Aus dem

Department für Diagnostische Labormedizin

der Universität Tübingen

Institut für Medizinische Mikrobiologie und Hygiene

Characterization of the murein endopeptidase MepM as a potential target for the development of adjuvants to overcome β-lactam resistance

Inaugural-Dissertation
zur Erlangung des Doktorgrades
der Medizin

der Medizinischen Fakultät
der Eberhard Karls Universität
zu Tübingen

vorgelegt von
Kemper, Johanna

2023

Dekan: Professor Dr. B. Pichler

1. Berichterstatter: Privatdozent Dr. E. Bohn
2. Berichterstatterin: Professorin Dr. B. Schittek

Tag der Disputation: 17.05.2021

Table of contents

List of figures

List of tables

Abbreviations

ATM	Aztreonam
Bp	Base pairs
CAZ	Ceftazidime
CDC	U. S. Centre for Disease Control and Prevention
cDNA	Complementary DNA
CF	Cystic Fibrosis
CP	Crossing point
dNTP	Desoxyribonucleosidetriphosphate
PBS	Phosphate Buffered Saline
dsDNA	Double stranded DNA
Ec	*Escherichia coli*
FEP	Cefepime
GlcNAc	N-acetyl-glucosamine
IMI	Imipenem
LB	Lysogeny Broth
LMM-PBP	Low molecular mass penicillin-binding protein
LPS	Lipopolysaccharides
LT	Lytic transglycosylases
MDR	Multidrug-resistant
MEM	Meropenem
MEP	Murein endopeptidase
MIC	Minimal inhibitory concentration
MurNAc	N-acetyl-muramic acid
OD	Optical density
Pa	*Pseudomonas aeruginosa*
PBP	Penicillin-binding protein
PCR	Polymerase chain reaction
PG	Peptidoglycan
PIP	Piperacillin
qRT-PCR	semi-quantitative Real-time PCR
RND	Resistance-nodulation-division

rpm	Revolutions per minute
RT-enzyme	Reverse transcriptase
SD	Standard deviation
SDS-PAGE	Sodium dodecyl sulfate polyacrylamide gel electrophoresis
SOC	Super optimal broth with catabolite repression
TBE buffer	5x TRIS-Borate-EDTA buffer
Tn	Transposon
TraDis	Transposon-directed insertion sequencing
TRIS	Tris(hydroxymethyl)aminomethane
TZP	Piperacillin/Tazobactam
VAP	Ventilator associated pneumonia
WHO	World Health Organisation
WT	Wildtype

1 Introduction

1.1 *Pseudomonas aeruginosa*

Pseudomonas aeruginosa (*Pa*) is a gram-negative, rod-shaped bacterium, which was first isolated by Gessard in 1882. Because of its unique blue-green colouration in cultures, he named it “Bacterium pyocyaneum”. The cause for the species-specific colouring is the production of the phenacyl-derivate pyocyanin (Hof and Schlüter, 2019).

Due to its low nutrient requirements, *Pa* can be found in a variety of different environments such as soil or water. It can also be detected in showers, sinks and even eye drops or insufficiently concentrated disinfectants. That is why *Pa* plays a major role in nosocomial infections (Hof and Schlüter, 2019). Being an opportunistic pathogen, *Pa* rarely infects patients with intact immunity. Many infections with *Pa* occur in generally immunosuppressed patients, such as AIDS patients or neutropenic patients undergoing chemotherapy (Lyczak et al., 2000). Furthermore, *Pa* infects tissues when a natural barrier of the host is breached, e.g. in burn wound infections or ulcerative keratitis after contact lens use (Hancock and Speert, 2000). In general, it can provoke various infections such as pneumonia, urinary tract infection, wound infection or blood stream infection (Weiner-Lastinger et al., 2019).

Compared to other bacteria, *Pa* has a relatively large genome comprising 5.5-7 million base pairs (bp). Moreover, *Pa* has more than 500 regulatory genes (Stover et al., 2000) and lots of genes encoding transporters, transcriptional factors and two-component regulatory systems. The great variability of its genome yields in *Pa*’s very flexible metabolism and its high ability to adapt to changing environments (Klockgether et al., 2011, Pang et al., 2019, Silby et al., 2011).

Besides, *Pa* employs several virulence factors to infect host cells leading to invasive infections and higher mortality of affected patients. To start with, it carries a polar flagellum and several type 4 pili, which facilitate bacterial adhesion to different kinds of tissues. Both annexes are essential for the bacterium’s motility and can provoke inflammatory response of the host (Gellatly and Hancock, 2013).

With the help of a type III secretion system, *Pa* can inject toxic effector proteins into the host cells (Hauser, 2009). Degradative enzymes such as elastases are secreted by *Pa*, leading to increased epithelial permeability through destruction of tight junctions (Azghani, 1996).

Pa is member of the group of the "ESKAPE" pathogens. "ESKAPE" is an acronym for 6 nosocomial pathogens (namely ***E****nterococcus faecium*, ***S****taphylococcus aureus*, ***K****lebsiella pneumoniae*, ***A****cinetobacter baumannii,* ***P****seudomonas aeruginosa* and ***E****nterobacter* spp.), whose treatment is complicated by increasing multidrug resistance and virulence (Rice, 2008). The World Health Organisation's (WHO) priority list of antibiotic-resistant bacteria ranks carbapenem-resistant *Pa* in the category of "critical priority", together with carbapenem-resistant *Acinetobacter baumannii* and carbapenem- and third-generation cephalosporin resistant *Enterobacteriaceae* (Tacconelli et al., 2018). In their report of 2019, the U. S. Centre for Disease Control and Prevention (CDC) classifies the threat of multidrug-resistant (MDR) *Pa* as "serious" (CENTRES FOR DISEASE CONTROL AND PREVENTION, 2019).

1.2 Infections caused by *Pseudomonas aeruginosa*

Pa is among the most common pathogens causing Healthcare Associated Infections (HAI's). Between 2015 and 2017 *Pa* made up 8 % of all nosocomial infections in adults, following *Ec* (17,5 %), *Staphylococcus aureus* (11.8 %) and selected *Klebsiella spp.* (8,8 %). This can be explained by the fact that *Pa* is able to colonize moist reservoirs like sinks or contact lens solutions (Wu et al., 2015) as well as surfaces of medical devices like catheters or ventilation equipment (Willmann et al., 2014, Percival et al., 2015, Lister et al., 2009). In the nosocomial setting, urinary tract infections, wound infections, blood stream infections and pneumonia are the most common infections following *Pa* colonization (Weiner-Lastinger et al., 2019).

Nearly all infections with *Pa* are associated with a compromised immune system of the patient. Thus, neutropenic patients undergoing chemotherapy, AIDS patients or patients with pharmacologically induced immunosuppression are at greater risk of infections with *Pa* (Lyczak et al., 2000, Shepp et al., 1994).

Furthermore, infections are facilitated by disruption of physiological barriers, such as epithelial tissues or the skin barrier. This can for example be observed in patients with severe burns (Lyczak et al., 2000), surgical wounds, permanent catheters or tracheostoma (Restrepo et al., 2018, Lister et al., 2009). Consequently, *Pa* often is a problem in intensive care units (Spencer, 1996). The mortality rates can rise up to 60 %, when the pathogen reaches the bloodstream provoking septicaemiae (Page and Heim, 2009). Further, it was shown that colonization and infection with *Pa* leads to a significantly higher mortality in burn patients (Armour et al., 2007).

Pa can cause acute and chronic respiratory infections, often in a nosocomial setting, but also community-acquired in immunocompromised patients (Gellatly and Hancock, 2013, Williams et al., 2010). The pathogen is the second most common pathogen isolated from patients with ventilator-associated pneumonia (VAP, (Weiner-Lastinger et al., 2019)). The European Centre of Disease Prevention and Control even ranks *Pa* as the microorganism most frequently isolated from pneumonia acquired in intensive-care units in 2017 (European Centre of Disease Prevention and Control, 2019). Patients suffering from VAP mostly have acquired damages of the respiratory epithelium e.g. after intubation of the trachea. As a result, *Pa* can colonize the plastic surface of endotracheal tubes building a biofilm that is difficult to remove (Williams et al., 2010, Gil-Perotin et al., 2012). Furthermore, *Pa* can use its type III secretion system to intoxicate the epithelial lung cells, thereby penetrating the pulmonal-vascular barrier and causing bacteraemia (Berube et al., 2016).

If *Pa* is not eradicated through antimicrobial therapy during the acute state of the infection, it starts growing as a biofilm resulting in a chronic infection. *Pa* isolated during the chronic infection state are less virulent, but also less sensitive to antimicrobial agents than isolates of *Pa* in the acute state of infection (Pang et al., 2019). Chronic respiratory infections most usually occur in patients who have previous illness of the respiratory system like patients with chronic obstructive pulmonary disease or patients suffering from cystic fibrosis (CF) (Gellatly and Hancock, 2013). CF is caused by a mutation of the gene encoding for the CF

transmembrane conductance regulator (CFTR) chloride channel. The CFTR channel is expressed in respiratory epithelium and submucosal glands and its defect leads to a thickened airway surface liquid resulting in severe impairment of the mucociliary clearance and the immune response of the host. This environment makes it easy for bacteria to colonize the airways of CF patients and to develop chronic infections. In 2001, Burns et al. showed that 97 % of all 3-year old children with CF are infected with *Pa* (Burns et al., 2001). Those patients, who move into a chronic stage may live with *Pa* for more than 20 years during which the infection accelerates the deterioration of their lung function (Jacques et al., 1998, Williams et al., 2010, Sadikot et al., 2005).

Besides the nosocomial infections, *Pa* can cause infections of the external ear, the so-called “swimmers’ ear” or otitis externa. As *Pa* prefers wet environments, it can colonize swimming pools. Here, it can easily infect the external ear canal of swimmers (Schaefer and Baugh, 2012). In addition, use of extensive-wear soft contact lenses increases the risk of a corneal infection by *Pa*. The possibly resulting ulcerative keratitis can lead to visual loss or perforation of the cornea (Weissman et al., 1984, Vazirani et al., 2015).

To conclude, *Pa* is responsible for a large range of infections, threatening especially patients with a weakened immune response. Different official authorities such as the CDC or the WHO frequently emphasize the threat of infections by MDR *Pa*.

1.3 Resistance mechanisms of *Pseudomonas aeruginosa*

The characteristic of *Pa* to resist many antibiotics is mediated by intrinsic, acquired and adaptive resistance mechanisms (Pang et al., 2019). Low permeability of the outer membrane, high expression of efflux pumps and expression of the inducible β-lactamase AmpC are main intrinsic resistance mechanisms of *Pa* (Breidenstein et al., 2011). As most antibiotics must pass the bacterial cell wall to interact with their intracellular targets, a low permeability of the cell wall counts as one of the intrinsic resistance mechanisms (Lambert, 2002). Bellido et al. (1992) propose that the outer membrane permeability of *Pa* is 12- to 100-fold lower than that of *Ec*. One possible explanation for this

phenomenon is that in *Pa* 95 % of the non-specific porin OprF, which is responsible for non-specific uptake of ions and saccharides, appear to be in a closed conformation (Sugawara et al., 2006).

The function of bacterial efflux pumps is to remove potentially toxic molecules from the cell, such as dyes, inhibitors or antibiotics (Poole, 2001). Consequently, a high expression of these efflux pumps contributes to high antibiotic resistance and the development of multidrug resistance in *Pa* (Cabot et al., 2011, Shigemura et al., 2015). Bacterial efflux systems responsible for expulsion of antimicrobials can be classified into 5 families: (i) the resistance-nodulation-division (RND) family, (ii) the small multidrug resistance (SMR) family, (iii) the major facilitator (MF) superfamily, (iv) the ATP-binding cassette (ABC) family and (v) the multidrug and toxic compound extrusion (MATE) family (Poole, 2007, Putman et al., 2000). In Gram-negative bacteria, transporters of the RND family expel a broad variety of antibiotics, catalysing an active efflux as proton/drug antiporters. RND transporters consist of cytoplasmic membrane transporters, periplasmic linker proteins and outer membrane porin channel proteins. All three domains form a tripartite complex (Li and Nikaido, 2009, Daury et al., 2016). Two RND family efflux pumps (MexAB-OprM and MexCD-OprJ) are mainly responsible for the expulsion of β-lactam antibiotics (Poole, 2001, Masuda et al., 2000).

The third intrinsic resistance mechanism is the production of antibiotic-inactivating enzymes such as the β-lactamase AmpC or aminoglycoside-modifying enzymes. β-lactamases are able to hydrolyse the amide bond of the β-lactam ring, which leads to inactivation of β-lactam antibiotics. AmpC belongs to the class C β-lactamases and inactivates antipseudomonal cephalosporins (Pang et al., 2019, Berrazeg et al., 2015). The expression of the *ampC* gene is usually low, but can be induced by subinhibitory concentrations of β-lactams (Gellatly and Hancock, 2013). Furthermore, extended-spectrum-β-lactamases have been found in *Pa* isolates, leading to resistance against many β-lactam antibiotics like penicillins, cephalosporins and aztreonam (Rawat and Nair, 2010, Paterson and Bonomo, 2005).

Besides the intrinsic resistance mechanisms, *Pa* can acquire resistance genes via horizontal gene transfer or through chromosomal mutations (Botelho et al., 2019). For instance, a reason for higher resistance especially against carbapenems is a mutationally deficient OprD porin, which usually mediates the uptake of carbapenems (Li et al., 2012, Shu et al., 2017). Other examples are mutations occurring in the genes encoding DNA gyrase (*gyrA*, *gyrB*) or topoisomerase IV (*parC*, *parE*). These enzymes provide the binding site for quinolone antibiotics. Thus, mutations of the corresponding genes result in deteriorated binding affinity of the quinolones and thereby in reduced effect on the *Pa* strains (Bruchmann et al., 2013). Also, mutations in the regulator genes of efflux pumps (*mexR*, *nalB*, *nalC*, *nalD* or *nfxB*) can effect overexpression of efflux systems leading to an increased expulsion of antibiotics (Pang et al., 2019). Braz et al. exemplarily showed that mutations of the *nalC* gene induce MexAB-OprM overexpression causing high resistance against aztreonam (Braz et al., 2016). Beyond that, resistance against cephalosporins and penicillins is greatly increased by mutations of the *ampC* gene (Berrazeg et al., 2015).

Using horizontal gene transfer, bacteria can acquire resistance genes, which are carried e.g. on plasmids or transposons (Breidenstein et al., 2011). For example, in *Pa* gene cassettes encoding metallo-β-lactamases are transferred into the *Pa* strains by genetic elements like integrons and plasmids. Through the mechanisms of transferring resistance genes in between the different species, the rate of microbial resistances increases dramatically, complicating the treatment of bacterial infections (Hong et al., 2015).

Adaptive antibiotic resistance describes the ability of bacteria to adapt transitionally to environmental conditions including subinhibitory concentrations of antibiotics or certain growth states such as swarming motility or biofilm formation. After being stimulated, the adaptation process occurs through alterations in gene and protein expression or in modification of antibiotic targets. To give an example, it has been shown, that a bacterial strain can tolerate higher concentrations of an antibiotic, if it has been exposed to lower concentrations before (Moradali et al., 2017, Fernandez et al., 2011).

Formation of a biofilm is one of the transient strategies of *Pa* to evade antimicrobial treatment. A biofilm is a growth state, in which the bacteria aggregate on surfaces together with a self-produced extracellular matrix, composed of exopolysaccharides such as alginate, proteins, lipids and extracellular DNA (Donlan, 2002, Hof and Schlüter, 2019). Bacteria growing in a biofilm are less sensitive to antimicrobial agents and host immune response (Stewart and Costerton, 2001). One reason for this phenomenon is that the biofilm acts as a chemical barrier, preventing antibiotic penetration (Hof and Schlüter, 2019, Stewart, 2002).

Moreover, the bacteria have the ability to communicate via quorum sensing systems: this communication through messenger substances allows the microorganisms to change their gene expression resulting in biofilm formation or differentiation into persister cells (Pang et al., 2019). A persister cell phenotype is a transient dormant state of a bacterium defined by slow growth, inactive metabolism and thus high tolerance against antibiotics (Moradali et al., 2017). The frequency of persister cells in a population is rather low (10^{-6} to 10^{-5} in *Ec* wildtype (WT))(Fasani and Savageau, 2015). Still, it is presumed that these persister cells are responsible for the difficulties in the treatment of chronic infections (Maisonneuve and Gerdes, 2014). High levels of persister cells have e.g. been found in patients with CF (Mulcahy et al., 2010). For *Pa*, another persister-like phenotype has been described, which was first discovered in *Vibrio cholerae*: upon exposure to normally lethal doses of β-lactams, bacteria including *Pa* can turn into viable, cell-wall deficient sphere phenotypes, which can re-establish their typical rod-shaped morphology after removal of the antibiotics (Weaver et al., 2018, Dörr et al., 2015).

1.4 The bacterial cell envelope

The cytoplasm of bacteria is surrounded by an envelope, which performs a variety of functions: it determines the bacterium’s shape and acts as an interface between the bacteria and their environment. Additionally, it controls uptake and release of substances and in pathogens it is responsible for interaction with the host (Braun et al., 2015).

Generally, the cell envelope consists of different layers that lie on top of each other. An inner membrane encircles the cytoplasm followed by a smaller or larger periplasmic space. The cell wall (murein sacculus), a layer of cross-linked peptidoglycans (murein), surrounds the periplasmic space. Depending on their cell wall structure, bacteria are categorized as Gram-negative or Gram-positive. In Gram-positive bacteria, the murein layer is thicker, whereas Gram-negative species possess a thin peptidoglycan-layer and an outer membrane on top of it. The outer membrane of Gram-negative bacteria is composed of phospholipids, different proteins and lipopolysaccharides (LPS) (Hof and Schlüter, 2019, Nikaido, 2003). *Pa* produces an LPS consisting of three structural domains: Lipid A anchors LPS into the outer membrane. It consists of a disaccharide backbone and several fatty acids. Moreover, it acts as an endotoxin, evoking inflammatory responses in the host. The second domain is a nine or ten-sugar, branched oligosaccharide core, which is attached to Lipid A. Furthermore, the third domain is called O-antigen or O-polysaccharide and consists of a repetitive carbohydrate polymer. *Pa* can produce two different O-antigens at once: the common polysaccharide antigen is a homopolymer of D-rhamnose and triggers a weak antibody response. On the contrary, the O-specific antigens are composed of five different sugars organized into repetitive O units inducing a strong immune response (King et al., 2009, Lam et al., 2011). In summary, LPS plays a decisive role in the interaction with host cells. In contrast, the cell wall is rather essential for stability of the cell envelope. Going more into detail regarding the composition of the bacterial cell wall, it is made up of alternating N-acetyl-muramic acid (MurNAc) and N-acetyl-glucosamine (GlcNAc) residues connected by β-1,4-glycosidic linkages. There is a short chain peptide linked to the MurNAc moiety, typically composed of five amino acids. In Gram-negative bacteria, the common amino acids are L-alanine, γ-D-glutamate, meso-diaminopimelic acid and D-alanyl-D-alanine (L-Ala-γ-D-Glu-*m*-DAP-D-Ala-D-Ala). Further, the adjacent peptidoglycan (PG) units are crosslinked between the third amino acid of one chain (*m*-DAP) and the fourth amino acid of the other (D-Ala) (Schleifer and Kandler, 1972). The outcome is a strongly tied, netlike structure, which confers high stability upon the cell wall (Dhar et al., 2018). Figure 1 shows schematically

the structure of the bacterial murein. The composition of the PG was thought to be relatively consistent among Gram-negative species. However, recent findings revealed that the PG structure of *Pa* includes 160 different muropeptides, meaning a higher variance in PG composition than previously believed (Anderson et al., 2020).

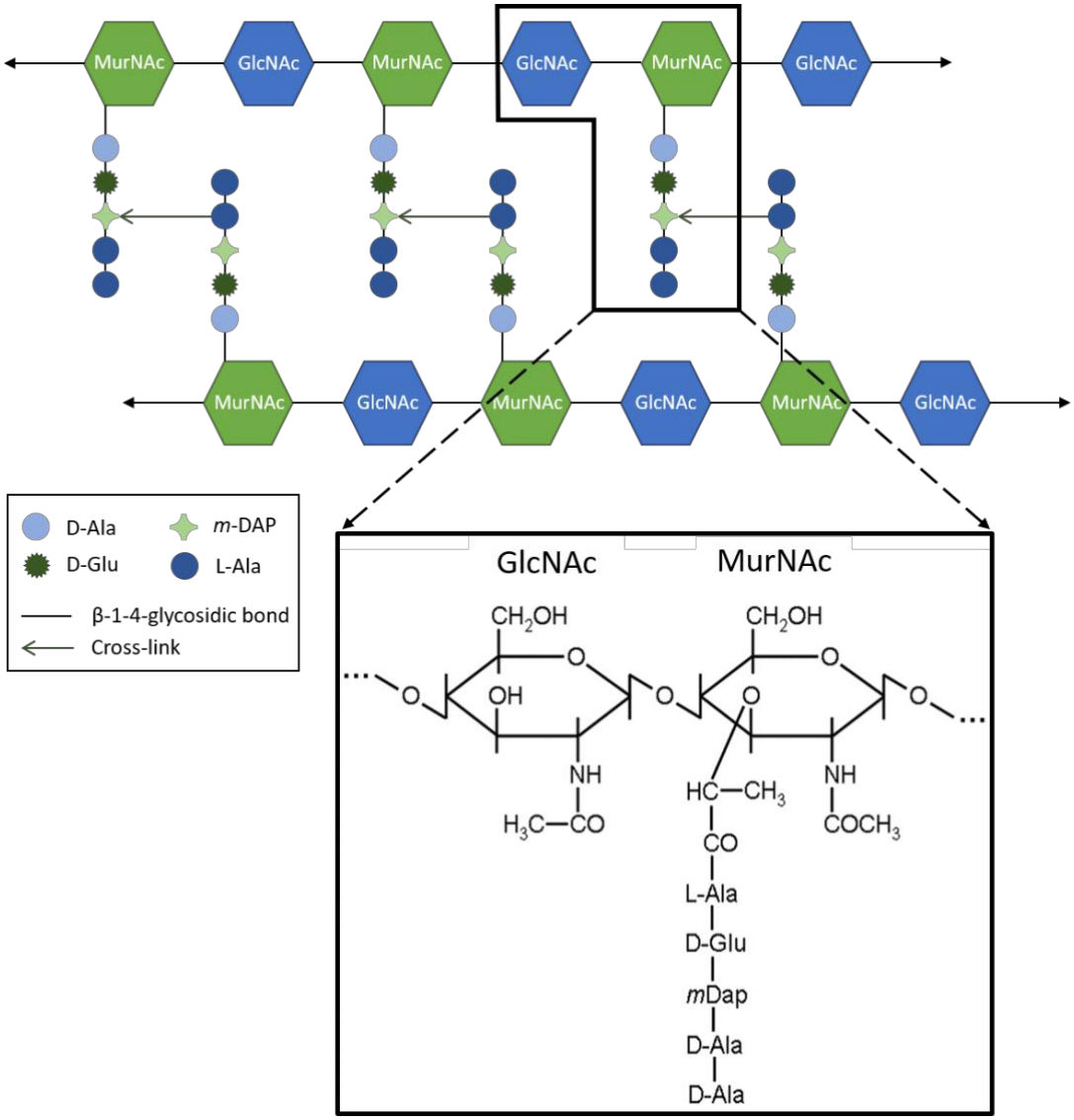

Figure 1: ***Structure of peptidoglycans in the bacterial cell wall***

One PG repeat unit consists of the two alternating amino sugars MurNAc and GlcNAc, connected via β-1,4-glycosidic bonds. A pentapeptide chain is attached to the MurNAc residue. Generally, it is composed of L-alanine, γ-D-glutamate, meso-diaminopimelic acid and D-alanyl-D-alanine (L-Ala-γ-D-Glu-m-DAP-D-Ala-D-Ala). Adjacent PG units are typically connected via crosslinks between m-DAP and D-Ala. Thus, a very stable and netlike structure is built, which can resist internal pressure. Parts of the figure were kindly provided by Roujeinikova (2008). Copyright (2008) National Academy of Sciences, U.S.A.

During cell growth and cell division it is crucial for bacteria to remodel their cell wall. To save resources, bacteria recycle almost 40-50% of their cell wall components including their muropeptides (Dhar et al., 2018, Doyle et al., 1988). Because an intact cell wall is essential for the survival of a bacterium, it has always been of interest as a target for antimicrobial therapy. Furthermore, it has been discovered, that cell wall biosynthesis and recycling are closely connected to the induction of β-lactamase AmpC via its transcriptional regulator AmpR (Mayer, 2019, Jacobs et al., 1994).

1.4.1 Peptidoglycan recycling pathway

During growth, lytic and anabolic activity upon the cell wall must be kept in balance to ensure bacterial survival. The degradation of the cell wall starts with the catabolic action of several enzymes: lytic transglycosylases (LTs) such as MltA, MltG or Slt cleave the glyosidic bond between GlcNAc and MurNAc (Lee et al., 2017), amidases such as AmpDh2 and AmpDh3 cleave between the sugar and the peptide moiety. Moreover, carboxypeptidases remove the C-terminal amino acid of the peptide chain and endopeptidases cut the peptide crosslinks (Irazoki et al., 2019, Dhar et al., 2018). Low molecular mass penicillin-binding proteins (LMM PBPs: PBP4, PBP5, PBP6, PBP7/8) have endopeptidase and/or carboxypeptidase activity. As a result of the activity of all these enzymes, N-acetyl-glucosamine-1,6-anhydro-N-acetyl-muramic acid (GlcNAc-1,6-anhydroMurNAc) tri-, tetra-, and pentapeptides are generated (Vollmer et al., 2008). Next, the GlcNAc-1,6-anhydroMurNAc peptides are transported through the inner membrane into the cytoplasm via the permease AmpG (Jacobs et al., 1994). In contrast to *Ec*, *Pa* additionally harbours a homologue of AmpG, the permease AmpP. However, its role concerning the transport of muropeptides into the cytoplasm has not yet been elucidated (Kong et al., 2010). Once in the cytoplasm, the GlcNAc-1,6-anhydroMurNAc-peptides are processed by the β-N-acetylglucosaminidase NagZ into units of GlcNAc and 1,6-anhydroMurNAc peptides (Stubbs et al., 2008). A carboxypeptidase named LdcA removes the terminal D-alanine from the tetrapeptides, whereby tripeptides are created (Templin et al., 1999, Korza and Bochtler, 2005). Afterwards, an amidase called AmpD cleaves the bond of the peptide chains, forming 1,6-anhydroMurNAc and

tri-, tetra- and pentapeptides (Dhar et al., 2018, Zhang et al., 2013). In *Pa*, the further processing of 1,6-anhydroMurNAc is catalysed by four different enzymes, namely AnmK, MupP, AmgK and MurU. During these steps 1,6-anhydro-MurNAc is metabolized into UDP-MurNAc, which is an intermediate product of the PG de novo synthesis (Gisin et al., 2013). From this step on, PG biosynthesis and recycling proceed convergently. By the activity of the ligases MurC, MurD, MurE and MurF, a peptide chain is gradually attached to UDP-MurNAc (Barreteau et al., 2008). The generated UDP-MurNAc-pentapeptide is coupled to undecaprenyl phosphate by the integral membrane protein MraY forming Lipid I (Ikeda et al., 1991, Bouhss et al., 2004). Another enzyme associated with the membrane (MurG) adds GlcNAc to Lipid I generating Lipid II (undecaprenol-pyrophosphate-UDP-GlcNAc-MurNAc peptide)(Brown et al., 2013, Vollmer and Bertsche, 2008). Lipid II is presumably transported into the periplasm via the suspected “flippases” FtsW and MurJ (Mohammadi et al., 2011, Sham et al., 2014, Dhar et al., 2018). Once in the periplasm, the precursor is incorporated into the nascent PG layer. These final steps are catalysed by high molecular mass penicillin-binding proteins with transglucosylase and/or transpeptidase activity (Vollmer and Bertsche, 2008, Handfield et al., 1997, Legaree et al., 2007). Figure 2 gives a schematic overview on PG turnover and synthesis.

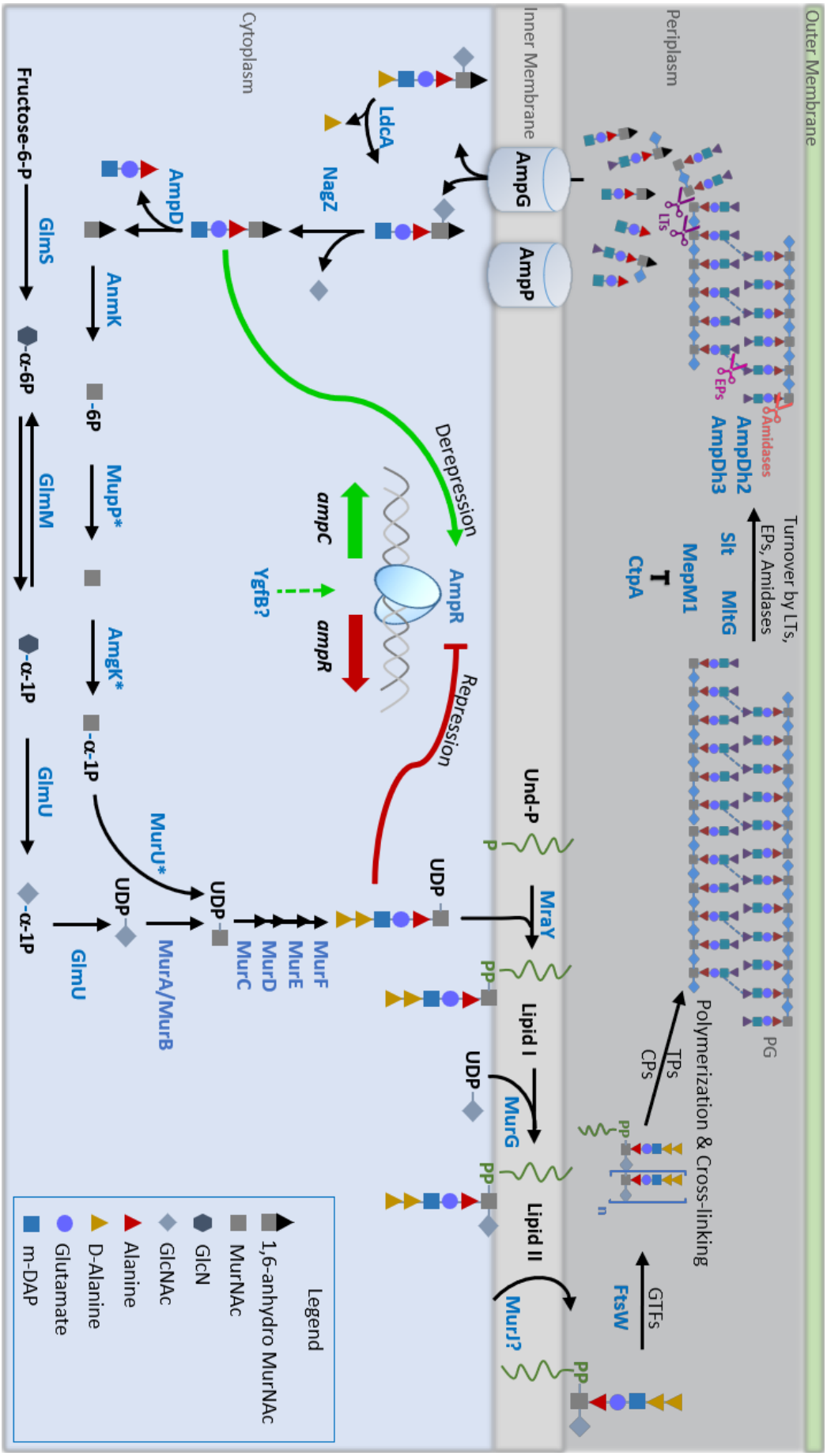
Outer Membrane
Periplasm
Inner Membrane
Cytoplasm
PG
Polymerization & Cross-linking
Turnover by LTs, EPs, Amidases
TPs
CPs
GTFs
FtsW
MurJ?
Lipid II
MurG
Lipid I
MraY
Und-P
UDP
PP
MurF
MurE
MurD
MurC
MurA/MurB
MurU*
GlmU
α-1P
AmgK*
MupP*
-6P
AnmK
GlmM
α-6P
GlmS
Fructose-6-P
AmpD
NagZ
LdcA
AmpG
AmpP
AmpR
Derepression
Repression
ampC
ampR
YgfB?
MepM1
MltG
Slt
CtpA
AmpDh2
AmpDh3
Amidases
EPs
LTs
Legend
1,6-anhydro MurNAc
MurNAc
GlcN
GlcNAc
Alanine
D-Alanine
Glutamate
m-DAP

Figure 2: ***Illustrative scheme of the PG recycling and synthesis in Pa***

De-novo biosynthesis of PG starts in the cytoplasm. Step by step, Fructose-6-phosphate is converted into UDP-GlcNAc by the enzymes GlmS, GlmM and GlmU. Next, MurA and B transform UDP-GlcNAc into UDP-MurNAc. The recycling pathway, which also results in the generation of UDP-MurNAc, starts in the periplasm. LMM PBPs, LTs, EPs and amidases cleave muropeptides from the PG strand. These muropeptides are transported into the cytoplasm, mainly via permease AmgG. The role of AmpP, a paralogue of AmpG has not been elucidated yet. Subsequently, the muropeptides are degraded: a β-N-acetylglucosaminidase (NagZ) cleaves the GlcNAc moiety and a carboxypeptidase (LdcA) cuts the terminal amino acid D-alanine. The resulting products (1,6-anhMurNAc-muropeptides) can induce ampC expression via the transcriptional regulator ampR. The 1,6-anhMurNAc-muropeptides are further processed by the amidase AmpD, which removes the rest of the peptide chain. Through the enzymatic action of the so-called salvage pathway (AnmK, MupP, AmgK and MurU), 1,6-anhMurNAc is processed to UDP-MurNAc. From this step on, PG biosynthesis and recycling proceed together. Following the formation of UDP-MurNAc, peptide chains are added by ligases such as MurC, MurD, MurE and MurF. The products (UDP-MurNAc-pentapeptides) can bind to ampR leading to a depression of ampC expression. Furthermore, a MurNAc-pentapeptide-translocase MraY converts the UDP-MurNAc-pentapeptides to Lipid I and the glycosyltransferase MurG attaches the GlcNAc moiety forming Lipid II. A putative flippase MurJ transports Lipid II into the periplasm, where it is assembled into the nascent PG strand by high molecular mass penicillin-binding proteins, glycosyltransferases, transpeptidases and DD-carboxypeptidases. Figure taken modified from: Sonnabend et al. (2019)

1.5 Cell-wall recycling and resistance against β-lactam antibiotics

The PG turnover and the regulation of the expression of the β-lactamase AmpC are closely connected. Through cytosolic intermediates of PG biosynthesis and degradation the cells sense the status of their cell walls (Mayer, 2019). The expression of the *ampC*-gene is thereby depending on the transcriptional regulator AmpR. Whereas the accumulation of the intermediate in PG synthesis UDP-MurNAc-pentapeptide decreases expression of *ampC* when bound to AmpR, the degradation product 1,6-anhydro-MurNAc-peptides can counteract this effect (Jacobs et al., 1997). Since the expression level of the inducible *ampC*-gene strongly influences resistance against β-lactam antibiotics, changes in PG recycling might respectively have impact on resistance. On this account, different players of the PG turnover have been analysed regarding their significance for resistance in *Pa*.

The first group of proteins identified to play a role for β-lactam resistance are those that produce the catabolites of PG leading to induction of *ampC* expression. For example, it has been shown that inactivation or mutation of the *dacB*-gene encoding the LMM PBP4 leads to an increased expression of *ampC* and thus to higher resistance. Mutations of the *dacB* are very prevalent in clinically isolated MDR *Pa* (Moya et al., 2009, Lee et al., 2015). Furthermore, the periplasmic LTs, which are mainly responsible for the generation of 1,6-anhydro-MurNAc muropeptides, play a role in resistance against β-lactams. Investigations by

Cavallari et al. (2013) demonstrate that deletion of the LT Slt decreases β-lactam resistance, whereas the loss of SltB1 and MltB1 leads to enhanced resistance. However, the increased resistance in SltB1 and MltB1 does not seem to be attributable to upregulated expression of *ampC* (Lamers et al., 2015). Deletion of the LT MltG caused strikingly reduced MICs due to a strongly decreased AmpC β-lactamase activity in *Pa* ID40 (Sonnabend et al., 2019).

After degradation of the PG in the periplasm by LTs and LMM PBPs, the intermediate products are transported into the cytoplasm by the permease AmpG. Consequently, absence of *ampG* prevents the accumulation of 1,6-anhydro-MurNAc muropeptides in the cytoplasm, thereby averting induction of *ampC* expression. Indeed, inactivation of *ampG* could restore the sensitivity of isolated pan-β-lactam-resistant clinical strains by completely blocking *ampC* induction (Zamorano et al., 2011, Dhar et al., 2018).

NagZ acts as a β-N-acetylglucosaminidase in the cytoplasm and generates the 1,6-anhydro-MurNAc muropeptides, that bind to AmpR, which is required for induction of *ampC* (Asgarali et al., 2009). Thus, it is not surprising that deletion of NagZ caused higher susceptibility to β-lactams through lower *ampC* expression. This was discovered in different MDR *Pa* including pan-β-lactam-resistant clinical isolates (Zamorano et al., 2010, Zamorano et al., 2011).

Moreover, the amidase AmpD degrades the 1,6-anhydro-MurNAc muropeptides by cutting off the peptide chains (Zhang et al., 2013). In this way, it promotes the further processing of the AmpR activators, leading to a decreased *ampC* expression. Accordingly, the absence of AmpD results in accumulation of 1,6-anhydro-MurNAc tripeptides, which promotes the overproduction of AmpC β-lactamases and thus high resistance against β-lactams (Langaee et al., 2000, Jacobs et al., 1995). Inactivating mutations of the *ampD* gene are common in clinical isolates of *Pa* (Schmidtke and Hanson, 2008, Juan et al., 2005). What remains to be mentioned is that the *Pa* genome encodes for another β-lactamase named PoxB, whose expression is regulated negatively by AmpR (Kong et al., 2005). In PAO1 it has been discovered, that deletion of PoxB does not alter β-lactamase activity or susceptibility to β-lactam antibiotics. Apart from this, a *poxB*-

overexpressing clone was observed to have lower minimal inhibitory concentrations (MICs) for meropenem and doripenem (Zincke et al., 2016).

To sum up, many of the players acting in the PG turnover have indirect influence on *ampC* expression and thereby on resistance against β-lactam antibiotics. Hence, these findings should be considered, when it comes to the development of future antimicrobial therapies.

1.6 Players of the Peptidoglycan Recycling as targets for antibiotic adjuvants in Pseudomonas aeruginosa

Since an intact cell wall is essential for the survival of bacteria, it has always been of interest as a target for antimicrobial therapies. β-lactam antibiotics act as covalent inhibitors of essential penicillin-binding proteins (PBPs). PBPs are enzymes involved in the final steps of cell wall biosynthesis catalysing the cross linkage between PGs. Additionally, they play an important role in degradation of PG. It was found that Penicillin G has a structural similarity to the terminal D-Ala-D-Ala dipeptide of the nascent PG (Bush and Bradford, 2016, Strominger and Tipper, 1965). If certain PBPs are inhibited, complex downstream consequences lead to an imbalance of cell wall synthesis and degradation consuming cellular resources and causing cell lysis (Cho et al., 2014, Mayer, 2019). However, resistance against β-lactam antibiotics is very common in pathogens like *Pa* mediated through a large number of mechanisms such as the production of β-lactamases (see 1.4). Hereby, the range of effective antibiotics is limited, when it comes to infections with MDR strains. To treat infection with MDR *Pa*, the use of colistin often remains the only option, even though it is known for its neuro- and nephrotoxicity (Chatterjee et al., 2016, Sabuda et al., 2008). To evade β-lactam resistance, combination therapies of antibiotics together with a new adjuvant molecule have been developed. In general, the adjuvant's role is to restore the antibiotics effectiveness, not necessarily to have antimicrobial effects itself (Douafer et al., 2019). The most successful adjuvants applied in clinical practice are β-lactamase inhibitors such as clavulanic acid, sulbactam or tazobactam (Bush and Bradford, 2016). Yet, not all β-lactamases are blocked to the same level by these inhibitors. Clavulanic acid, for example, effects induction of *ampC*

in *Pa* (Lister et al., 1999). In contrast to direct inhibition of the β-lactamase, new approaches aim different players of the induction pathway of *ampC*, which includes the PG turnover (Mayer, 2019). As described in 1.5, many enzymes involved in the cell wall recycling influence AmpR-AmpC-mediated β-lactam resistance. For NagZ several small molecule inhibitors have been designed and tested (Stubbs et al., 2007, Mondon et al., 2013). It has been most challenging to find selective inhibitors, which do not concomitantly inhibit functionally related human enzymes. However, compounds were found that exhibit a 20-50-fold higher selectivity towards NagZ over the human enzymes (Stubbs et al., 2013). Moreover, the first *in vivo* validations have shown that inactivation of NagZ reverts β-lactam resistance and additionally reduces virulence in terms of mice mortality (Torrens et al., 2019).

To conclude, in search of new adjuvants to cope with *ampC*-mediated resistance, the strategy of interfering with the regulatory processes of *ampC* expression seems like a promising approach.

1.7 Murein endopeptidases

The focus of this work lies on the further characterization of five different murein endopeptidases (MEPs) in *Pa*. In *Ec* more investigations on these enzymes have already been accomplished. LytM protein YebA/MepM and NlpC/P60 peptidase members Spr/MepS and YdhO/MepH were newly identified as murein hydrolases in 2012. It was shown that they cleave D-Ala-*m*-DAP crosslinks, which is important for the incorporation of new murein. Additionally, they are essential for PG growth and viability of *Ec*: absence of all three endopeptidases leads to cell lysis presumably through autolysins (Singh et al., 2012). Recently, it was suggested that the outer membrane protein NlpI regulates the hydrolytic activity of several endopeptidases including MepM and MepS by scaffolding them in a multi-enzyme complex (Banzhaf et al., 2020). Earlier, it had been reported that NlpI together with the protease Prc degrade *Ec* MepS (Su et al., 2017). In *Vibrio cholerae* YebA, the homologue of *Ec* MepM, was described to play an important role in sphere formation of the pathogen, which resulted in high antibiotic tolerance of the bacteria (Dörr et al., 2015).

So far, knowledge about MEPs in *Pa* is very poor. In 2018, Srivastava et al. found four putative MEPs (PA0667, PA1199, PA1198, PA4404) to be substrates of a proteolytic complex consisting of the carboxy-terminal processing protease CtpA and its binding partner LbcA. It had already been known that a CtpA-deficient mutant has a defective type III secretion system and decreased cytotoxicity against host cells. Moreover, CtpA was assessed to be important for the virulence of *Pa* (Seo and Darwin, 2013, Srivastava et al., 2018). During their study, Srivastava et al. discovered, that the MEPs they had identified as substrates of CtpA have orthologous genes in *Ec*. They found PA0667 to be 35 % identical to *Ec* MepM. PA1199 and PA1198 are both homologous to *Ec* MepS. The functional similarity of the *Pa* endopeptidases was also confirmed: deletion of CtpA resulted in reduced cross-linked PGs. This observation is assumed to be due to an accumulation of MEPs in CtpA-deficient mutants leading to excessive cleavage of cross-links.

In 2015, Yakhnina et al. published a phylogenetic tree (Figure 3) showing LytM proteins (lysostaphin family of proteins) of *Ec* and *Pa*. These proteins usually function as zinc metalloendopeptidases and possess intrinsic PG hydrolytic activity (Firczuk et al., 2005). They found nine proteins with LytM domain in *Pa* including PA0667/mepM, PA4404, PA3787 and PA5363. The tree also includes MepM of *Ec* and confirms its relation to *Pa* MepM (Yakhnina et al., 2015).

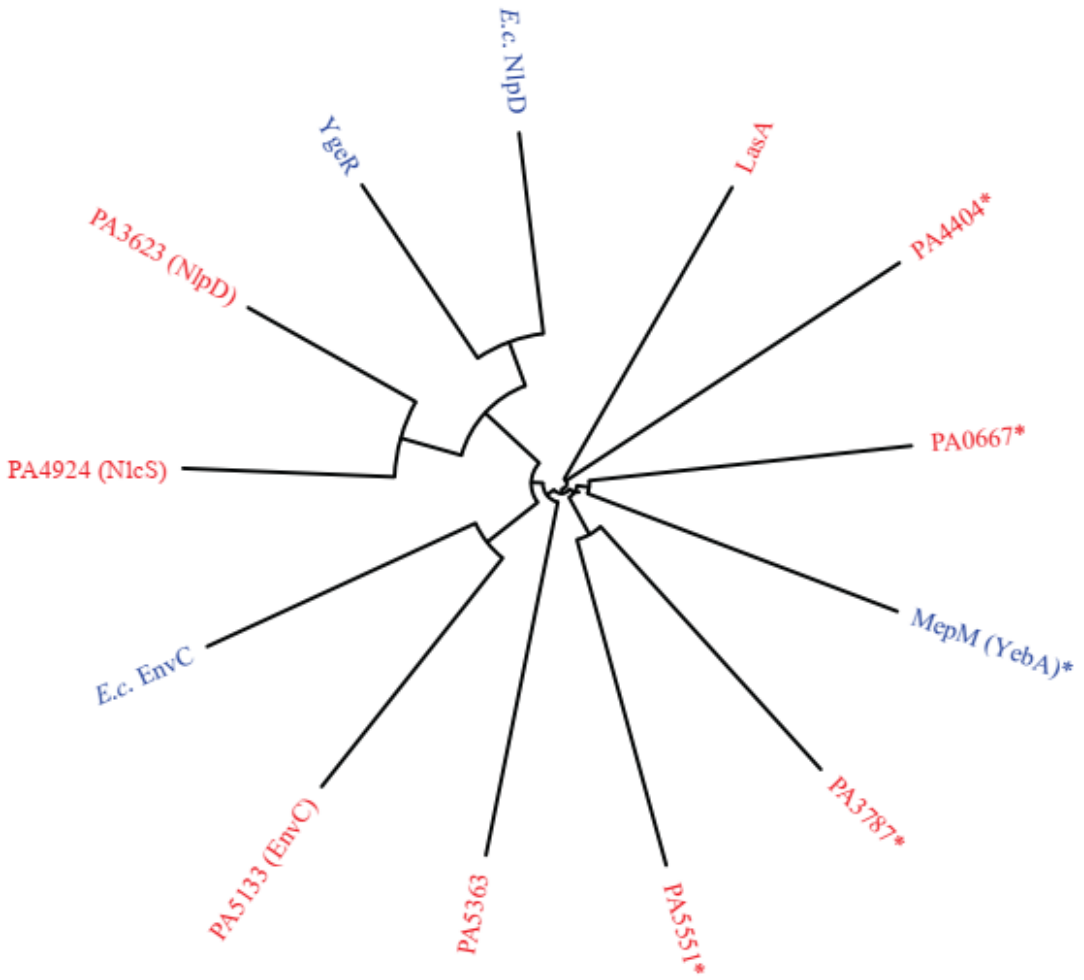

Figure 3: ***Phylogenetic tree of Pa and Ec LytM proteins***

Whole-protein alignment of factors containing LytM domain was performed via ClustalW and plotted via iTOL (Interactive Tree of Life) programs. The Ec proteins are depicted in blue and the Pa proteins are presented in red. Moreover, dLytM factors are shown:they have degenerated active sites, acting as regulators of other peptidases. Asterisks denote the factors that retain functional active sites and PG hydrolase activity. Figure taken from Yakhnina et al. (2015)

Of all MEPs in *Pa*, MepM is so far the one, which is best characterized. MepM has a Sec-dependent signal sequence that ensures the proteins transport across the cytoplasmic membrane to the periplasmic space. Besides, it has a LysM PG-binding domain and a LytM/M23 peptidase domain (Srivastava et al., 2018). About the functionality of MepM it is known that an additional deletion of *mepM* in a CtpA-deficient mutant (Δ*ctpA* Δ*mepM*) was able to restore a normal type III secretion system and cytotoxicity phenotype. Thus, it seems proved that these characteristics of the Δ*ctpA* mutant are attributable primarily to elevated MepM activity (Srivastava et al., 2018).

Recently, Sonnabend et al. performed a Transposon-directed insertion sequencing (TraDis) with a transposon library of the MDR clinical bloodstream isolate *Pa* ID40, which consists of 100000 unique transposon (Tn) insertions distributed across the whole genome. This means that in a pool of 10^7 bacteria (equalling mutants each with one unique Tn insertion) in average 100 bacteria would exist with the same Tn insertion. Such a library was grown with or without subinhibitory concentrations of meropenem (MEM) or cefepime (FEP) for 24h. The isolated genomic DNA was then isolated and used for transposon-directed sequencing. Each sequence read corresponds to one Tn mutant. By bioinformatic analysis for all conditions (no antibiotics or antibiotics) the number of all Tn insertions for every gene could be determined and normalized to the whole number of Tn insertion sequence reads. By statistical analysis significant changes of the number of Tn insertion mutants (affecting one gene) could be identified. The change of the number of Tn insertion sequence reads of each gene with antibiotics or without can be expressed as a ratio of normalized reads derived from bacteria grown with antibiotics related to those normalized reads derived from bacteria grown with only lysogeny broth (LB) medium.

Their results indicated that several MEPs are involved in maintaining antibiotic resistance against MEM and FEP (see Table 1). They validated the data for *Pa* MepM and showed that deletion of *mepM* in *Pa* ID40 increased sensitivity against β-lactam antibiotics due to reduced *ampC* expression and activity. Moreover, the deletion mutant ID40 Δ*ctpA* revealed increased *ampC* expression and activity resulting in hyperresistance. This hyperresistant phenotype could be reversed by further deletion of *mepM* to some extent (Sonnabend et al., 2019). In their work they referred to *Pa mepM*/PA0067 as *mepM1* and to PA3787 as *mepM2*. This nomenclature will be adopted for this thesis. Furthermore, the gene names depicted in Table 1 will be used. Table 1 shows the results regarding MEPs of the TraDis screening performed by Sonnabend et al.

Table 1: ***Results of the TraDis screening conducted by Sonnabend et al.***

The ID40 Transposon library was grown in Lysogeny Broth with or without 2 µg/ml meropenem or 8 µl/ml cefepime. Afterwards the genomic DNA of the surviving bacteria was used for sequencing of the Transposon-genome junctions. The left side of the table shows the function, orthologues and assigned gene names of MEPs and the carboxypeptidase CtpA. The differences in insertion sequence abundance in a distinct gene are expressed as the mean of the ratio of the normalized sequence read numbers of antibiotic-treated culture in relation to the normalized sequence read numbers of the LB control culture of the Tn library. Significant differences in the normalized read counts (representing the ratios of Tn insertion mutants in a distinct gene compared to all Tn insertion mutants) determined after both antibiotic treatment and treatment without antibiotics are highlighted with bold numbers (adjusted p-value p<0,05).

Gene name/ Orthologs	**Function/Family**	**Ratio MEM/LB**	**Ratio FEP/LB**
mepM1/ PA0067	murein-DD endopeptidase, LytM/M23 peptidase family	**0,051**	**0,073**
mepM2/ PA3787	Murein DD-endopeptidase MepM, unknown function, LytM/M23 peptidase family	**0,140**	**0,370**
mepM3/ PA4404	Murein DD-endopeptidase MepM, unknown function, LytM/M23 peptidase family	**0,484**	1,260
mepM4/ PA5363	Murein DD-endopeptidase MepM, unknown function, LytM/M23 peptidase family	1,020	0,85
lytH/ PA5551	peptidoglycan LD-endopeptidase, LytM/M23 peptidase family	1,000	0,775
mepH1/ PA1199	Murein DD-endopeptidase, NlpC/P60 family	0,930	0,84
mepH2/ PA1198	Murein DD-endopeptidase, NlpC/P60 family	**0,483**	**0,517**
mepH3/ PA3472	Murein DD-endopeptidase	0,812	0,917
ctpA/ PA5134	Carboxy-terminal processing protease	**4,026**	2,19

According to the results depicted in Table 1, the low ratio for MepM1 shows that the abundance of *mepM1* Tn insertion mutants was strongly reduced under

treatment with MEM or FEP. A significant reduction of the abundance of Tn insertion after treatment of at least one of the two antibiotics was found for the Tn insertion mutants affecting the genes *mepM2*, *mepM3* and *mepH2.* Since the impact of a Tn insertion on the function of a gene depends on the site where it is integrated in the gene, the data of the TraDis screening are only predictions that remain to be validated.

1.8 Aim of this work

MDR *Pa* strains are emerging worldwide due to accumulation of multiple resistance mechanisms. Epidemiological studies revealed high prevalence of extensively drug resistant phenotypes among clinical isolates of *Pa* varying from 9% in the USA to 33% in Iran (Eichenberger and Thaden, 2019). Thus, the development of new antimicrobial agents for the treatment of MDR *Pa* is urgently needed (Tacconelli et al., 2018). Besides common antibiotics, new strategies such as phage therapy (Vandenheuvel et al., 2015) or lectin inhibition (Krachler and Orth, 2013) have been investigated in the past years. The treatment using adjuvants such as β-lactamase inhibitors in addition to approved antibiotics has prevailed in clinical practice over a long period (Drawz and Bonomo, 2010). However, not all β-lactamases are effectively inhibited by the existing agents. As described in 1.6, investigation on inhibitors of NagZ as representative of the players of the PG turnover has been quite successful. Aim of this thesis is to assess the suitability of MEPs as targets for the development of antimicrobial adjuvants.

As demonstrated by the TraDis screening of Sonnabend et al., MEPs seem to influence resistance against β-lactam antibiotics in *Pa* ID40. For MepM1, they validated the data of the screening by generation of a knockout mutant. ID40 Δ*mepM1* showed higher susceptibility to β-lactam antibiotics due to higher *ampC* expression and activity.

For the development of an adjuvant to re-sensitize strains resistant against treatment with β-lactam antibiotics, the following considerations have been taken into account: the effect of the MepM1-knockout alone did not seem to be strong enough to become a candidate for a potential inhibitor target. Hence, a new idea

was the usage of an inhibitor that blocks not only one but several MEPs. Therefore, the following approach was elaborated: a structure-analysis of MepM2 and MepM1 run by Thales Kronenberger, (Universitätsklinikum Tübingen, Internal Medicine VIII, Medical Oncology and Pneumology) revealed similarities regarding the active sites of the proteins (see Figure 4). The idea is that an agent could possibly bind to both active sides, inhibiting the two enzymes simultaneously.

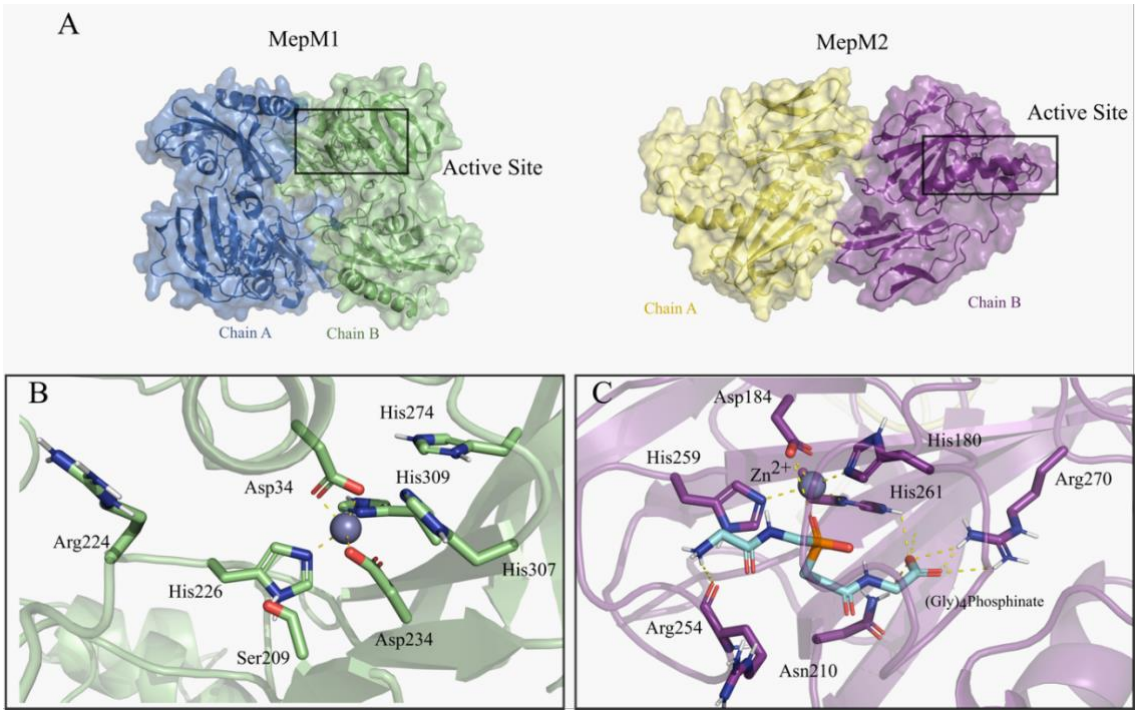

Figure 4: ***Quaternary structures of MepM1 and MepM2 of Pa***

(A) *shows the quaternary structure of MepM1, result from a homology model, and MepM2 (PDB ID: 2HSI), both structures are proposed to work as dimers with MepM1 relying on the flexible loop to integrate the dimerization interface and MepM2 showing a rather smaller interface. Despite the overall dissimilar structure, both active sites are highly conserved among them, with a catalytic Zinc ion coordinated by histidine and aspartate amino acids. Structural water molecules are omitted. Snapshots from the molecular dynamics simulation show stable pockets for both MepM1* ***(B)*** *and for the MepM2 complexed with the potential inhibitor* $(Gly)_4$*Phosphinate* ***(C)****. Figure kindly provided by Thales Kronenberger (Universitätsklinikum Tübingen)*

With this work, we aimed to validate the TraDis results by Sonnabend et al. referring to the other MEPs. Therefore, it was planned to accomplish further deletions of MEPs in ID40 and to perform tests on susceptibility of the different mutants. To find out if the knockouts of several MEPs have a redundant or synergistic effect on susceptibility, double and triple deletions should be

generated. On the basis of the achieved results, we intend to provide a better assessment concerning the adequacy of MEPs as targets of a potential adjuvant.

2 Materials and Methods

2.1 Materials

2.1.1 Instruments

Table 2: Instruments

Instrument	**manufacturer**
Bench Thermo HeraSafe HS18	Heraeus INSTRUMENTS, Hanau
Branson sonifier 250	Branson Ultrasonics, Danbury (USA)
Centrifuge 5415 R and 5417 R	Eppendorf, Hamburg
Centrifuge mini Spin plus	Eppendorf, Hamburg
DensiChek plus	BioMérieux, Nürtingen
Dymo Label Manager 210D	Dymo Corporation, USA
Function Line B20 incubator	Heraeus INSTRUMENTS, Hanau
Gel documentation system FAS-V	NIPPON Genetics, Düren
HAT incubator shaker	Infors HT, Bottmingen (CH)
HFC 586 Basic freezer	Heraeus INSTRUMENTS, Hanau
Light Cycler 480 II	Roche, Basel (CH)
Mini-PROTEAN® Tetra System	Bio-Rad, München
Mini-Sub-Cell GT and Sub-Cell GT chambers for gel electrophoresis	Bio-Rad, München
Multichannel pipette (5-50 µl, 50-300 µl)	Thermo Fisher Scientific, Schwerte
Multifuge 3 S-R	Heraeus INSTRUMENTS, Hanau
Nanodrop One spectrometer	Thermo Fisher Scientific, Schwerte
Photometer, BioPhotometer	Eppendorf, Hamburg
Pipettes (10 µl, 20 µl, 100 µl, 200 µl, 1000 µl)	Eppendorf, Hamburg
Power supply PowerPac 300	Bio-Rad, München
Premium NoFrost freezer	Liebherr, Biberach a. d. Riß
Sartorius CPA225D semimicro balance	Sartorius, Göttingen

Scout Pro scale	OHAUS, Parsippany (USA)
Severin MW 7825 microwave	Severin, Sundern
Sonorex Super RK 510 sonificator	Bandelin, Berlin
Tecan reader infinite 200® PRO	Tecan, Männedorf (CH)
Thermo-Cycler C1000 Touch	Bio-Rad, München
Thermomixer comfort	Eppendorf, Hamburg
Vortex Genie 2	Scientific Industries, Bohemia (USA)

2.1.2 Software

Table 3: Software

Name	**Manufacturer**
Adobe Photoshop CS6	Adobe Systems, Mountain View (USA)
EndNote	Thomson Reuters, New York City (USA)
GraphPad Prism 8.1.0	Graph Pad Software, San Diego (USA)
i-control 1.11 (for Tecan infinite reader)	Tecan, Crailsheim
ImageJ	Java, National Institutes of Health (USA), (Rueden et al., 2017)
LightCycler® 480 Software 1.5	Roche, Basel (CH)
Microsoft Office 2010 + 2016	Microsoft, Redmond (USA)
Snap Gene	GSL Biotech LLC, Chicago (USA)

2.1.3 Consumables

Table 4: Consumables

Product	**manufacturer**
24-well-plate	Greiner Bio-One, Frickenhausen
96-well-plate	Greiner Bio-One, Frickenhausen
Black 96-well-plate	Greiner Bio-One, Frickenhausen
Cellulose membrane, ZelluTrans (3.5 kDa)	Carl Roth, Karlsruhe
Cuvettes (plastic), 1.5 ml	SARSTEDT, Nümbrecht
DNA LoBind tubes, 1.5 ml	Eppendorf, Hamburg
Falcon tubes (15 ml)	Greiner Bio-One, Frickenhausen
Falcon tubes (50 ml)	Corning Life Sciences, Corning (USA)
Inoculation loops	Greiner Bio-One, Frickenhausen
Kryo-tubes, 1.5 ml	Thermo Fisher Scientific, Schwerte
Low Residual Volume Reagent Reservoir	Integra LifeSciences, Plainsboro Township (USA)
Micronaut-S Pseudomonas MIC plates	Merlin, Bruker Company, Billerica (USA)
PCR 96-well TW-MT-plate, white	Biozym Scientific, Hessisch Oldendorf
PCR reaction tubes single cap 8er soft stripes 0,2 ml	Biozym Scientific, Hessisch Oldendorf
Petri dishes	Greiner Bio-One, Frickenhausen
Pipette filter-tips (10 µl, 100 µl, 200 µl, 1000 µl)	Nerbe plus, Winsen
Pipette tips 10 µl	Brand, Wertheim
Pipette tips 1000 µl	Ratiolab, Dreieich
Pipette tips 200 µl	SARSTEDT, Nümbrecht
Pipettes (5 ml, 10 ml, 25 ml, 50 ml)	Corning Life Sciences, Corning (USA)
Polystyrene round-bottom tubes (14 ml)	Corning Life Sciences, Corning (USA)
Reaction tubes, 1.5 and 2 ml	SARSTEDT, Nümbrecht

SC Micro Tubes, 2.0 ml	SARSTEDT, Nümbrecht
SDS gel, Mini-protean TGX™ Precast Gels (4-20%)	Bio-Rad, München
Sensititre™ EUX2NF MIC plates	Thermo Fisher Scientific, Schwerte
Sensititre™ GN2F MIC plates	Thermo Fisher Scientific, Schwerte

2.1.4 Chemicals

Table 5: Chemicals and Reagents

Name	**manufacturer**
4 x Laemmli sample buffer	Bio-Rad, Hercules (USA)
Acidic acid	Carl Roth, Karlsruhe
Acidic hydrolysate of casein	BD Biosciences, Freiburg
Agar agar	Carl Roth, Karlsruhe
Aqua ad injectabilia	B. Braun, Melsungen
Beef extract	BD Biosciences, Freiburg
Boric acid	Sigma-Aldrich, Taufkirchen
Chloroform	Applichem, Darmstadt
Clarity™ Western ECL Substrate	Bio-Rad, Hercules (USA)
Dulbecco's Phosphate Buffered Saline (Dulbecco's PBS), 1x	Gibco Life Technologies, Carlsbad (USA)
Ethanol	VWR, Darmstadt
Ethanol	Applichem, Darmstadt
Gene ruler 1 kb Plus DNA Ladder	Thermo Fisher Scientific, Schwerte
Glycerine	Merck, Darmstadt
Hoechst 33342	Thermo Fisher Scientific, Schwerte
Isopropanol	VWR, Darmstadt
L-rhamnose	Sigma-Aldrich, Taufkirchen
Methanol dried p.A.	AppliChem, Darmstadt
Nuclease-free water	Thermo Fisher Scientific, Schwerte
Orange G	Sigma-Aldrich, Taufkirchen

PageRuler™ Prestained Protein Ladder	Thermo Fisher Scientific, Schwerte
SeaKem® LE Agarose	Lonza, Basel (CH)
Skimmed Milk Powder	TSI Consumer Goods GmbH, Zeven
Sodium chloride (NaCl)	VWR, Darmstadt
Starch (soluble)	BD Biosciences, Freiburg
Sucrose BioXtra	Sigma-Aldrich, Taufkirchen
SYBR safe DNA gel stain (0.01 %)	Thermo Fisher Scientific, Schwerte
The RNA Storage Solution	Invitrogen by Thermo Fisher Scientific, Carlsbad (USA)
Tris(hydroxymethyl)aminomethan (TRIS)	Applichem, Darmstadt
TRIzol	Thermo Fisher Scientific, Schwerte
Trypton	Applichem, Darmstadt
Tween-20	Bio-Rad, Hercules (USA)
Yeast extract	Carl Roth, Karlsruhe
Zirkonia/Silica Beads 0,1 mm (Nr. 11079101z)	Biospec products, Bartlesville (USA)
β-Mercaptoethanol	AppliChem, Darmstadt

2.1.5 Antibiotics

Table 6: Antibiotics

Name	**Manufacturer**
Gentamicinsulfate	Appli Chem, Darmstadt
Irgasan	Sigma-Aldrich, Taufkirchen

2.1.6 Buffers

Table 7: Buffers

Name	**Manufacturer/components**
1 x transfer buffer	100 ml 10x Transfer buffer 200 ml Methanol (20%)

	H_2O ad 1 L
10 x TBS buffer	60.6g TRIS-base 87.6 g NaCl H_2O ad 1 L pH was adjusted to 7,6
10 x Transfer buffer	30 g TRIS-base 144.4 g glycine H_2O ad 1 L
4x Laemmli loading dye	900 µl 4x Laemmli sample buffer 100 µl β-Mercaptoethanol
5 x SDS running buffer	60.55 g TRIS-base 288.15 g glycerine 10 g sodium dodecyl sulfate (SDS) H_2O ad 2 L
5x TRIS-Borat-EDTA buffer (TBE-buffer)	54 g TRIS 27.5 g boric acid 20 ml 0.5M EDTA pH 8.3 was adjusted using acetic acid H_2O ad 1L
TBS-T buffer (1 x TBS + 0.1% Tween-20)	100 ml 10x TBS buffer 1 ml Tween-20 H_2O ad 1 L

2.1.7 Culture media

Table 8: Culture media

Name	**Components/supplier**
Lysogeny Broth (LB) agar	15 g bactoagar LB-medium ad 1L
LB-medium pH 7,5	10 g Trypton 5 g yeast extract 10 g NaCl

	pH 7,5 was adjusted using NaOH purified water ad 1L
Mueller Hinton II Broth Micronaut	BioTrading Benelux B.V.
Super optimal broth with catabolite repression (SOC)	20 g Trypton 5 g yeast extract 10 ml 1M MgSO4 10 ml 1M MgCl2 10 ml 1M KCl 2 ml 5M NaCl 20 ml 1M Glucose Purified water ad 1000 ml

2.1.8 Enzymes

Table 9: Enzymes and enzyme mixes

Name	**manufacturer**
Desoxyribonucleosidetriphosphate (dNTPs) (10mM)	Roche Diagnostics, Rotkreuz (CH)
DpnI restriction enzyme	Thermo Fisher Scientific, Schwerte
Gibson Mix	Kindly provided by Andrea Eipper (Tübingen); contains • T5 Exonuclease (10 U/µl); Epicentre, Madison (USA) • Phusion DNA Polymerase; New England Biolabs, Ipswich (UK) • Taq DNA Ligase (40 U/µl); New England Biolabs, Ipswich (UK) • 5X isothermal (ISO) reaction buffer (25% PEG-8000, 500 mM Tris-HCl pH 7.5, 50 mM

	MgCl2, 50 mM DTT, 1 mM each of the 4 dNTPs, and 5 mM NAD)
MangoMix PCR reaction mix	Bioline, London (UK)

2.1.9 Commercial Kits

Table 10: Kits of commercial manufacturers

Name	**Manufacturer**
Beta-Lactamase Activity Kit	BioVision, Milpitas (USA)
DNAse I recombinant, RNAse free Kit	Sigma Aldrich, St. Louis (USA)
DNeasy® UltraClean® Microbial Kit	Qiagen, Hilden
KAPA HiFi PCR Kit	Roche, Basel (CH)
Monarch® Plasmid Miniprep Kit	New England BioLabs, Ipswich (USA)
QuantiFast® SYBR® Green RT-PCR Kit	Qiagen, Hilden
Turbo DNA-free Kit	Invitrogen by Thermo Fisher Scientific, Carlsbad (USA)
Wizard® SV Gel and PCR Clean-Up System	PROMEGA, Madison (USA)

2.1.10 Antibodies

Table 11: Antibodies

Name	**origin**
rabbit anti-OprD (1:2000)	Kindly provided by Thilo Köhler, University of Geneva
rabbit anti-RpoB (1:2000, *Ec)*	Abcam #mAb EPR18704
horseradish-peroxidase-conjugated goat anti-rabbit antibody (1:5000)	Thermo Fisher Scientific, Schwerte; #31460

2.1.11 Bacterial strains

2.1.11.1 Provided bacterial strains used in this work

Table 12: Provided bacterial strains used in this work

bacterial strain	**Characteristics**	**origin**
Pa ID40	Multi-drug resistant clinical isolate from bloodstream infection	Willmann et al. 2019
Pa PA14	Laboratory *Pseudomonas aeruginosa* strain	DSMZ (Nr. 19882)
Pa ID40 ΔmepM1	In-frame deletion mutant of *Pa* ID40	Sonnabend et al. (2020)
Ec Top 10	Chemically competent *Ec*	Thermo Fisher Scientific, Schwerte
Ec SM10λpir	Chemically competent *Ec*	Hmelo et al. (2005)

2.1.11.2 In-frame deletion mutants of *Pa* ID40 generated in this work

Table 13: In-frame deletion mutants of Pa ID40 generated in this work

Deletion mutant	**Deleted gene(s)**
Pa ID40 Δ*mepM2*	*mepM2*
Pa ID40 ΔmepM3	*mepM3*
Pa ID40 Δ*mepH1/2*	*mepH1, mepH2*
Pa ID40 Δ*mepM1* Δ*mepM2*	*mepM1, mepM2*
Pa ID40 Δ*mepM1* Δ*mepM3*	*mepM1, mepM3*
Pa ID40 Δ*mepM1* Δ*mepM2* Δ*mepM3*	*mepM1, mepM2, mepM3*

2.1.12 Plasmids

Table 14: Plasmids

Name	Characteristics	Origin
pEXG2	Cloning-vector with selective *sacB*-gene, pBR origin and gentamicin resistance cassette	Hmelo et al. (2015)
pEXG2 Δ*mepM2*	pEXG2 derivative for in-frame deletion of the *mepM2* gene	This work
pEXG2 Δ*mepM3*	pEXG2 derivative for in-frame deletion of the *mepM3* gene	This work
pEXG2 Δ*mepH1/2*	pEXG2 derivative for in-frame deletion of the genes *mepH1* and *mepH2*	This work

2.1.13 Oligonucleotides

2.1.13.1 Primer for Gibson cloning

Table 15: Primer for Gibson cloning

Name	Sequence 5'-3'
pEXG2_mepM2_up_f	AGCTAATTCCACACATTATACGAGCCGGAAGTGGTTCTGCACCACGAAGTAG
pEXG2_mepM2_up_r	CGCGTTGCTCACTTCTCAGGGCTGGAAGGCTAGGGTGCGGGGCATCGG
pEXG2_mepM2_dn_f	CGAGTCGAGAAGCCGATGCCCCGCACCCTAGCCTTCCAGCCCTGAGAAGTG
pEXG2_mepM2_dn_r	CGAGTCGAGAAGCCGATGCCCCGCACCCTAGCCTTCCAGCCCTGAGAAGTG
pEXG2_mepM3_up_f	AGCTAATTCCACACATTATACGAGCCGGAACCTCGTCGATGAGGATCGAG
pEXG2_mepM3_up_r	ATGCACATCATTTTTCTGAGCCGGCACCATTTCATCGCACGCGCGTC
pEXG2_mepM3_dn_f	TCACTCGGAAACAGACGCGCGTGCGATGAAATGGTGCCGGCTCAGAAAAATG

pEXG2_mepM3_dn_r	TCGAGCCCGGGGATCCTCTAGAGTCGACCTATCCTGGATGCCATCGG
pEXG2_MepH1/2_up_f	AGCTAATTCCACACATTATACGAGCCGGAAGACCTGATCTACGCCATGTATTCGCG
pEXG2_MepH1/2_up_r	CCCATGCTTAAACGCTTAGCACCCCTCGTGTTGGCGCGGGTGCCCTGA
pEXG2_MepH1/2_dn_f	GACCTCCCCGCCTCAGGGCACCCGCGCCAACACGAGGGGTGCTAAGCG
pEXG2_MepH2_dn_r	TCGAGCCCGGGGATCCTCTAGAGTCGACCTGAACGCATCCTGGTCATCACC

2.1.13.2 Deletion-flanking primers to verify deletions

Table 16: Deletion-flanking primers to verify deletions

Name	**Sequence 5'-3'**
pEXG2_seq_f	TACTGTGTTAGCGGTCTG
pEXG2_seq_r	GATCCGGAACATAATGGTG
MepM1_seq_f	TGGGTAGGTAATGGGAAGCG
MepM1_seq_r	GAAGATCACCTGATGCCCCA
MepM1_inside_r	ACGAGTTCCAGATCAATGG
MepM2_seq_f	TCGGGAAGATCGATGTCCTTG
MepM2_seq_r	AGCCAGAGGAAGGTGGTTAG
MepM2_inside_r	CTCGCACTTCCAGCTTCTG
MepM3_seq_f	CATTTCGGCGATCTTGCC
MepM3_seq_r	CAACTGGGTCGATGCCTG
MepM3_inside_r	GGATGGCCGGGTAATGAATC
MepH1/2_seq_f	CTGTAGCCGGTGAAGGTG
MepH1/2_seq_r	AATGACAGGACGAGCCTTAG
MepH1/2_inside_r	AACAGCTACTGGCAACGC

2.1.13.3 Primers for real-time semi-quantitative PCR (qRT-PCR)

Table 17: Primers for qRT-PCR

Name	**Sequence 5'-3'**
PA14_gyrB_f	CGTAACCTGAACAACTACATCGAG
PA14_gyrB_r	AAGTACTTGCCCATCTCCTGTTC
ID40_ampC neu_f	TGCTGCTCCATGAGTCGTTC
ID40_ampC neu_r	CGCCTCTATTCCAACCCGAG
ID40_OXA_f	TTCGCCCTGAACATCGACAT
ID40_OXA_r	GCAGTATCCCGAGAGCCTTG

2.2 Microbiological Methods

2.2.1 Cultivation of bacteria

The cultivation of the *Ec* and *Pa* strains (see Table 12 + 13) was performed in a standardized way. 5 ml LB medium were inoculated with bacteria of a frozen cryo-culture and incubated overnight at 37 °C with shaking at 200 revolutions per minute (rpm). *Ec* and *Pa* strains carrying pEXG2 plasmids encoding for resistance against gentamicin were grown in the presence of 15 µg/ml or 75 µg/ml gentamicin respectively.

To generate subcultures, overnight cultures were diluted in a 1:20 ratio with fresh LB medium. The cells were cultured for 3h at 37 °C and 200 rpm.

To cultivate bacteria on LB-agar-plates, material of a cryo-culture was spread on the plate with an inoculation loop. The plates were incubated overnight at 37 °C.

2.2.2 Production of Glycerol-cultures for the collection of bacterial strains

For conservation, the bacterial strains were stored at -80 °C in LB medium containing 20 % glycerol. The glycerol prevents formation of crystals in the cytoplasm of the cells and is therefore essential for their survival at -80 °C.

5 ml overnight cultures were centrifuged at 4495*g for 5 minutes, the supernatant was decanted, and the pellet was resuspended in 4 ml LB medium + 20% glycerol. 1 ml of the suspension was transferred to a cryo-tube (1.5 ml), which was stored in the freezer at -80 °C.

2.2.3 Photometric measurement of bacterial count

To generate cultures with a standardized number of bacteria (e.g. for growth curves), the optical densities (OD) of the cultures were determined. For this purpose, the cultures were diluted in LB medium or PBS in a plastic cuvette and the OD was measured with a photometer at a wavelength of 600 nm. To adjust the cultures to a certain OD, the following formula was used:

$$V_1 \times c_1 = V_2 \times c_2 \rightarrow V_1 = V_2 \times \frac{c_2}{c_1}$$

V_1= volume of the culture
c_1 = measured OD_{600nm}
V_2 = final desired volume
c_2 = desired OD_{600nm}

For *Pa*, an OD_{600nm} of 1 corresponds to 10^9 bacteria.

2.2.4 Growth curves

To observe the growth of the different bacterial strains, growth curves were performed.

The OD_{600nm} of overnight cultures was adjusted to 0.01 by dilution with LB medium (see 2.2.3). 1 ml of this dilution was pipetted into a 24-well plate (2 technical replicates per mutant). LB medium was used as a blank. Then, the OD_{600} of each well was measured 50 times in a time range of 15 hours using the Tecan Infinite® 200 Pro.

2.2.5 Microbroth dilution assay

One hypothesis of this work is that the deletion mutants are more susceptible to β-lactam antibiotics than the ID40 WT. To verify this, a microbroth dilution assay was performed applying the mutant strains on 3 different microtiter plates (Micronaut-S Pseudomonas MIC plates (Merlin), Sensititre™ EUX2NF MIC plates (Thermo Fisher Scientific) and Sensititre™ GN2F MIC plates (Thermo Fisher Scientific)). In this assay, the bacteria are exposed to varying concentrations of different antibiotics to finally detect the MIC. The MIC is defined as the lowest concentration of an antibiotic, which inhibits the growth of a bacterial strain.

First, bacteria were cultivated on LB-agar plates overnight (see 2.2.1). To get a comparable number of bacteria into each well, the grown material was resuspended in isotonic sodium chloride solution until no visible clumps could be seen. The suspension was diluted with sodium chloride solution until a McFarland Standard of 0.5 was measured with the DensiChek plus (BioMérieux). Then, 62.5

µl of the dilution were added to 15 ml of Mueller Hinton II Broth Micronaut (BioTrading). Following the instructions of the manufacturer, 50-100 µl of the suspension were applied into each well of one of the microbroth dilution microtiter plates with a 12-channel pipette. Sensititre™ EUX2NF MIC plates and Sensititre™ GN2F MIC plates were carefully sealed with a foil. The plates were stored in the incubator at 37 °C for 18 hours, after which the OD_{600} was measured using the Tecan Infinite® 200 Pro. Plates filled with just Mueller Hinton II Broth Micronaut were used as blanks.

2.2.6 Efflux Assay

A common resistance mechanism of MDR bacteria is the (over)expression of efflux-pumps, which remove antimicrobial substances from the cells before they can take effect (Puzari and Chetia, 2017).

The aim of this assay was to find out, if the reduced resistance of the *mepM* deficient mutants is caused by a lower activity of efflux pumps in *Pa* ID40. For this purpose, a dye (Hoechst 33342) was used that can pass through the bacterial cell envelope, bind to double-stranded DNA and by this emit blue fluorescence, that can be detected (Coldham et al., 2010). Further, Hoechst 33342 is a substrate for a wide range of multidrug resistance transporters such as MexAB-OprM and can therefore be used to evaluate their transport activity (van den Berg van Saparoea et al., 2005, Coldham et al., 2010, Siriyong et al., 2017).

Subcultures were inoculated and grown as described in 2.2.1. Afterwards, the subcultures were centrifuged at 4495*g for 5 minutes and the supernatant was discarded. The pellets were resuspended in 5 ml Dulbecco's PBS and the OD_{600nm} was measured as described in 2.2.3 and adjusted to 0.3 using Dulbecco's PBS. 180 µl of the diluted cultures were pipetted into the wells of a black 96-well plate with a flat bottom, always applying duplicates of each strain. A duplicate of Dulbecco's PBS was used as a blank. 20 µl of Hoechst 33342 (100 µM) were added to each well. The plate was immediately placed into the Tecan Infinite® PRO reader (Tecan), which measured the fluorescence. The following settings were chosen:

Table 18: ***Settings of the Tecan Infinite® PRO reader for the Efflux Assay***

excitation	355 nm
emission	460 nm
flashes per well	5
measurements per well	3*3
interval of measurement	60 s
number of cycles	60

2.2.7 β-Lactamase Activity Assay (Nitrocefin Assay)

β-lactamases as e.g. AmpC have the ability to hydrolyse β-lactam antibiotics such as penicillins or cephalosporins, which are thereby deactivated. As a consequence, expression of β-lactamases promotes resistance against β-lactam antibiotics.

This assay was performed to detect the difference in β-lactamase activity of the different deletion mutants in comparison to *Pa* ID40 WT. The method is based on the chromogenic cephalosporin Nitrocefin. When Nitrocefin is hydrolysed, a red-coloured product (OD 490 nm) is generated directly proportional to the amount of enzymatic activity of β-lactamases (BioVision).

For the quantification of β-lactamase activity, the β-Lactamase Activity Colorimetric Assay Kit (BioVision) was applied, following the instructions of the manufacturer. As samples subcultures of the different strains were used and prepared as described in 2.2.1. The weights of the pellets were determined by Sartorius CPA225D semimicro balance (Sartorius) and the pellets were resuspended in 10-30 µl β-lactamase assay buffer per mg pellet. To lysate the bacteria, three different approaches were performed: the bacteria were treated with ultrasound in an ultrasonic bath (Sonorex Super RK 510 sonificator (Bandelin)) for 5 min or they were sonicated for either 3 or 5 min using the Branson sonifier 250 (Branson Ultrasonics). After centrifugation, the supernatant of the sonified bacteria was diluted 1:50 in β-lactamase assay buffer and 50 µl reaction mix containing 2 µl nitrocefin were added (2 µl nitrocefin/100 µl in each well). The absorbance (OD 490 nm) was measured every minute for 1 hour using

the Tecan Infinite® 200 PRO Reader. Moreover, the results were calculated as described in the manufacturer's protocol.

2.3 Molecular biological Methods

2.3.1 Polymerase chain reaction

The polymerase chain reaction (PCR) is used to amplify DNA fragments, which are defined by an upstream and a downstream primer. In this work, it was used to screen bacterial strains for deletions after mutagenesis, to generate and amplify DNA fragments for Gibson cloning and to measure the length of a defined DNA fragment.

2.3.1.1 PCR using KAPA HiFi PCR Kit

The PCR using KAPA HiFi PCR Kit was applied to generate DNA-fragments, which were afterwards cloned into the pEXG2 plasmid by Gibson cloning.

Table 19: ***Components and quantities of the KAPA HiFi PCR***

Component	**Quantity**
Kapa HiFi GC buffer	5 µl
10 mM dNTP Mix	0.75 µl
Kapa Polymerase	0.5 µl
Primers • forward [10 pmol] • reverse [10 pmol]	 0.75 µl 0.75 µl
Template	20 ng genomic DNA of *Pa* ID40
H_2O	X µl (adjust to 25 µl)
All	25 µl

The PCR tubes were placed into the thermo cycler Thermo-Cycler C1000 Touch (Bio-Rad) employing the following temperatures:

Table 20: ***PCR programme of the KAPA HiFi PCR***

Reaction	**Temperature**	**Duration**
Initial Denaturation	95 °C	5 min
Denaturation	95 °C	0:30 min
Annealing	52 °C	0:30 min
Extension	72 °C	0:30 min per kb
Final Extension	72 °C	5 min
Pause	4 °C	∞

30 cycles

2.3.1.2 PCR using MangoMix

This type of PCR was used to screen bacterial strains for a certain mutation or to measure the length of DNA fragments. As templates isolated genomic DNA or the supernatant of lysed colony material (see Colony-PCR in 2.3.6) were applied. The employed MangoMix is an industrially produced mix containing MangoTaq™ DNA Polymerase, $MgCl_2$ and ultra-pure dNTPs.

Table 21: ***Components and quantities of the PCR using MangoMix***

Component	**Quantity**
MangoMix	7.5 µl
Template • Isolated genomic DNA or • Supernatant of lysed colony material	 20-40 ng 3 µl
Primers • Forward-Primer • Reverse-Primer	 0.5 µl 0.5 µl
H_2O	X (adjust to 15 µl)
All	15 µl

The PCR tubes were placed into the thermo cycler Thermo-Cycler C1000 Touch (Bio-Rad) employing the following temperatures:

Table 22: ***PCR programme of the PCR using MangoMix***

Reaction	Temperature	Duration
Initial Denaturation	95 °C	5 min
Denaturation	95 °C	0:30 min
Annealing	52-63 °C	0:30 min
Extension	72 °C	0:30 min per kb
Final Extension	72 °C	5 min
Pause	4 °C	∞

30 cycles

2.3.2 Agarose gel electrophoresis

Agarose gel electrophoresis is a method that uses electric current to separate DNA fragments based on their different sizes. DNA is negatively charged and therefore moves to the cathode within electric fields. Shorter DNA fragments move faster than long fragments in the agarose gel, so that a distinction between different sized fragments is possible. In this work, agarose gel electrophoresis was used to visualize the sizes of the DNA fragments that were amplified by PCR. To produce an 1 %-agarose gel, 1 g agarose was mixed with 100 ml of 0.5x TBE-buffer and boiled in a microwave until the agarose had dissolved completely. Before filling the gel chambers, SYBR safe DNA gel stain was added in ratio of 1:10000. The hot gel was poured into the gel chambers and an appropriate comb was positioned. The gel cooled down for at least 30 minutes. Then, the pockets were loaded with 6 µl of the PCR products (PCR using MangoMix (see 2.3.1.2)) or 5 µl of the PCR sample plus 3 µl Orange G dye (PCR using Kapa polymerase (see 2.3.1.1)). As marker 4 µl of Gene Ruler 1 kb Plus DNA ladder (750–20.000 bp) were applied. The gel electrophoresis was run at 100 V for 45 minutes. Finally, pictures of the gels were taken and documented with FAS-V documentation system.

2.3.3 Purification of PCR products

The DNA-fragments, which were generated via PCR as described in 2.3.1.1, were purified using the Wizard® SV Gel and PCR Clean-Up System. The kit was applied following the instructions of the manufacturer's protocol. Finally, the purified DNA was eluted with 50 µl H_2O and stored at -20 °C.

2.3.4 Gibson cloning for the generation of mutator plasmids

As described by Gibson et al. (2009), Gibson cloning is a method, which is used to ligate and amplify multiple DNA molecules. In this work, it is employed to assemble the linearized vector pEXG2 with two fragments, that are flanking a target gene and that were produced by PCR as described in 2.3.1.1. The reaction occurs as displayed in Figure 5:

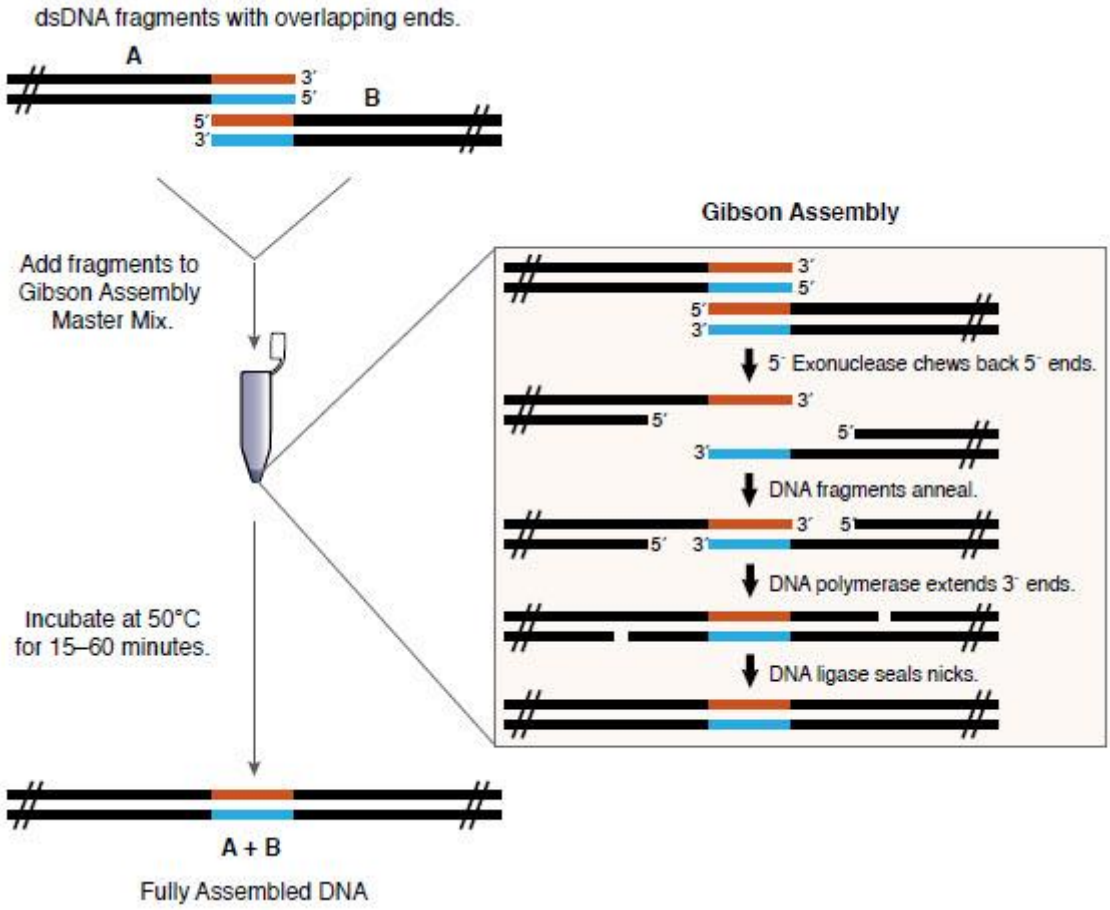

Figure 5: ***Overview of the Gibson Assembly (Gibson et al., 2009)***

Double-stranded DNA (dsDNA) fragments with up to several hundred kilobases can be assembled with this method. The reaction occurs at a stable temperature of 50 °C as follows: the 5'-ends are removed by a 5'-exonuclease, so that the overlapping 3'-regions are left in a single-stranded state. Now, the overlapping ends can anneal to each other. A DNA polymerase elongates the 3'-ends and a DNA ligase seals the nicks. Figure kindly provided by: New England Biolabs Gibson Assembly Master Mix Instruction Manual (product E2611)

In a first step, a 5'-exonuclease chews back the 5'-ends of the DNA single strands leaving behind overlapping "sticky ends" at the 3'-end. The overlaps anneal to complementary bases of the fragment they are supposed to connect to. Then, a

5'-3'-DNA-polymerase elongates the 3'-ends and a DNA ligase connects the molecules. All needed enzymes were components of the employed Gibson Mix.

After purification of the synthetized DNA fragments as described in 2.3.3, the concentration of DNA was determined by a Nanodrop One spectrometer (Thermo Fisher Scientific). 50-100 ng of each DNA fragment and 50-100 ng of the linearized plasmid pEXG2 were added to an Eppendorf cup containing 10 µl Gibson Mix and incubated at 50 °C for 30 minutes. The Gibson Mix was kindly produced by Andrea Eipper (Universitätsklinikum, Tübingen). The next step was to digest remaining template DNA, adding 1 µl of DpnI restriction enzyme to the reaction mix. The tubes were incubated for 1 hour at 37 °C.

2.3.5 Transformation into chemical competent Ec

Transformation means a process of horizontal gene transfer, in which bacteria take up foreign DNA, mostly using a plasmid as a vector. The plasmids used in this work were generated by Gibson cloning as described in 2.3.4. For the transformation, a tube with 100 µl chemical competent *Ec* Top10 or *Ec* SM10λpir was thawed on ice and 40-100 ng of plasmid DNA were added. The cells were incubated on ice for 20 minutes and then placed into a water bath with a temperature of 42 °C for 30 seconds. After incubating the cells for another 2 minutes on ice, the cup was filled with 1 ml SOC medium and incubated at 37 °C with shaking at 200 rpm for 1 hour. Afterwards, the tube was centrifuged at 10000*g for 1 minute and the supernatant was decanted. The pellet was resuspended and the suspension (10 µl and 100 µl respectively) was plated on two LB-agar plates containing gentamicin (15 µg/ml). Technically, the gentamicin plates are selective for those bacteria, which have taken up the plasmid containing the gentamicin resistance cassette. The plates were placed into an incubator at 37 °C overnight.

2.3.6 Colony-PCR

Colony-PCR was used to screen different individual clones for a deletion, or a plasmid insert. First, a single colony was picked with a pipette tip from a LB-agar plate. The material was resuspended in 50 µl of sterile Braun water in an Eppendorf cup and boiled at 95 °C for 5 minutes to lysate the bacteria. Afterwards

the cups were centrifuged at 3000 rpm for 5 minutes. Avoiding the pellet, 3 µl of the supernatant were used as template for a PCR using MangoMix (see 2.3.1.2).

2.3.7 Isolation of plasmid DNA

Ec Top10 containing a pEXG2 plasmid with confirmed insert were grown in 20 ml LB medium with 30 µl gentamicin overnight. On the next day, Monarch® Plasmid Miniprep Kit was performed, following the protocol of the manufacturer. To make sure that the Gibson assembly had been successful the plasmid DNA was sequenced by Eurofins Genomics.

2.3.8 Generation of in-frame deletion mutants by allelic exchange

Aim of allelic exchange in this work was the in-frame deletion of the genes *mepM2*, *mepM3* or the operon encoding both *mepH1* and *mepH2*. The goal is to interchange the functional target gene of the bacteria with a shortened and unfunctional version of the target gene, that was inserted into the pEXG2 plasmid. In Figure 6, the principle of allelic exchange is presented.

The first step of allelic exchange was the conjugation of a *Pa* ID40 WT or deletion mutant with an *Ec* SM10λpir carrying the suicide vector pEXG2 with the corresponding gene insert. Aim of the conjugation was the uptake and integration of the plasmid into the genome of the *Pa* strain by a single crossover. For this purpose, overnight cultures were inoculated as described in 2.2.1 adding 15 µl gentamicin to the *Ec* SM10λpir strain. On the next day, 400 µl of the *Pa* ID40 strain and 200 µl of the *Ec* SM10λpir were mixed, centrifuged at 10000*g for 1 minute and resuspended in 100 µl fresh LB medium. The suspension was pipetted as a droplet on a LB-plate and carefully stored in the incubator at 37 °C overnight.

With an inoculation loop the grown material was completely transferred and resuspended in 2 ml LB. 100 µl of the suspension were plated on a LB-agar plate containing 75 µg/ml gentamicin and 20 µg/ml irgasan. 20 µl of the suspension were plated on a second plate and both plates were incubated at 37 °C overnight. During this step, positive selection of all merodiploid *Pa* was achieved. As opposed to *Pa*, *Ec* bacteria are sensitive to irgasan and did therefore not grow on

plates containing irgasan. Further, only those *Pa* clones survived the presence of gentamicin, which had integrated the plasmid vector implying the gentamicin resistance cassette.

After overnight incubation at 37 °C, 4 clones were picked and streaked on LB-agar plates using an inoculation loop. The plates were incubated at 37 °C until the next day. On the LB-agar plates, the merodiploid strains are grown without any selection pressure. During this time, a second crossover may occur in some of the bacteria. The second crossover may result either in the completed deletion of the target gene or in the return to WT genotype.

To select those bacteria, in which the second crossover has taken place, further steps were carried out: on the following day, some material was picked and used to inoculate 4 tubes with 5 ml LB medium containing 22,5 % sucrose. The culture was incubated overnight at 37 °C and with shaking at 200 rpm.

The grown material was streaked on no-salt-lysogeny-broth (NSLB) plates containing 15 % sucrose. They were also incubated at 37 °C overnight. As mentioned before, the sucrose counterselection aimed to select *Pa*, who have undergone a second crossover. The principle is as follows: the pEXG2-plasmid contains the selective gene *sacB*, which encodes an enzyme called levansucrase. This enzyme catalyses the hydrolysis of sucrose resulting in the synthesis of the toxic metabolite levan. As the production of levan is lethal for *Pa*, sucrose-containing LB-agar plates select those bacteria, which lost the *sacB* gene accordingly during the second crossover.

Next, 8-100 clones were picked with a pipette tip of the plate containing 15 % sucrose. The pipette tip was first streaked onto a plate containing 75 µg/ml gentamicin and secondly on a plain LB-agar plate. The plates were incubated overnight at 37 °C. This step is performed, because sensitivity to gentamicin is another indicator that the clone has lost the plasmid and thus undergone second crossover. On this account, Colony-PCR was realised the next day to see if the gentamicin-sensitive streaks had in fact lost the target gene.

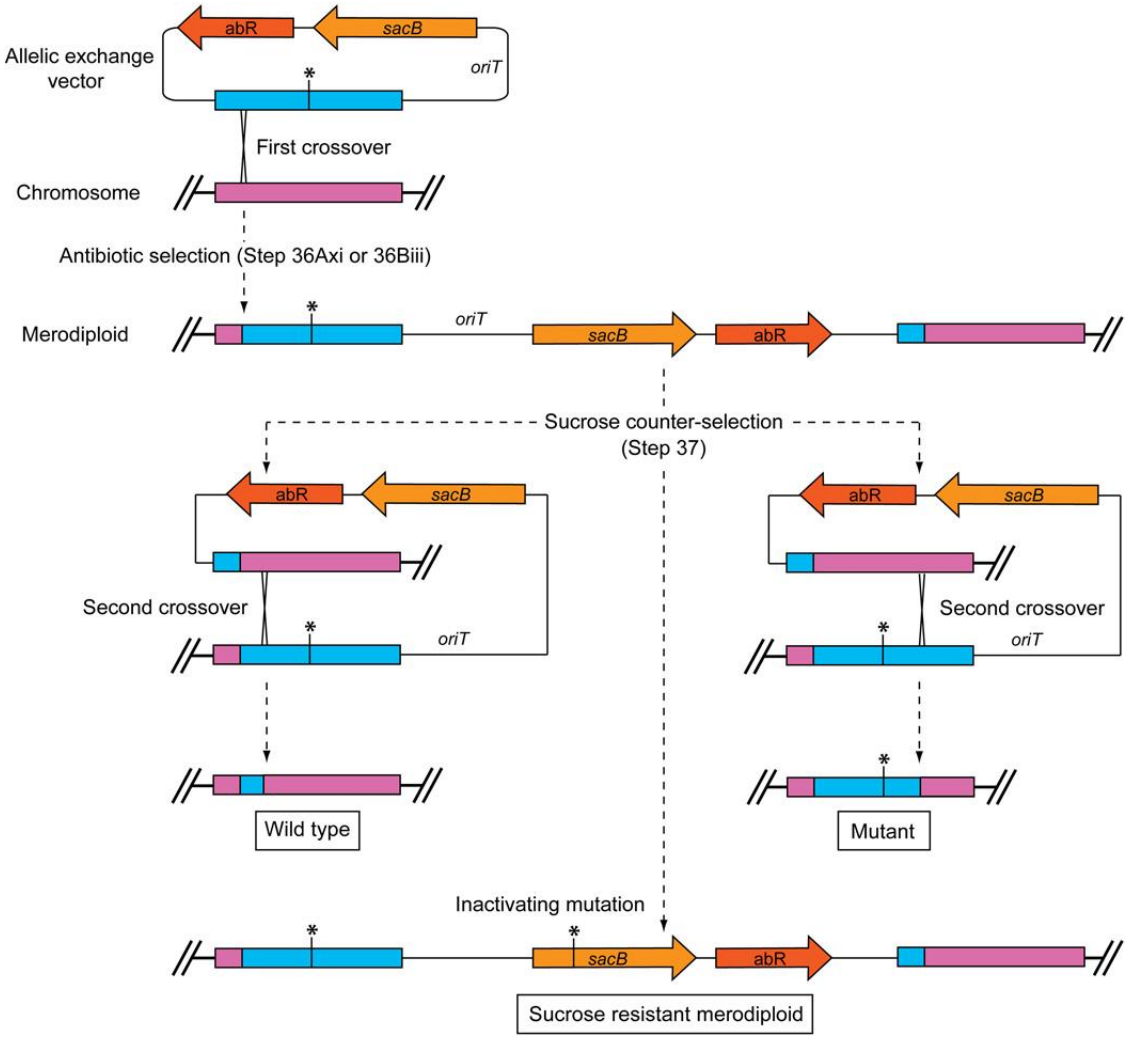

Figure 6: ***Scheme for illustration of allelic exchange***

The allelic exchange vector contains an antibiotic resistance cassette, a sacB gene and sequences flanking the target gene. Via horizontal gene transfer, the suicide vector is transferred into the Pa target strain. The first crossover happens coincidentally at one of the homologues sequences. Thereby, the plasmid is integrated into the bacterial chromosome resulting in merodiploid strains. If a second crossover occurs, there are two possibilities regarding the outcome: either the deletion of the target gene is completed, or the WT genotype is restored. By sucrose counter-selection it can be differentiated, which bacteria have undergone the second crossover. Exceptionally, strains that carry an inactivating mutation in the sacB gene can survive the sucrose treatment. Reprinted by permission from NATURE SPRINGER: Nat Protoc, 10, 1820-41. Precision-engineering the Pseudomonas aeruginosa genome with two-step allelic exchange, HMELO, L. R., BORLEE, B. R., ALMBLAD, H., LOVE, M. E., RANDALL, T. E., TSENG, B. S., LIN, C., IRIE, Y., STOREK, K. M., YANG, J. J., SIEHNEL, R. J., HOWELL, P. L., SINGH, P. K., TOLKER-NIELSEN, T., PARSEK, M. R., SCHWEIZER, H. P. & HARRISON, J. J. COPYRIGHT 2015

2.3.9 Isolation of genomic DNA

For isolation of genomic DNA DNeasy® UltraClean® Microbial Kit (QIAGEN) was applied on 1.8 ml overnight culture. The protocol of the manufacturer was followed in detail. The isolated genomic DNA was eluted in 50 µl elution buffer, the concentration of DNA was determined with Nanodrop One spectrometer and stored at –20 °C in the freezer.

2.3.10 Isolation of RNA

RNA was isolated, so that the expression of different proteins could be determined by qRT-PCR.

First, 10 ml subcultures of each strain were prepared as described in 2.2.1. After 3 hours, the cells were harvested by centrifuging them at 4495*g for 5 minutes. From this step on, RNAse-free pipette tips and tubes were used. On ice, the pellet was resuspended in 1 ml TRIzol and the suspension was transferred into a tube filled with 0.25 ml Zirkonia Silicium Beads. To open the cells mechanically, the tubes were vortexed horizontally at 4 °C for 2 minutes. Afterwards, 200 µl chloroform were added. The tubes were inverted for 60 seconds and incubated for 3 minutes at room temperature. Then, they were centrifuged at 4 °C at 12000*g for 15 minutes. 400 µl of the upper aqueous layer was transferred into a new Eppendorf cup and 500 µl isopropanol were added. The suspension was incubated at room temperature for 10 minutes and centrifuged at 4 °C and 12000*g for 30 minutes. Next, the supernatant was removed and 500 µl ethanol (70 %) was added, after which the tubes were centrifuged again (12000*g, 4 °C) for 5 minutes. After decanting the supernatant, two more centrifugation steps of 12000*g at 4 °C for 3 minutes were implemented, each time removing the supernatant with pipette tips. To completely air dry the RNA pellets, the tubes were left under a laminar air flow bench for at least 60 minutes with open tabs. Hereafter, 50 µl of RNA-Storage solution were added, the pellet was resuspended, and the tubes were incubated for 10 minutes at 55 °C with shaking at 1000 rpm. The tubes were vortexed once after 5 minutes. Finally, the concentration of RNA was measured with Nanodrop One spectrometer and the tubes were stored at -80 °C.

2.3.11 Digestion using Deoxyribonuclease

To further purify the isolated RNA, Deoxyribonuclease (DNase) is used to cut the remaining single or double stranded DNA fragments into oligonucleotides.

For the purification DNAse I recombinant, RNAse free Kit (Sigma Aldrich) was applied. 5 µg RNA were diluted in 50 µl of nuclease-free water. Afterwards, 5µl 10x Incubation Buffer, 2 µl DNase I and 1 µl RNAsin were mixed, vortexed and

then added to the RNA dilution. The samples were incubated at room temperature for 30 minutes. Hereafter, 6 µl of a DNase-inactivation enzyme were pipetted to each tube. The tubes were shaken at 1000 rpm and room temperature on a shaking platform for 3 min. Finally, the samples were centrifuged at 10000 rpm for 1 minute and the supernatant was transferred into a clean low-binding tube and stored at -80 °C.

2.3.12 Real-time semi-quantitative PCR (qRT-PCR)

Compared to a conventional PCR, qRT-PCR not only amplifies nucleic acids, but also quantifies them. For this purpose, a dye that intercalates with nucleic acids is used and its fluorescence is measured after elongation of each cycle. The fluorescence of the dye increases proportionally with the amount of PCR products.

In this work, we wanted to quantify the expression of the genes *ampC* and *poxB*, both encoding β-lactamases. As reference gene, the housekeeping gene *gyrB* was chosen. A housekeeping gene is a gene, which is expressed at a relatively constant rate and mostly encodes for proteins important for preservation of basic cell functions.

SYBR Green RT-PCR Kit (QIAGEN, no. 204154) was employed following the instructions of the manufacturer, using SYBR Green I as dye. The Kit contains a reverse transcriptase (RT-enzyme) that generates complementary DNA (cDNA) from the RNA template. The utilised primers had already been established by Klein et al. (2019): they had generated a standard curve by dilution of one sample and calculated the efficiency of the PCR (Klein et al., 2019). According to their results, the efficiency of *gyrB* was 2.363, of *ampC* it was 2.480 and of *poxB* it was 2.467.

First, the purified RNA was diluted with RNase-free water in a ratio of 1:10. Then, a mastermix was prepared comprising SYBR-Green 2x Mastermix, RNase-free water, primers and the RT-enzyme. The wells of a 96-well TW-MT-plate were each filled with 9 µl of this mastermix (see Table 23) and 1 µl of the diluted RNA. The plate was kept on ice during the whole procedure.

Table 23: ***Components and quantities of the qRT-PCR***

Component	**Quantity**
SYBR-Green 2x Mastermix	5 µl
H_2O (RNase-free)	1,9 µl
Primers • Forward-Primer • Reverse-Primer	 1 µl 1 µl
RT-enzyme	0,1 µl
RNA-template	1 µl
All	10 µl

Subsequently, the 96-well plate was sealed with a foil and centrifuged for 5 seconds at around 400*g. For the measurement, Light Cycler 480 II (Roche) and LightCycler® 480 Software 1.5 (Roche) were used. The settings were chosen as described in the protocol of the manufacturer.

Table 24: ***Programme of the qRT-PCR***

Reaction	**Temperature**	**Duration**
Reverse transcription	50 °C	10 min
PCR initial activation step	95 °C	5 min
Denaturation	95 °C	0:10 min
Combined annealing/extension	60 °C	0:30 min — 40 cycles

For the semi-quantitative analyses of the qRT-PCRs a method published by Pfaffl in 2001 was conducted (Pfaffl, 2001). To apply this mathematical model, crossing points (CP) must be determined for each transcript. The CP is defined as the point at which the fluorescence rises notably above the background fluorescence. It is determined using the LightCycler® 480 Software 1.5. The method by Pfaffl provides relative quantification of a target gene transcript in comparison to a reference gene transcript and uses the following formula:

$$ratio = \frac{(E_{target})^{\Delta CP_{target}(control-sample)}}{(E_{ref})^{\Delta CP_{ref}(control-sample)}}$$

E_{target} = PCR efficiency of a target gene transcript
E_{ref} = PCR efficiency of a reference gene transcript
ΔCP_{target} = CP deviation of control – sample of the target gene transcript
ΔCP_{ref} = CP deviation of control – sample of the reference gene transcript

2.3.13 Sodium dodecyl sulfate polyacrylamide gel electrophoresis (SDS-PAGE)

To separate proteins based on their molecular weights, SDS-PAGE can be performed. After denaturation, sodium dodecyl sulphate forms complexes with the proteins and thereby masks the protein's differing charges. In addition, SDS is negatively charged. When the complexes are applied to a polyacrylamide gel and an electric field, they move through the pores of the gel to the cathode. As the smaller proteins move faster through the gel than the larger complexes, the proteins are hereby separated according to their molecular weight.

To denature the cells and the proteins, 5 x 10^8 bacteria per ml grown in subcultures (see 2.2.1) and 2.5 x Laemmli buffer supplemented with 10% β-Mercaptoethanol were heated up to a temperature of 95 °C for 10 minutes. A 4 - 20 % Mini-PROTEAN® TGX™ Precast Protein gel was used to perform SDS-PAGE. It was run at 110 V for 60 minutes. 5 x 10^6 bacteria and 3.5 µl of protein ladder were applied into the lanes of the gel.

2.3.14 Western Blot analysis

The outer membrane protein OprD regularly mediates the uptake of carbapenems in *Pa*. In this work, western blot analysis was performed to quantify the expression of OprD-channels of the bacterial strains. The Western Blot is a method that provides the specific detection of a certain protein using two antibodies. The first antibody binds specifically to the protein, whereas the secondary antibody binds to the first one. Usually, the secondary antibody is conjugated to an enzyme, which catalyses a reaction that results in the emission of a detectable, chemiluminescent signal.

First, an SDS-PAGE was realized as described in 2.3.13. Subsequently, the proteins were transferred to a nitrocellulose membrane via electroblotting. Therefore, the Western Blot was assembled in an ice tank filled with Transfer Buffer. The blotting was performed at 0.3 Ampère (constant current) at 4 °C for 1 hour. In order to saturate the membrane with protein, it was blocked with 10 ml TBS-T buffer containing 5 % skim milk at 4 °C overnight. Afterwards, the membrane was incubated with the primary antibodies (rabbit anti-OprD (1:2000) and rabbit anti-RpoB (1:2000)) for 1 hour at room temperature in 10 ml TBS-T buffer containing 5% skim milk. The membrane was washed three times with 30 ml TBS-T buffer for 5 minutes and incubated with the secondary antibody (horseradish-peroxidase-conjugated goat anti-rabbit antibody (1:5000)) in 10 ml 5 % skim milk TBS-T buffer for another hour. Again, the membrane was washed as described before using TBS buffer and additionally with 1x PBS. For detection of the proteins, 800 µl Clarity™ Western ECL Substrate was pipetted on the membrane and Fusion Solo S imager was used to detect the chemiluminescent signal. The protein bands were quantified using ImageJ (Rueden et al., 2017). RpoB was used as a loading control for quantification.

3 Results

3.1 Generation of MepM and MepH deletion mutants

The main question of this thesis was to investigate whether the MEPs found to possibly be involved in β-lactam resistance of ID40 contribute to antibiotic resistance or not.

The generation of deletion mutants was the basic requirement to answer this question. Basically, the genes encoding the different MEPs were excised from the ID40 genome leaving only 15-30 bp at the beginning and at the end of the gene. Thereby, the mutated strains formed only short, non-functional peptides. This effect is comparable to the effect of a possible inhibitor of these proteins in the best case. Therefore, the generation of deletion mutants serves as a simulation of a potential inhibitor effect.

The implemented tests intended to provide an overview of how the MEPs influence resistance and growth of the *Pa* ID40 strain. For this purpose, results of the ID40 WT were compared with those of the deletion mutants. Furthermore, the effects on the different mutants were compared to determine, whether the impacts on the phenotypes acted in a redundant or synergistic way.

For the generation of the deletion mutants, suicide vectors for each gene or operon (*mepM2*, *mepM3* and *mepH1/2*) were assembled via Gibson cloning (2.3.4) and transformed into *Ec SM10λpir* (2.3.5). Afterwards, the plasmids were transferred by conjugation into ID40 WT or into ID40 deletion mutants for the generation of double or triple deletion mutants using allelic exchange (2.3.8). In the following, each step will be explained in detail.

3.1.1 Gibson-Cloning and Transformation into Ec SM10λpir

The first step for the generation of deletion mutants, was to generate suicide vectors using the Gibson assembly reaction 2.3.4. The elements assembled via Gibson reaction were: the linearized vector pEXG2 and two fragments, which were synthesized by PCR as described in 2.3.1.1. These fragments were designed implying the flanking regions of the target gene, but also the first and

the last amino acids of the particular gene. The so-called upstream fragments contained 30 bp of the beginning of the target gene and about 800 bp of the sequence before the target gene. The downstream fragments contained 30 bp of the end of the gene and about 800 bp of the sequence after the target gene. As the genes *mepH1* and *mepH2* are located in one operon, only one suicide vector for the synchronous knock out of both genes was designed. Therefore, the upstream fragment contained a sequence of the region upstream of *mepH1* and the first 30 bp of the coding sequence of *mepH1* and the downstream fragment contained the last 30 bp of the 3' end of the coding sequence of *mepH2* and approximately 800 bp of the upstream flanking region of *mepH2*. In this work, the operon will be referred to as *mepH1/2*. Figure 7 illustrates the general principle for the generation of the fragments and its integration into the vector. After successful Gibson assembly, only few base triplets ("gene-scar") are left of the original target gene. The inserted sequences can still be transcribed and translated, but the resulting product is a shortened and unfunctional version of the protein. Because some parts of the gene remain inside the genome, unwanted regulatory effects on flanking genes should be avoided.

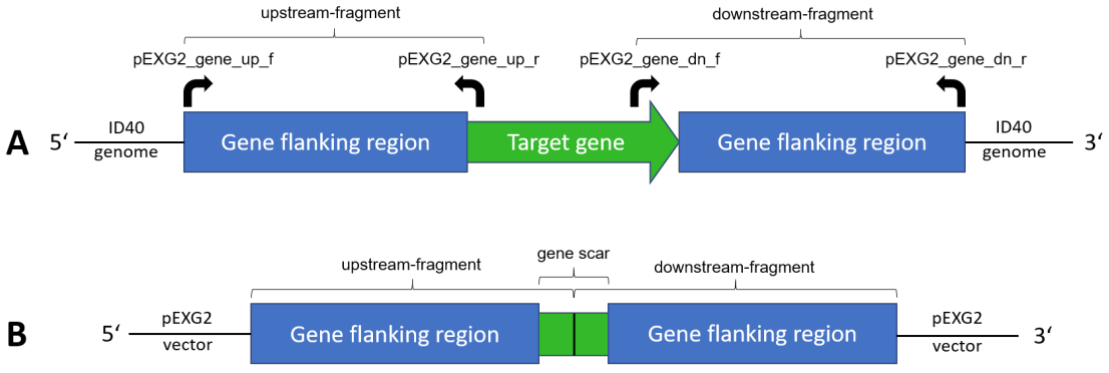

Figure 7: ***Simplified scheme on fragment synthesis and Gibson reaction***

(A) *shows the primer binding sites for fragment synthesis in ID40 genomic DNA. The generated fragments contain flanking regions of the target gene and about 30 bp of the beginning and the end of the target gene.* ***(B)*** *shows the result of a successful Gibson reaction: the fragments are integrated into the pEXG2 vector. The "gene scar" contains only few base triplets of the former target gene. About 800 bp build up the flanking regions.*

Table 25 shows the primer pairs used for the synthesis of the different up- and downstream fragments. Moreover, the fragment's lengths determined using Snap Gene (GSL Biotech LLC) are shown in Table 25. All these fragments were

synthesized by PCR (2.3.1.1) and verified by Agarose-gel electrophoresis (2.3.2, see Figure 8).

Table 25: ***Primer pairs for the synthesis of up- and downstream fragments for Gibson cloning and lengths of the synthesized fragments***

Fragment	**Primer**	**Fragment length**
mepM2 5' upstream fragment	pEXG2_mepM2_up_f pEXG2_mepM2_up_r	862 bp
mepM2 3' downstream fragment	pEXG2_mepM2_dn_f pEXG2_mepM2_dn_r	921 bp
mepM3 5' upstream fragment	pEXG2_mepM3_up_f pEXG2_mepM3_up_r	878 bp
mepM3 3' downstream fragment	pEXG2_mepM3_dn_f pEXG2_mepM3_dn_r	890 bp
mepH1/2 5' upstream fragment	pEXG2_MepH1/2_up_f pEXG2_MepH1/2_up_r	881 bp
mepH1/2 3' downstream fragment	pEXG2_MepH1/2_dn_f pEXG2_MepH1/2_dn_r	878 bp

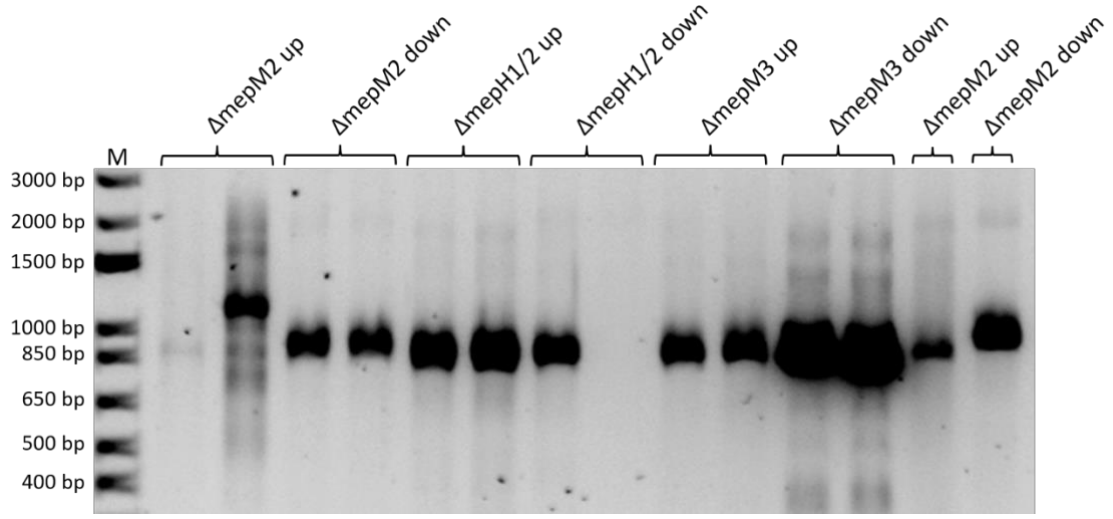

Figure 8: ***Agarose gel electrophoresis of the amplified upstream and downstream fragments***

Upstream and downstream fragments of mepM2, mepM3 and mepH1/2 were amplified by PCR. The expected fragment sizes are shown in Table 25.

After verifying the amplification of the correct PCR fragments, they were purified (2.3.3) and used for the Gibson reaction. The next step was to transform the

obtained pEXG2 derivates into chemically competent *Ec* Top10 (see 2.3.5). Afterwards, a Colony-PCR (2.3.6) was performed to check if the Gibson assembly had been successful. For this purpose, the primers pEXG2_seq_f and pEXG2_seq_r, which bind before and after the insertion, were used (see Figure 9). Suicide vectors for the deletion of *mepM2*, *mepM3* and *mepH1/2* could effectively be created and transformed into *Ec* Top10. The expected lengths of the PCR products are shown in Table 26.

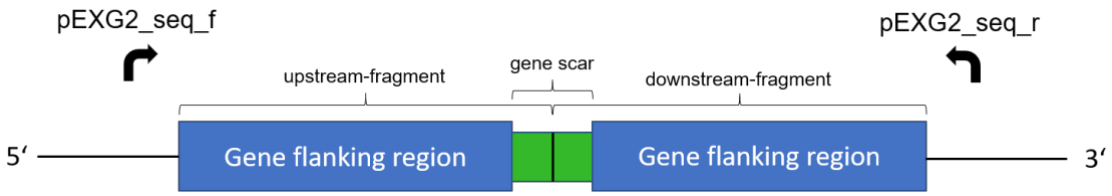

Figure 9: ***Binding sites of the primers used for Colony-PCR of Ec Top10 clones***

The Colony-PCR was used to screen the clones for a successful Gibson assembly and transformation into Ec Top10. The primers pEXG2_seq_f and pEXG2_seq_r bind a few bp before and after the insertion. Thus, clones with vectors carrying the insertion produced longer PCR products than those with the initial, unmodified pEXG2 plasmids.

Table 26: ***Expected lengths of the PCR products of the Colony-PCR after transformation into Ec Top10***

Plasmid	**Length of PCR fragment**
pEXG2	755 bp
pEXG2 *mepM2* suicide vector	2391 bp
pEXG2 *mepM3* suicide vector	2378 bp
pEXG2 *mepH1/2* suicide vector	2369 bp

Moreover, to ensure that the suicide vectors had not acquired mutations during the cloning procedure, the plasmids were sequenced by Eurofins Genomics. For this purpose, the plasmid DNA was isolated (see 2.3.7) and prepared according to the company's instructions. Error-free suicide vectors for all three genes were confirmed.

Next, another transformation was performed. The *Ec* Top10 strain had been elected, because of its high transformation efficiency. However, since it is not able to transfer plasmids via conjugation into *Pa*, the plasmid DNA of the confirmed suicide vectors was transformed into *Ec* SM10λpir as described in 2.3.5. To confirm a successful transformation of the pEXG2 derivatives, another

Colony-PCR was applied screening colonies of *Ec* SM10λpir. Again, the primers pEXG2_seq_f and pEXG2_seq_r were used and the fragment lengths complied with the lengths depicted in Table 26. Clones with the correct fragment length were used for the mating with *Pa* ID40.

3.1.2 Allelic exchange

Aim of the allelic exchange in the genome of ID40 was to replace the functional genes (*mepM2*, *mepM3*, *mepH1* and *mepH2*) by the short, unfunctional gene scar inserted into the pEXG2 vector. The pEXG2 derivates were designed carrying target gene flanking regions. This part of the sequence is homologous in both ID40 WT genome and the pEXG2 suicide vectors. Based on the homologous recombination of this region, the insert of the pEXG2 vector was interchanged with the functional gene via allelic exchange. For a detailed description on how the allelic exchange was performed, see 2.3.8. The first step was the conjugation of a *Pa* ID40 strain with *Ec* SM10λpir carrying the vector. Table 27 gives an overview about how the *Pa* ID40 strains and *Ec* strains were combined to generate the deletion mutants. Not only single deletion mutants were created, but also double and triple deletion mutants. As they are located in one operon, the genes *mepH1* and *mepH2* were always deleted simultaneously using the pEXG2 Δ*mepH1/2* vector.

Table 27: ***Overview on how the conjugation was performed to generate the deletion mutants***

As described in 2.3.8, 200 µl of Ec SM10λpir strain were conjugated with 400 µl of Pa ID40 strains. Deletion mutants of ID40 WT were used to create double or triple mutants.

ID40 strain	***Ec*SM10λpir strain**	**Deletion mutant**
ID40 WT	*Ec*SM10λpir Δ*mepM2*	ID40 Δ*mepM2*
ID40 WT	*Ec*SM10λpir Δ*mepM3*	ID40 Δ*mepM3*
ID40 WT	*Ec*SM10λpir Δ*mepH1/2*	ID40 Δ*mepH1/2*
ID40 Δ*mepM1*	*Ec*SM10λpir Δ*mepM2*	ID40 Δ*mepM1* Δ*mepM2*
ID40 Δ*mepM1*	*Ec*SM10λpir Δ*mepM3*	ID40 Δ*mepM1* Δ*mepM3*
ID40 Δ*mepM1*	*Ec*SM10λpir Δ*mepH1/2*	ID40 Δ*mepM1* Δ*mepH1/2*
ID40 Δ*mepM1* Δ*mepM3*	*Ec*SM10λpir Δ*mepM2*	ID40 Δ*mepM1* Δ*mepM2* Δ*mepM3*

ID40 Δ*mepM1* Δ*mepM3*	*Ec*SM10λpir Δ*mepH1/2*	ID40 Δ*mepM1* Δ*mepM3* Δ*mepH1/2*

After conjugation, the homologous recombination occurred successively on different selective culture media as described in detail in 2.3.8. To create a proper deletion mutant, two crossovers must occur incidentally. The first crossover leads to the integration of the plasmid into the genome of ID40 after conjugation, resulting in merodiploids. Further, the second crossover leads either to a clean deletion of the target gene or to return to WT genotype. Finally, a Colony-PCR was performed to screen the gentamicin-sensitive clones for suspected deletions. Table 28 depicts the applied primers and the fragment lengths indicating if the gene has either ID40 WT or deletion length. Figure 10 shows the binding sites of the primers.

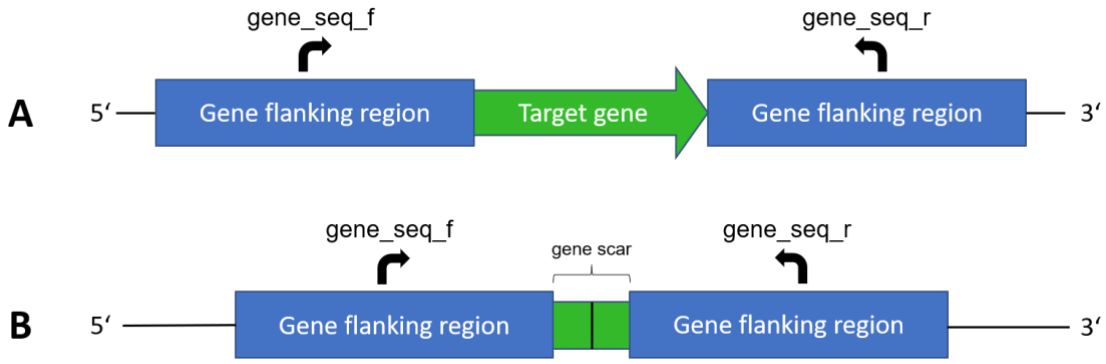

Figure 10: ***Binding sites of the primers used for Colony-PCR to verify the deletions after allelic exchange***

The primers bind to a small sequence located inside the target gene flanking regions. ***(A)*** *shows the gene with WT length.* ***(B)*** *depicts the DNA sequence of a deletion mutant after a successful second crossover. The resulting product of the Colony-PCR is shorter than the product of an ID40 WT clone.*

*Table 28****: Primer pairs and expected fragment lengths for verification of the deletions via Colony-PCR:*** *After performing allelic exchange, the gentamicin sensitive clones were screened for the putative mutations via Colony-PCR.*

Potential mutation	**Primers**	**Fragment length**	
		WT	**Mutation**
Δ*mepM1*	MepM1_seq_f MepM1_seq_r	1948 bp	634 bp

Δ*mepM2*	MepM2_seq_f MepM2_seq_r	1604 bp	806 bp
Δ*mepM3*	MepM3_seq_f MepM3_seq_r	1467 bp	621 bp
Δ*mepH1/2*	MepH1/2_seq_f MepH1/2_seq_r	1599 bp	417 bp

For validation of the deletions, the clones were checked again with another two PCRs: First, the suspected deletion mutants were cultivated overnight. Next, the genomic DNA of the putative mutants was isolated (2.3.9) and served as template for the PCRs. For the first PCR, the gene-flanking primers depicted in Table 28 (gene_seq_f and gene_seq_r) were used again. The PCR products were just as long as the products of the Colony-PCR (Table 28). Besides, a Proof-PCR was performed to verify the mutants: as forward primers the gene_seq_f primers (see Table 28) were used, which bind to the 5' target gene flanking region. The second primer was called "inside primer", because its homologous sequence lies inside the target gene. If the screened genomic DNA still had an intact target gene, the inside primer could bind to its homologous sequence, resulting in a PCR product with a certain length (see Table 29). If the genomic DNA carried the suspected deletion, the inside primer could not bind to the template. Hence, no band was detected in the Agarose-gel picture, which confirmed the deletion mutant. Figure 11 schematically shows the binding sites of the primers during the Proof-PCR.

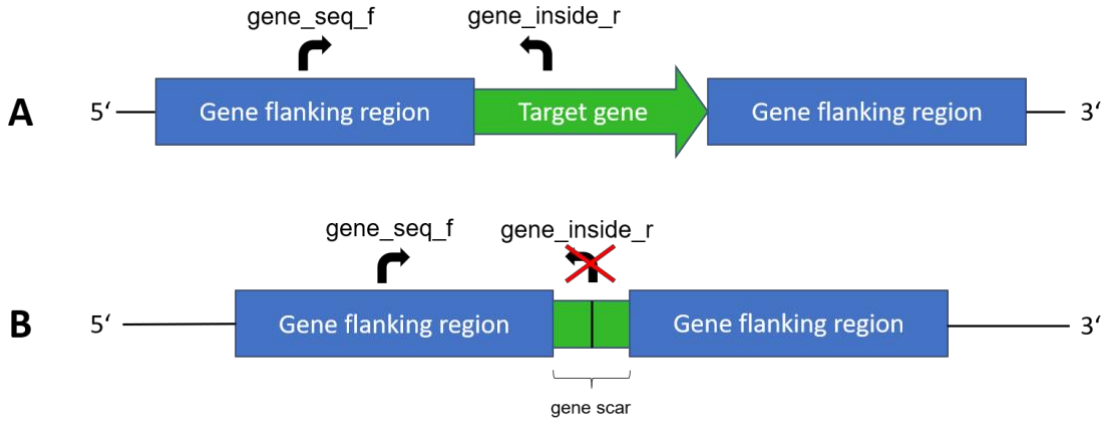

Figure 11: ***Binding sites of the primers used for Proof-PCR to confirm putative deletion mutants***

Just like in Figure 10, the gene_seq_f primer, which binds to the gene flanking region is used as forward primer. ***(A)*** *The inside primer binds to the target gene sequence, if the gene is still intact within the WT genome.* ***(B)*** *In the genomic DNA of a deletion mutant, the inside primer has no homologous sequence that it can bind to. As a result, no band can be seen on the Agarose-gel picture.*

Table 29: ***Primer pairs and fragment lengths for verification of the deletions via Proof-PCR***

Potential mutation	**Primers**	**Fragment length**	
		WT	**Mutation**
Δ*mepM1*	MepM1_seq_f MepM1_inside_r	658 bp	No band
Δ*mepM2*	MepM2_seq_f MepM2_inside_r	600 bp	No band
Δ*mepM3*	MepM3_seq_f MepM3_inside_r	496 bp	No band
Δ*mepH1/2*	MepH1/2_seq_f MepH1/2_inside_r	321 bp	No band

For the Proof-PCR isolated genomic DNA of the putative mutants was used as template. The applied inside primer binds to the target gene sequence, if the gene is still intact within the WT genome. If no band could be seen on the Agarose-gel picture, the clone was assessed a proved deletion mutant. This follows from the fact that the primer cannot bind its homologous sequence, if the target gene has successfully been deleted.

Pictures of the Agarose gel electrophoreses of both the PCR using gene-flanking primers as well as the Proof-PCR are displayed in Figures 12-18. For ID40 WT and each mutant the integrity and length of the genes encoding the different MEPs was analysed.

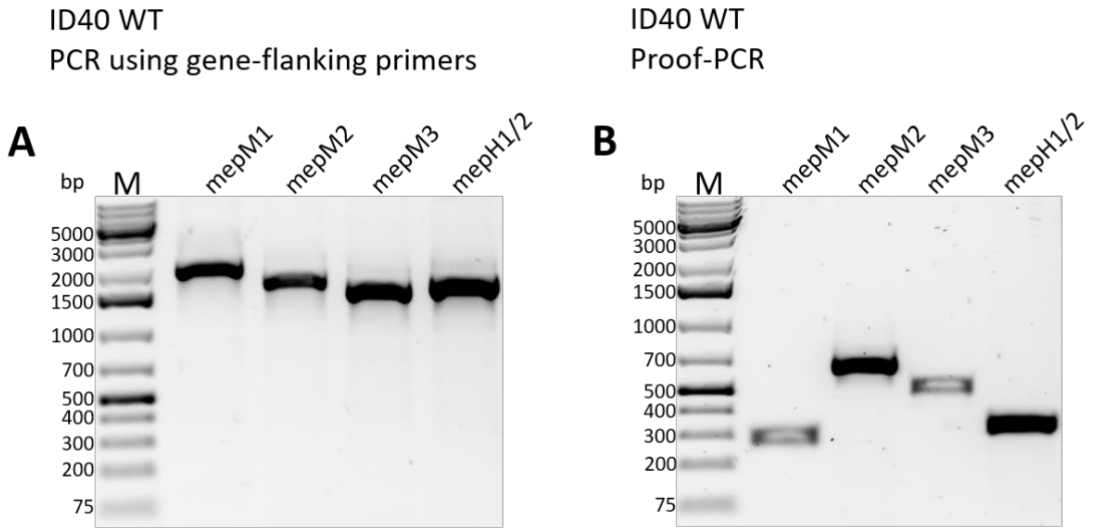

Figure 12: ***Agarose gel electrophoresis of PCR products (gDNA of ID40 WT)***

(A) *The gel shows DNA fragments of the gDNA of ID40 WT produced by the PCR using gene-flanking primers. The heights of the bands indicate, whether the respective genes have either WT length or mutant length. If the gene has been successfully deleted during allelic exchange, only a short, unfunctional gene-scar is left, represented by a shorter fragment on the gel picture. This picture demonstrates that the genes mepM1, mepM2, mepM3 and mepH1/2 of ID40 WT have WT length (see Table 28).* ***(B)*** *Picture B shows the Agarose gel electrophoresis of the Proof-PCR products generated with gDNA of ID40 WT. Four bands with WT length can be seen on the picture (see Table 29). If one of the genes had been deleted, no band would have appeared on the picture. Hence, the inside primer could bind to the corresponding gene sequences and none of the selected genes is deleted.*

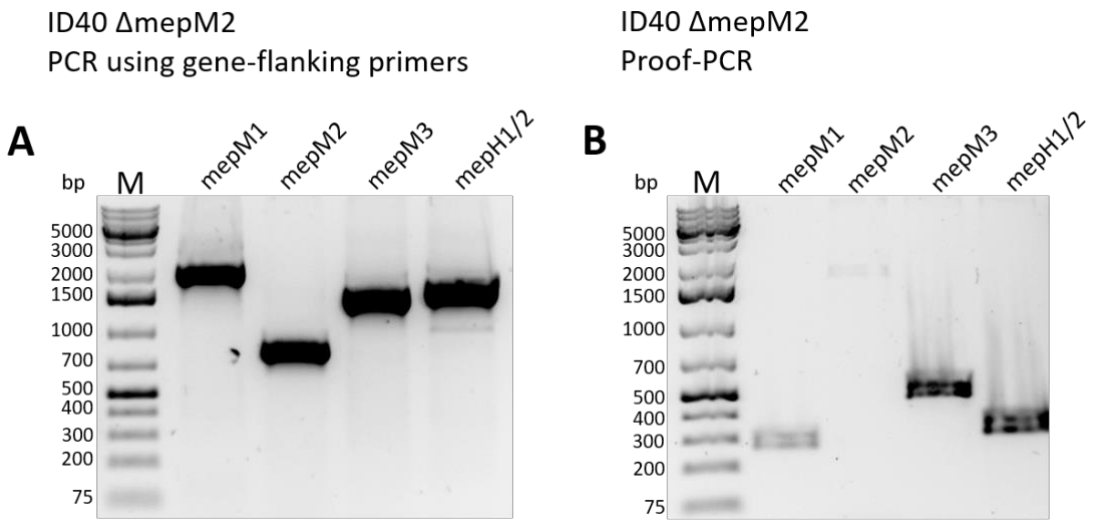

Figure 13: ***Agarose gel electrophoresis of PCR products (gDNA of ID40 ΔmepM2)***

(A) *The gel shows DNA fragments of the gDNA of ID40 ΔmepM2 produced by the PCR using gene-flanking primers. The heights of the bands indicate, whether the respective genes have either WT length or mutant length. If the gene has been successfully deleted during allelic exchange, only a short, unfunctional gene-scar is left, represented by a shorter fragment on the gel picture. This picture demonstrates that the genes mepM1, mepM3 and mepH1/2 of ID40 ΔmepM2 have WT length, whereas mepM2 is deleted (see Table 28).* ***(B)*** *Picture B shows the Agarose gel electrophoresis of the Proof-PCR products generated with gDNA of ID40 ΔmepM2. Three bands with WT length can be seen on the picture (mepM1, mepM3 and mepH1/2; see Table 29). Because the inside primer could not bind to the sequence of mepM2, no band appears on the gel for mepM2. This result confirms the deletion of mepM2.*

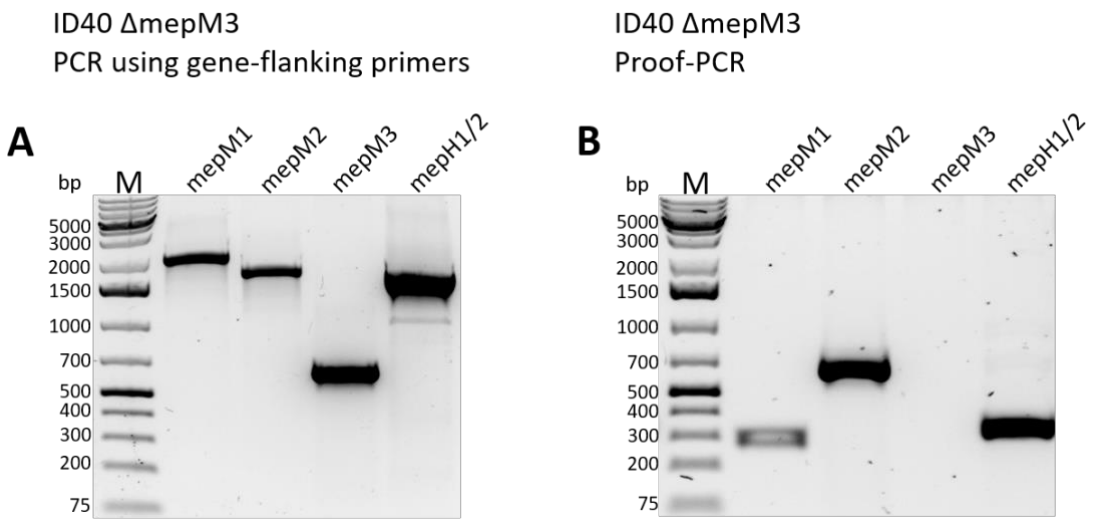

Figure 14: ***Agarose gel electrophoresis of PCR products (gDNA of ID40 ΔmepM3)***

(A) *The gel shows DNA fragments of the gDNA of ID40 ΔmepM3 produced by the PCR using gene-flanking primers. The picture demonstrates that the genes mepM1, mepM2 and mepH1/2 of ID40 ΔmepM3 have WT length, whereas mepM3 is deleted (see Table 28).* ***(B)*** *Picture B shows the Agarose gel electrophoresis of the Proof-PCR products generated with gDNA of ID40 ΔmepM3. Three bands with WT length can be seen on the picture (mepM1, mepM2 and mepH1/2; see Table 29). No band appears on the gel for mepM3, confirming its deletion.*

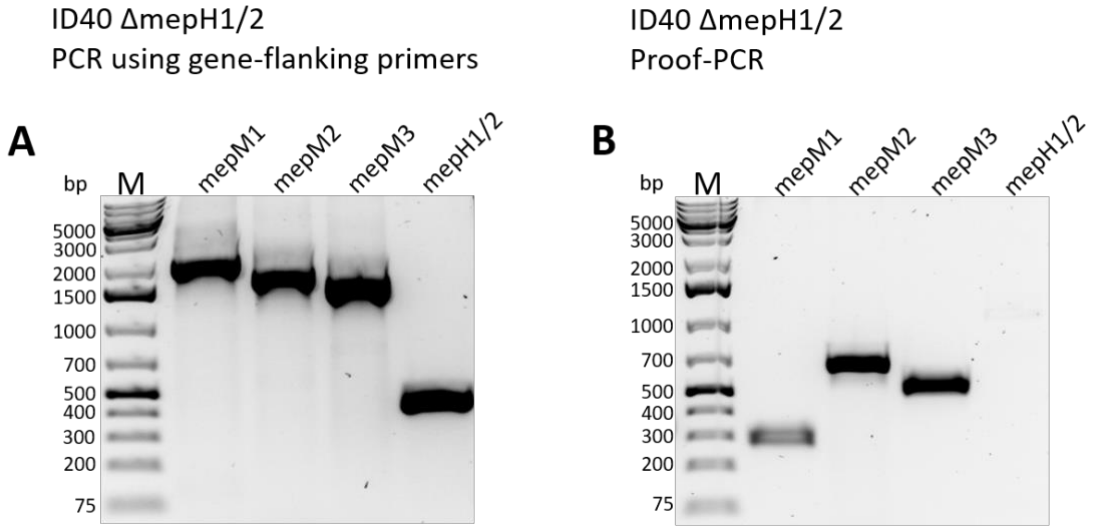

Figure 15: ***Agarose gel electrophoresis of PCR products (gDNA of ID40 ΔmepH1/2)***

(A) *The gel shows DNA fragments of the gDNA of ID40 ΔmepH1/2 produced by the PCR using gene-flanking primers. The picture demonstrates that the genes mepM1, mepM2 and mepM3 of ID40 ΔmepH1/2 have WT length, whereas mepH1/2 is deleted (see Table 28).* ***(B)*** *Picture B shows the Agarose gel electrophoresis of the Proof-PCR products generated with gDNA of ID40 ΔmepH1/2. Three bands with WT length can be seen on the picture (mepM1, mepM2 and mepM3; see Table 29). No band appears on the gel for mepH1/2, confirming its deletion.*

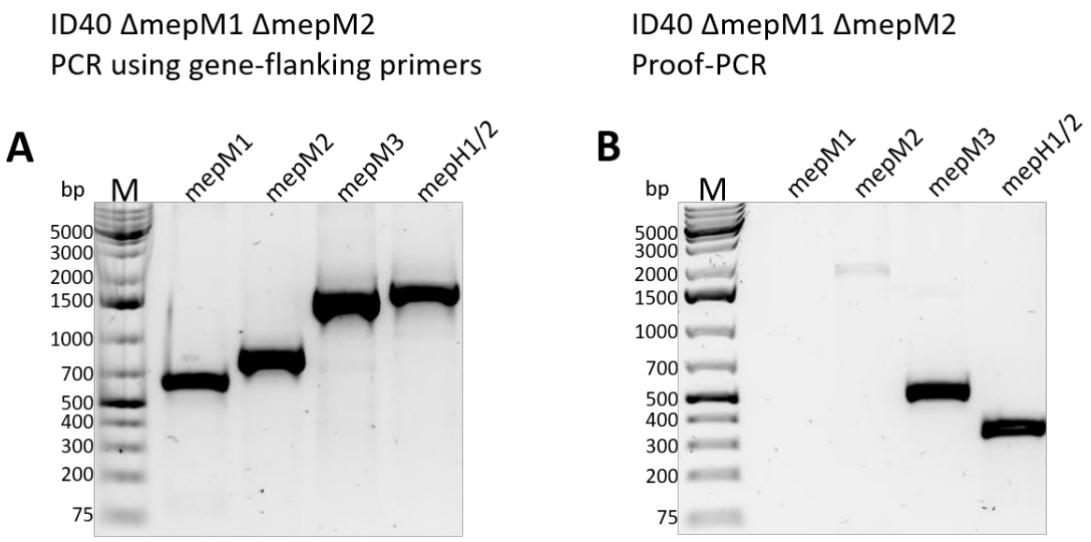

Figure 16: ***Agarose gel electrophoresis of PCR products (gDNA of ID40 ΔmepM1 ΔmepM2)***

(A) *The gel shows DNA fragments of the gDNA of ID40 ΔmepM1 ΔmepM2 produced by the PCR using gene-flanking primers. The picture demonstrates that the genes mepM3 and mepH1/2 of ID40 ΔmepM1 ΔmepM2 have WT length, whereas mepM1 and mepM2 are deleted (see Table 28).* ***(B)*** *Picture B shows the Agarose gel electrophoresis of the Proof-PCR products generated with gDNA of ID40 ΔmepM1 ΔmepM2. Two bands with WT length can be seen on the picture (mepM3 and mepH1/2; see Table 29). No bands appear on the gel for mepM1 and mepM2, confirming their deletion.*

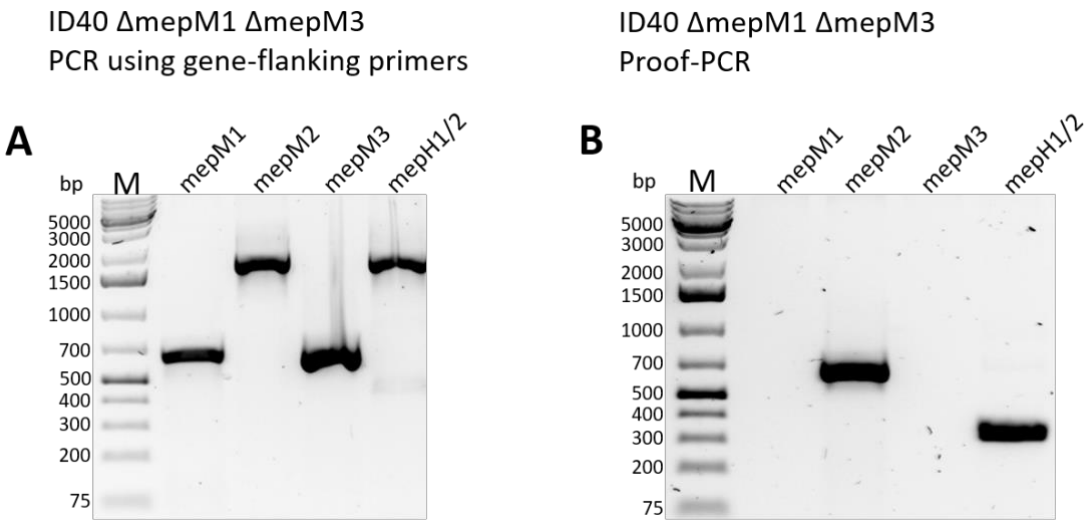

Figure 17: ***Agarose gel electrophoresis of PCR products (gDNA of ID40 ΔmepM1 ΔmepM3)***

(A) *The gel shows DNA fragments of the gDNA of ID40 ΔmepM1 ΔmepM3 produced by the PCR using gene-flanking primers. The picture demonstrates that the genes mepM2 and mepH1/2 of ID40 ΔmepM1 ΔmepM3 have WT length, whereas mepM1 and mepM3 are deleted (see Table 28).* ***(B)*** *Picture B shows the Agarose gel electrophoresis of the Proof-PCR products generated with gDNA of ID40 ΔmepM1 ΔmepM3. Two bands with WT length can be seen on the picture (mepM2 and mepH1/2; see Table 29). No bands appear on the gel for mepM1 and mepM3, confirming their deletion.*

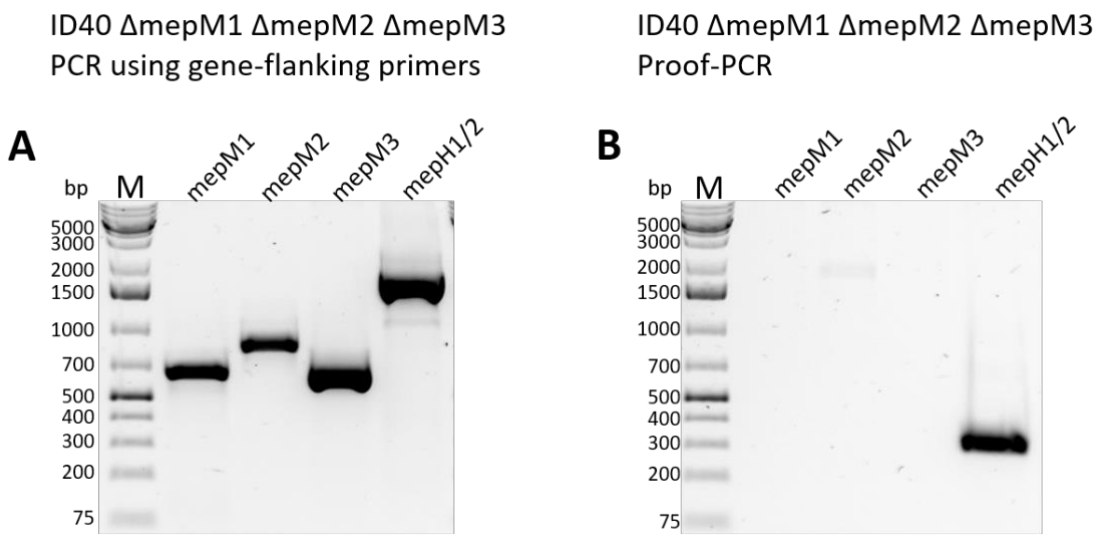

Figure 18: ***Agarose gel electrophoresis of PCR products (gDNA of ID40 ΔmepM1 ΔmepM2 ΔmepM3)***

(A*) The gel shows DNA fragments of the gDNA of ID40 ΔmepM1 ΔmepM2 ΔmepM3 produced by the PCR using gene-flanking primers. The picture demonstrates that the operon mepH1/2 of ID40 ΔmepM1 ΔmepM2 ΔmepM3 has WT length, whereas mepM1, mepM2 and mepM3 are deleted (see Table 28).* ***(B)*** *Picture B shows the Agarose gel electrophoresis of the Proof-PCR products generated with gDNA of ID40 ΔmepM1 ΔmepM2 ΔmepM3. One band with WT length can be seen on the picture (mepH1/2; see Table 29). No bands appear on the gel for mepM1, mepM2 and mepM3, confirming their deletion.*

Most of the planned deletion mutants shown in Table 27 could successfully be generated by allelic exchange (see Figures 12-18). However, the deletion mutants ID40 Δ*mepM1* Δ*mepH1/2* and ID40 Δ*mepM1* Δ*mepM3* Δ*mepH1/2* could not be created.

3.2 Growth curves

Using the generated deletion mutants, further experiments were performed for characterization of the new strains. The growth of bacteria is a very general indicator of the fitness of the strains. To investigate whether the deletions had any influence on the growth of the bacteria, growth of ID40 WT and all deletion mutants in LB medium was observed over a course of 15 hours (see 2.2.4). During this time, the OD_{600nm} was measured in 50 cycles. Three independent experiments were conducted, and Figure 19 representatively shows the result of one experiment. Technical duplicates of each biological replicate were prepared. Further, LB medium was used as a blank.

Looking at the graphs (Figure 19), the typical course of bacterial growth can be observed for all mutants. After a lag phase with almost no increase in OD_{600nm}, a period of exponential growth follows. At the end of the measurement, the slope of the graphs and thus the velocity of growth decreases, approaching a stationary phase. However, there are differences to be named comparing the ID40 WT with the deletion mutants: at the beginning, the curve progression of all strains looks quite similar with exception of ID40 Δ*mepM1* Δ*mepM2*. Yet, after about 9 hours, the curves of the deletion mutants seem to flatten, whereas the curve of ID40 WT keeps its slope. At the end of the measurement, ID40 WT reaches an OD_{600nm} of around 1.0. The deletion mutants except ID40 Δ*mepM1* Δ*mepM2* attain values between 0.7 and 0.9. The curve of ID40 Δ*mepM1* Δ*mepM2* differs from all other results. From the beginning, the OD_{600nm} rises slower than the OD_{600nm} of all other strains. Finally, its OD_{600nm} reaches only values of around 0.5 as maximum.

Taken together, the ID40 WT grows slightly better in LB medium than the deletion mutants. ID40 Δ*mepM1* Δ*mepM2* seems to have a stronger growth deficit than the other deletion mutants, reaching an OD_{600nm} only about half as high as the OD_{600nm} of ID40 WT.

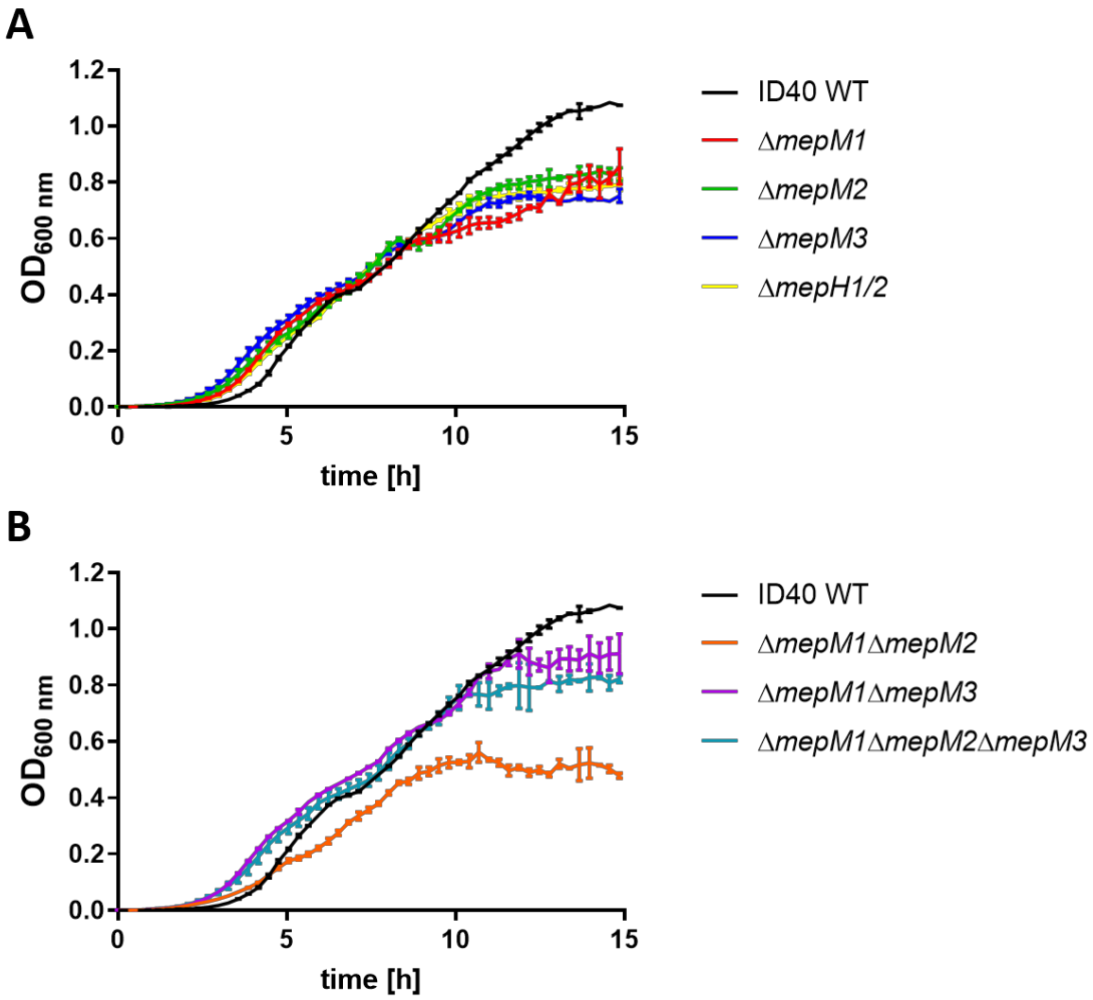

Figure 19: ***Growth curves of ID40 WT and the deletion mutants***

Figure 19 shows the temporal course of the growth of the different strains in LB medium. The $OD_{600\ nm}$ (Y-axis) was measured over 50 cycles in a time range of 15 hours (X-Axis) using the Tecan Infinite® 200 Pro. LB medium served as a blank, which was subtracted from all the values. ***(A)*** *Growth curves of ID40 WT and the deletion mutants ID40 ΔmepM1, ID40 ΔmepM2, ID40 ΔmepM3 and ID40 ΔmepH1/2 are depicted.* ***(B)*** *Growth curves of ID40 WT and the deletion mutants ID40 ΔmepM1 ΔmepM2, ID40 ΔmepM1 ΔmepM3 and ID40 ΔmepM1 ΔmepM2 ΔmepM3 are depicted.*

3.3 Influence of the knockouts on resistance of *Pa* ID40

3.3.1 Determination of minimal inhibitory concentrations (MICs)

To get more knowledge about the influence of the different MEPs on resistance against β-lactam antibiotics, microbroth dilution assays were accomplished with the ID40 WT and the deletion mutants. The test evaluates, whether the bacterial strain can grow in the presence of certain antibiotic concentrations. Thereby, the MICs of selected β-lactam antibiotics were determined. An equal number of bacteria was grown in Mueller Hinton II Broth Micronaut for 18 hours, being exposed to different concentrations of certain antibiotics. After the incubation time, the OD_{600nm} was measured as indicator for growth of the bacteria. The chosen antibiotics were meropenem (MEM), imipenem (IMP), cefepime (FEP), ceftazidime (CAZ), piperacillin (PIP), piperacillin/tazobactam (TZP) and aztreonam (ATM). After subtraction of the determined blank (Mueller Hinton II Broth Micronaut), a strain was rated “resistant” against the concentration of the antibiotic in the well, when the OD_{600nm} revealed a value >0.05. If the OD_{600nm} was ≤0.05, the strain was rated “sensitive” against the present concentration of the antibiotic. The results of the three different microtiter plates (Micronaut-S Pseudomonas MIC plates (Merlin), Sensititre™ EUX2NF MIC plates (Thermo Fisher Scientific) and Sensititre™ GN2F MIC plates (Thermo Fisher Scientific)) are presented in Table 30. For each deletion mutant, the assay was performed two times with each plate. As a result, at least 4 different MIC values for each antibiotic were determined (depending on which antibiotic is tested using which plate). The ID40 WT served as a control. As MIC breakpoints, the current EUCAST Clinical Breakpoint Tables were used.

In accordance with former studies by Sonnabend et al. (2020) and regarding the current EUCAST Clinical Breakpoint Tables, the ID40 WT was resistant against all listed β-lactam antibiotics except MEM. As can be seen in Table 30, the MIC values for all depicted antibiotics are reduced in ID40 Δ*mepM1*. For FEP and ATM the values decrease below the MIC breakpoint. ID40 Δ*mepM2* shows lower MIC values for all listed antibiotics except IMP and CAZ and breaks resistance against ATM. In ID40 Δ*mepM3* the MIC values are slightly reduced for MEM, FEP

and TZP. A minor increase of the MIC can be identified for IMP. The MIC values of ID40 Δ*mepH1/2* are all diminished in comparison to the WT except IMP. The deletion of *mepH1/2* restores sensitivity against ATM. For ID40 Δ*mepM1* Δ*mepM3* the results are comparable to Δ*mepM1*: MICs are reduced compared to the WT and resistance against ATM and FEP is broken. The double mutant ID40 Δ*mepM1* Δ*mepM2* shows immensely higher susceptibility to the stated antibiotics, lowering the MIC values below the breakpoint for all antibiotics with exception of IMP. ID40 Δ*mepM1* Δ*mepM2* Δ*mepM3* shows similar results with slightly more diminished values compared to ID40 Δ*mepM1* Δ*mepM2*.

To summarize, deletion of *mepM1* has the greatest impact concerning resistance against β-lactam antibiotics in ID40. However, deletions of *mepH1/2*, *mepM2* and *mepM3* increase the strain's sensitivity to β-lactam antibiotics as well. A double knock-out of *mepM1* and *mepM2* seems to have a synergistic effect and breaks resistance against most of the investigated antibiotics. The MIC values are clearly reduced compared to a single deletion of *mepM1*.

Table 30: ***Minimal inhibitory concentrations of ID40 WT and deletion mutants***

(MEM: meropenem; IMP: imipenem; FEP: cefepime; CAZ: ceftazidime; PIP: piperacillin; TZP: piperacillin/tazobactam; ATM: aztreonam) The MICs were determined by microbroth dilution. The table shows a summary of the detected MIC values of three different microtiter plates. Each mutant was applied twice on each plate. At the end, at least 4 MIC values for each mutant and for each antibiotic could be determined. The colouration was chosen as follows: MICs of the deletion mutants are highlighted in green, if they are lower than the MIC of the WT. Bold green means that the MIC value is below the MIC breakpoint according to the current EUCAST Clinical Breakpoint Tables. The red colour stands for MIC values higher than the ID40 WT.

	MIC Breakpoint (mg/L)		*ID40 WT*	*ID40 ΔmepM1*	*ID40 ΔmepM2*	*ID40 ΔmepM3*	ID40 *ΔmepH1/2*	ID40 *ΔmepM1 ΔmepM2*	*ID40 ΔmepM1 ΔmepM3*	*ID40 ΔmepM1 ΔmepM2 ΔmepM3*
	S ≤	R >								
MEM	2	8	8	2 - 8	4	4 - 8	2 - 4	**≤1 - 2**	2 - 4	**≤1 - 1**
IMP	4	4	32	16	32	32 - 64	32	8	16	4 - 8
FEP	8	8	16 - 32	**8**	8 - >8	16	8 - >8	**4**	**8**	**4**
CAZ	8	8	32 - >32	16 - 32	32 - >32	32 - >32	16 - 32	**8**	16 - 32	**4 - 8**
PIP	16	16	128 - >128	16 - 32	32 - 64	>128	32 - 64	**8 - 16**	32	**8**
TZP	16	16	128 - >128	32 - 64	32 - 64	64 - 128	32	**8 - 16**	32	**8 - 16**
ATM	16	16	16 - 32	**8 - 16**	**16**	16 - 32	**8**	**4 - 8**	**8 - 16**	**4**

3.3.2 Quantification of β-lactamase expression

For the ID40 genome it is known that it encodes two different β-lactamases: AmpC and PoxB. Usually, the β-lactamase AmpC is mainly contributing to β-lactam resistance, whereas PoxB does not. However, in *poxB*-overexpressing clones a higher susceptibility to carbapenems was described (Zincke et al., 2016).

To investigate whether the higher susceptibility to β-lactam antibiotics results from a reduced expression of the *ampC*-gene, a qRT-PCR was performed quantifying the expression level of *ampC* (see 2.3.12). Beforehand, RNA isolation and digestion of remaining DNA had successfully be accomplished for all deletion mutants and ID40 WT (2.3.10; 2.3.11). For the qRT-PCR using the SYBR Green RT-PCR Kit, 1:10 dilutions of the purified RNA were used as templates. After each PCR cycle the fluorescence of SYBR Green I was measured, which increases proportionally with the amount of PCR products. Using the method by Pfaffl, the expression level of *ampC* in comparison to the reference gene *gyrB* was calculated. Figure 20A displays the results of three independent experiments. All numbers were normalized to ID40 WT.

As Figure 20A shows, deletion of *mepM1*, *mepM1* and *mepM2*, *mepM1* and *mepM3* as well as the deletion of *mepM1*, *mepM2* and *mepM3* reduces the mRNA expression of the β-lactamase *ampC* significantly by more than half. Moreover, the deletion mutant ID40 Δ*mepH1*/*2* shows a non-significant decrease, whereas the deletions of *mepM2* and *mepM3* seem to even slightly elevate *ampC* expression. The results of ID40 Δ*mepM1* correspond directly to the measured MIC values. Comparing the level of reduction in ID40 Δ*mepM1* with the ones of the double and triple mutant, no significant difference can be seen. This perception does not reflect the difference in MIC values found in the susceptibility tests. Besides, the unchanged *ampC* expression of ID40 Δ*mepM2* does not fit to the higher susceptibility identified by microbroth dilution.

As the quantification of *ampC* expression did not adequately correspond to all the results found in the antibiotic sensitivity testing, we decided to also quantify the expression of the *poxB* gene. The outcome was as follows: no significant

reduction in *poxB* expression can be observed in any of the deletion mutants (Figure 20B).

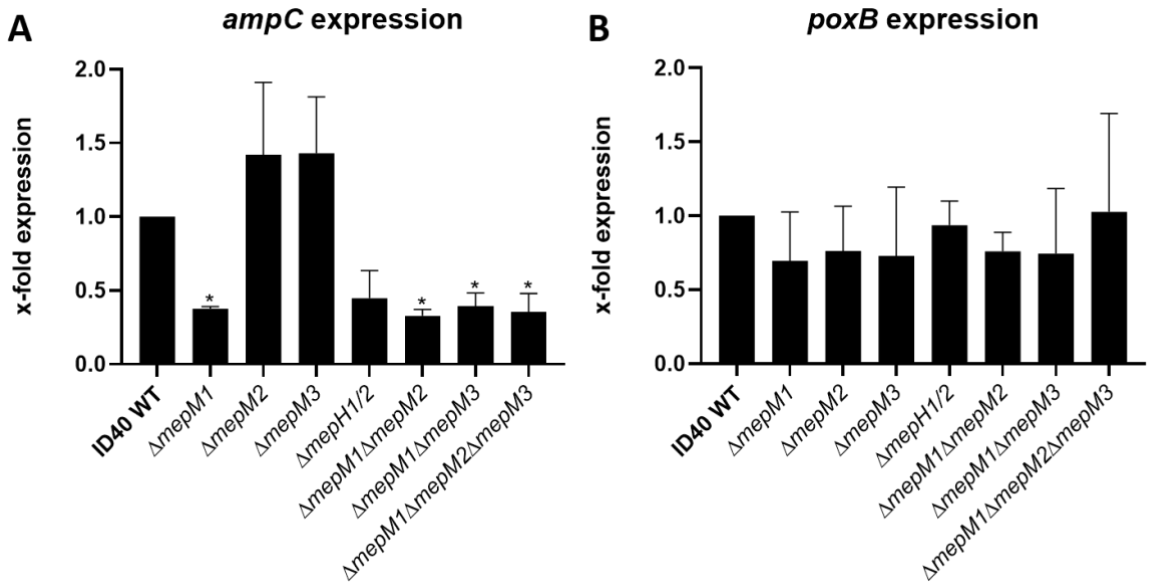

Figure 20: ***ampC and poxB expression in ID40 WT and the deletion mutants***

The expression of the genes ampC ***(A)*** *and poxB* ***(B)*** *was determined by qRT-PCR. The figures show data of three technical and three biological replicates. Means and standard deviations (SD) are depicted. The WT-values were normalized to 1 and the other bars show the relative expression compared to the WT. An ordinary one-way ANOVA was performed for each mutant strain in comparison to the WT (adjusted p-values: * p < 0.05).*

To conclude, deletion of *mepM1* resulted in a strong reduction of *ampC* expression, whereas deletion of *mepM2* and *mepM3* did not have any effect on β-lactamase expression. ID40 Δ*mepH1*/*2* displayed a lower *ampC* expression, but does not reach a significant reduction. No remarkable changes in *poxB* expression could be observed for any of the deletion mutants.

3.3.3 Quantification of β-lactamase activity

In addition to the quantification of β-lactamase expression on mRNA level, β-lactamase activity assay (nitrocefin assay) was performed (see 2.2.7). Our hypothesis was that the results of the *ampC* expression would be confirmed. The assay is based on the hydrolysis of the chromogenic cephalosporin nitrocefin. By hydrolysis of nitrocefin a red-coloured product is produced and can be detected with multi-well spectrophotometers. The measured absorbance reflects the

immediate amount of enzymatic activity of β-lactamases. For preparation of the experiment, the bacteria were subcultured for 3 hours. Then, three different strategies were performed to lyse the cells. The first two experiments included treatment of the bacteria in an ultrasonic bath for 5 minutes (Figure 21A+B). The second approach included sonification for 3 minutes (Figure 22) and the third experiment implied sonification for 5 minutes (Figure 23). The assay buffer provided in the applied kit, served as a blank. For evaluation of absolute values, a standard curve from different concentrations of hydrolysed nitrocefin (after subtraction of the blank) was plotted. Moreover, the linear interval of the nitrocefin turnover was defined. The change in absorption in the defined time range was calculated. Now, the amount of hydrolysed nitrocefin in nmol could be calculated with the help of the standard curve equation. The following equation was applied:

$$Sample\ \beta\ lactamase\ activity = \frac{B}{\Delta \mathrm{T} * \mathrm{V}} * D = \frac{\frac{nmol}{min}}{ml}$$

B = amount of nitrocefin from the Standard Curve (nmol)
ΔT = reaction time (min.)
V = sample volume added into the reaction well (ml)
D = sample dilution factor

Figure 21 shows the results of the two experiments, in which the bacteria were lysed using the ultrasonic bath. In Figure 21A, ID40 WT reaches a nitrocefin turnover of about 73.8 nmol/min/mg. A strong decrease in β-lactamase activity was recognisable for ID40 Δ*mepM1* (29.2 nmol/min/mg) and even stronger for ID40 Δ*mepM1* Δ*mepM2* (16.0 nmol/min/mg) in comparison to the ID40 WT. A slight reduction can be observed for ID40 Δ*mepM3* and ID40 Δ*mepM1* Δ*mepM2* Δ*mepM3*. Figure 21B shows a β-lactamase activity of ID40 WT of 132.5 nmol/min/mg. Moreover, it displays a strong reduction in β-lactamase activity for both ID40 Δ*mepM1* (58.2 nmol/min/mg) and ID40 Δ*mepM1* Δ*mepM2* (58.4 nmol/min/mg) compared to the ID40 WT. A minor decrease for ID40 Δ*mepM2*, ID40 Δ*mepM3* and ID40 Δ*mepH1/2* is noticeable.

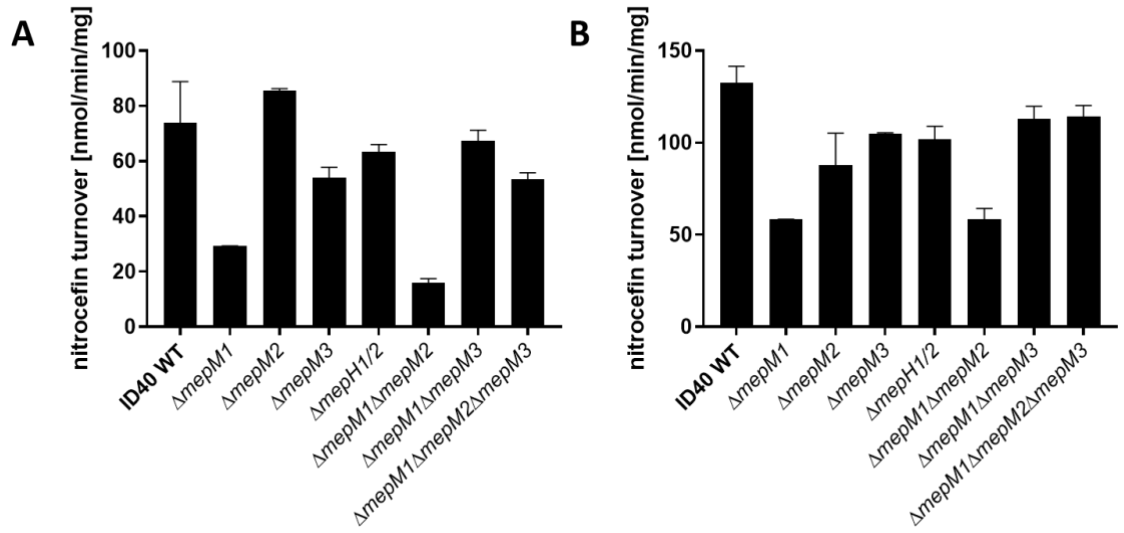

Figure 21: ***β-Lactamase Activity Assay of ID40 WT and the deletion mutants***

Absolute nitrocefin turnover is depicted in nmol/min/mg. The figure shows means and SDs of technical duplicates of two independent experiments. For cell lysis, bacteria were treated in the ultrasonic bath for 5 min.

Figure 22 displays the result of the approach, in which the bacteria were sonified with the sonificator for 3 min. ID40 WT reached an absolute nitrocefin turnover of 158.7 nmol/min/mg. The β-lactamase activity of ID40 Δ*mepM1* (64.3 nmol/min/mg) and ID40 Δ*mepM1* Δ*mepM2* (78.4 nmol/min/mg) was about half as high as the activity of ID40 WT. The other deletion mutants did not show a remarkable decrease in β-lactamase activity.

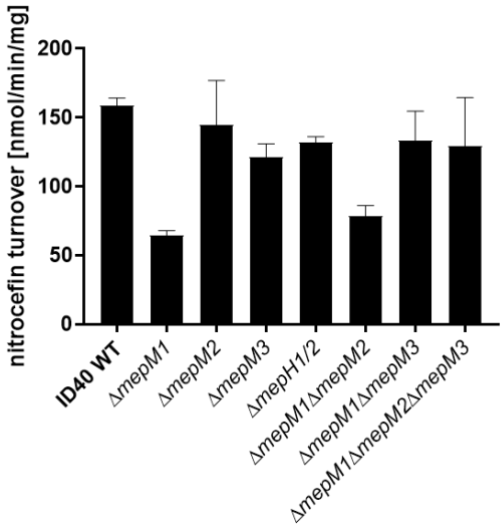

Figure 22: ***β-Lactamase Activity Assay of ID40 WT and the deletion mutants***

Absolute nitrocefin turnover is depicted in nmol/min/mg. The figure shows means and SDs of technical duplicates of one experiment. For cell lysis, bacteria were sonified with the sonificator for 3 min.

Figure 23 reproduces the results of measured β-lactamase activity after sonification of the bacteria for 5 min. In this approach, the β-lactamase activity of ID40 WT was 368.9 nmol/min/mg. All deletion mutants showed a reduced β-lactamase activity compared to the ID40 WT. For ID40 Δ*mepM1* an approximately five-fold reduction is depicted (64.3 nmol/min/mg), for ID40 Δ*mepM1* Δ*mepM2* the reduction is about three-fold (99.2 nmol/min/mg). ID40 Δ*mepM1* Δ*mepM2* Δ*mepM3* reached an activity of 141.8 nmol/min/mg, which approximately means a 2.5–fold reduction compared to the ID40 WT. Moreover, deletion of both *mepM1* and *mepM3* lead to a clearly decreased β-lactamase activity. Single deletions of *mepM2*, *mepM3* or *mepH1/2* resulted in a slightly minimised nitrocefin turnover.

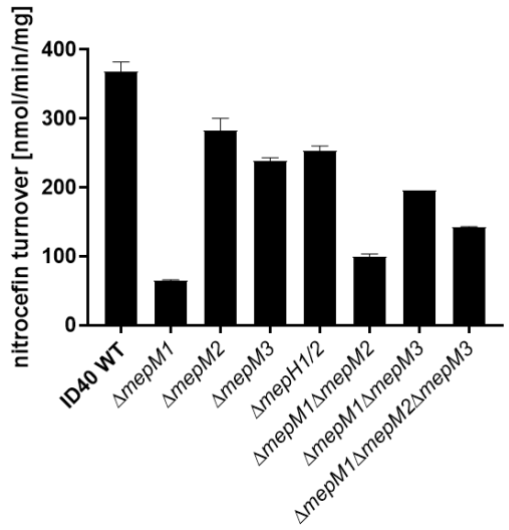

Figure 23: ***β-Lactamase Activity Assay of ID40 WT and the deletion mutants***

Absolute nitrocefin turnover is depicted in nmol/min/mg. The figure shows means and SDs of technical duplicates of one experiment. For cell lysis, bacteria were sonified with the sonificator for 5 min.

The different approaches of the nitrocefin assay lead to results with widely varying absolute numbers. To facilitate comparison between the different experiments, the absolute values were normalized to ID40 WT. Figure 24 shows a summary of all four conducted experiments using the relative nitrocefin turnover. Both, ID40 Δ*mepM1* and ID40 Δ*mepM1* Δ*mepM2* exhibited only 35% of the ID40 WT's β-lactamase activity. Further significant reductions could be noticed for ID40 Δ*mepM3* and ID40 Δ*mepM1* Δ*mepM2* Δ*mepM3*. The β-lactamase activity of ID40 Δ*mepM2, ID40* Δ*mepH1/2* and ID40 Δ*mepM1* Δ*mepM3* decreased only to a very small extent.

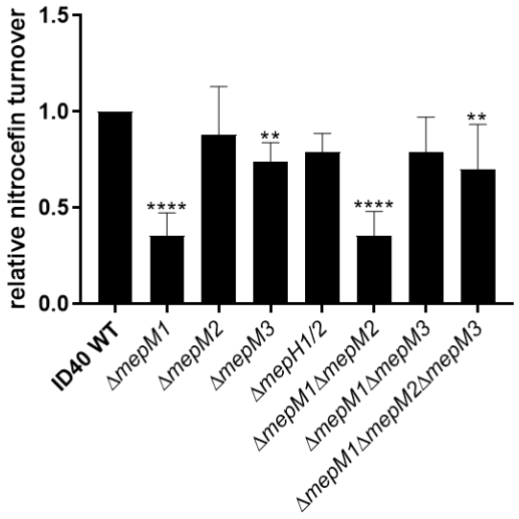

Figure 24: ***β-Lactamase Activity Assay of ID40 WT and the deletion mutants***

*The figure shows the results of the same experiments presented in Figure 21-23. To facilitate comparison of all four conducted experiments, relative nitrocefin turnover is depicted. The figure shows means and SDs of technical duplicates for each experiment. For cell lysis, four different approaches have been chosen. Bacteria were treated in the ultrasonic bath for 5 min or sonified either for 3 or 5 min. An ordinary one-way ANOVA was performed for each mutant strain in comparison to the WT (adjusted p-values: ** p < 0.01, **** p < 0.0001).*

To sum up, single deletion of *mepM1* and the double deletion of *mepM1* and *mepM2* lead to strongly reduced β-lactamase activities in all four experiments. However, their relative reduction in comparison to the ID40 WT varied. Opposed to our hypothesis, ID40 Δ*mepM1* Δ*mepM3,* ID40 Δ*mepM1* Δ*mepM2* Δ*mepM3* and ID40 Δ*mepH1/2* did not show significantly reduced β-lactamase activity. Moreover, the last experiment, in which the bacteria were sonified for 5 min, showed different results than the first experiments: all deletion mutants displayed lower β-lactamase activity. For example, the nitrocefin turnover of ID40 Δ*mepM1* Δ*mepM3* and ID40 Δ*mepM1* Δ*mepM2* Δ*mepM3* is about half as high as the turnover of ID40 WT. Furthermore, the absolute values of nitrocefin turnover are much higher.

3.3.4 Quantification of OprD porins

In *Pa*, OprD porins are commonly responsible for the uptake of carbapenems into the cells. Thus, reduced expression of OprD porins can lead to higher resistance against carbapenems. In order to find out, whether the expression level of OprD

porins in ID40 WT differs from the expression level in the deletion mutants, a Western Blot analysis was performed (see 2.3.14). Western Blot analysis can be applied to detect specific proteins displayed as bands on a nitrocellulose membrane (Figure 25A). The density of the bands could be determined using ImageJ software and correlates with the expression level of the protein. Therefore, by comparison of the band densities, a relative quantification can be achieved. To minimize errors due to differences regarding the initial loading amount, the ratio of the density of the OprD bands compared to density of the RpoB bands was calculated (Figure 25B). For this, it is assumed that the expression level of RpoB is the same in all strains.

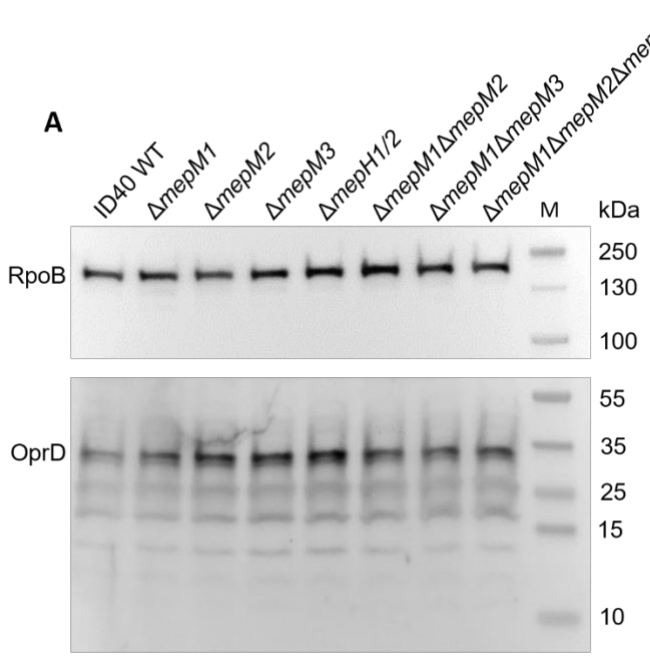

B

Strain	OprD/RpoB
ID40 WT	0,77112478
Δ*mepM1*	0,94672823
Δ*mepM2*	0,97282356
Δ*mepM3*	1,08440246
Δ*mepH1/2*	1,13122088
Δ*mepM1* Δ*mepM2*	0,77978224
Δ*mepM1* Δ*mepM3*	0,93563415
Δ*mepM1* Δ*mepM2* Δ*mepM3*	1,17585446

Figure 25: ***Western Blot analysis of OprD and RpoB of ID40 WT and the deletion mutants***

(A) *Image of the Western Blot of OprD and RpoB of ID40 WT and the deletion mutants; The bacteria were subcultured, grown for 3 hours and then harvested for the preparation of whole cell lysates. (B) Quantification of the bands displayed in the Western Blot analysis; For quantification, ImageJ software was used to assess the density of the different bands. To compensate differences in initially applied loading amount, the ratio of the densities of OprD bands in comparison with the RpoB bands was calculated.*

The picture (Figure 25A) of the Western Blot does not reveal any striking differences in expression of OprD. Furthermore, the calculated relative quantifications of ID40 WT and deletion mutants (Figure 25B) do not differ a lot.

3.3.5 Impact of the deletions on efflux of Hoechst 33342

Overexpression of efflux-pumps is one of the main resistance mechanisms of MDR *Pa*. To find out, if the increased susceptibility of the deletion mutants against β-lactam antibiotics is attributable to a reduced activity of efflux-pumps, an efflux assay was performed using Hoechst 33342 (see 2.2.6). This dye penetrates the bacterial cell wall and emits blue fluorescence when binding to dsDNA. Furthermore, it is a substrate of different efflux-pumps. Hence, the fluorescence signal reflects the proportion of influx and efflux. High activity of efflux-pumps would result in low fluorescence levels, as the dye would quickly be removed from the cell. Of this assay three independent experiments were implemented, each time measuring two technical replicates. PA14 strain was used as a control and reference, because of its low efflux activity. Dulbecco's PBS served as a blank and was subtracted from all values. Figure 26 shows the results representatively. The fluorescence levels are displayed in the course of 1 hour.

In the course of time, the fluorescence in PA14 rises gradually and then faster after about 10 minutes. The slope of the curve decreases again after about 30 minutes. The fluorescence in PA14 seems to reach a saturation stage. At the end of the measurement, the values are about 10-fold higher than in the beginning. The fluorescence of all other strains (ID40 WT and deletion mutants) stays at a very low level over the whole time of measurement. This means, that almost no Hoechst 33342 could bind to the dsDNA of these strains due to high efflux activity.

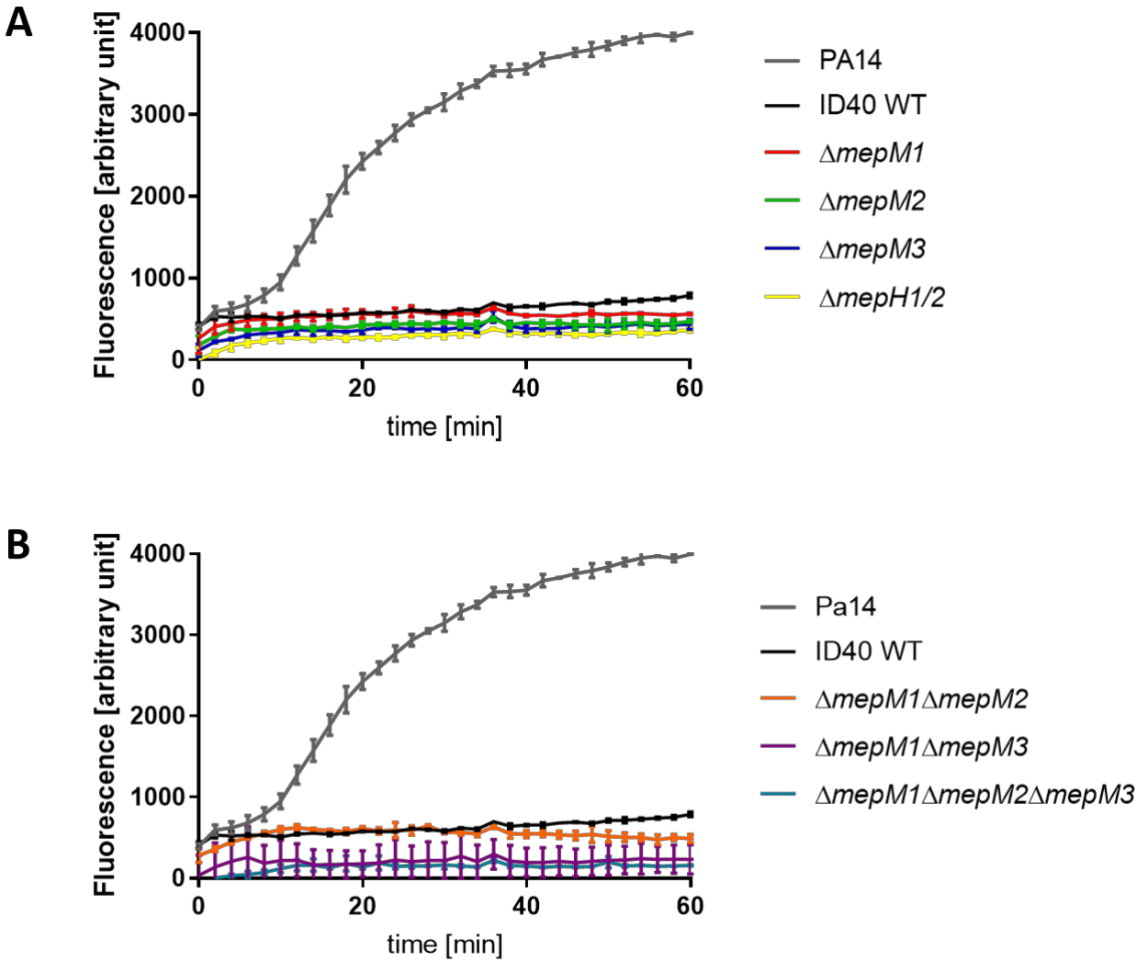

Figure 26: ***Efflux-activity in PA14, ID40 and the deletion mutants***

Representing efflux-activity, the graphs show the development of emitted fluorescence over a time range of 60 minutes. PA14 strain was used as a control and reference. The figure shows representatively the results of three independent experiments, each time measuring three technical replicates. The two graphs show data of the same experiment. To get a clear overview, the data were split into two graphs. Values for Dulbecco's PBS, which was used as a blank, were subtracted from each value. ***(A)*** *Figure 26A shows the results for PA14, ID40 WT and deletion mutants ID40 ΔmepM1, ID40 ΔmepM2, ID40 ΔmepM3 and ID40 ΔmepH1/2.* ***(B)*** *Figure 26B shows the results for PA14, ID40 WT and deletion mutants ID40 ΔmepM1 ΔmepM2, ID40 ΔmepM1 ΔmepM3 and ID40 ΔmepM1 ΔmepM2 ΔmepM3.*

4 Discussion

Aim of this work was the better characterization of the MEPs MepM1, MepM2, MepM3, MepH1 and MepH2 concerning their influence on resistance and growth of the MDR clinical isolate *Pa* ID40. Sequencing of this strain had revealed several common resistance genes like the β-lactamase genes *ampC* (PDC-3), *blalpoxB* and a point mutation in *dacB* encoding PBP4. As mutations in the *dacB* gene have been described to cause an increase of the MIC for CAZ from 1 µg/ml to 32 µl/ml in PAO1, it is presumably the main explanation for the resistance of ID40 against all β-lactam antibiotics (Sonnabend et al., 2019, Moya et al., 2009). Apart from *dacB*, many other genes are involved in resistance formation of *Pa*. The selection of the proteins analysed in this thesis was based on the TraDis results recently published by Sonnabend et al. Their resistome screening had identified several MEPs to play a role for resistance against FEP or MEM. For the further analysis of these enzymes, deletion mutants lacking the different endopeptidases were generated including the double mutants ID40 Δ*mepM1* Δ*mepM2,* ID40 Δ*mepM1* Δ*mepM3* and the triple deletion mutant ID40 Δ*mepM1* Δ*mepM2* Δ*mepM3* (see 3.1).

With the successfully generated deletion mutants, different tests were performed regarding growth and antibiotic resistance of the strains. In the following, the results of the tests on the deletion mutants and ID40 WT are discussed.

4.1 Deletions of *mepM* and *mepH* result in higher susceptibility to β-lactam antibiotics

Antibiotic resistance of MDR pathogens is a serious health threat. The development of new therapeutics for the so-called priority pathogens is one of the urgent concerns of the WHO. Among others, carbapenem-resistant *Pa* strains are ranked as pathogens of critical priority (Tacconelli et al., 2018). The treatment of *Pa* infections has always been complicated by the bacterium's high intrinsic resistance. In chronic infections, e.g. in patients with CF, the treatment is especially hampered, because *Pa* starts growing as a biofilm resulting in reduced sensitivity to antimicrobial therapeutics (Pang et al., 2019). In the clinical practice,

Pa infections are treated according to antibiograms with β-lactams, aminoglycosides or quinolones and with combinatory concepts of these antibiotics (Hof and Schlüter, 2019). Nevertheless, the number of MDR strains is increasing especially in south-eastern European countries. For infections with 4-MRGN (MDR gram negative) *Pa* a combinatory therapy with colistin and meropenem is suggested, even though colistin has strong side effects such as nephro- and neurotoxicity (Fritzenwanker et al., 2018). Thus, it seems obvious that new therapeutic strategies must be developed to further guarantee adequate treatment of *Pa* infections. The concept of adjuvants that help antibiotics to regain their effectiveness, has endured over years. For example, β-lactamase inhibitors such as sulbactam or clavulanic acid have been used in clinical practice for decades. In the course of time, however, resistances against these inhibitors have evolved (Bush and Bradford, 2016). Additionally, many of the clinically used β-lactamase inhibitors are not affecting the activity of β-lactamase AmpC, which is mainly responsible for resistance against β-lactams in *Pa* (Lister et al., 1999, Mayer, 2019). In search of new adjuvants, latest approaches target the induction pathway of the *ampC* gene, which is closely connected to the metabolism of the cell wall (Mayer, 2019; see 1.5). PG degradation products can bind to the transcriptional regulator AmpR, thereby inducing *ampC* expression and promoting resistance against β-lactams (Jacobs et al., 1997).

Peculiarly, inactivation of enzymes responsible for cell wall degradation can either strengthen or weaken the effect of β-lactam antibiotics. Whereas loss or mutation of PBP4 increases resistance, inactivation of the LT Slt leads to increased susceptibility to β-lactams (Moya et al., 2009, Lamers et al., 2015). In any case, several enzymes of the PG turnover appeared in the TraDis screening performed by Sonnabend et al. (2019) including DD-endopeptidases.

Since one of the aims of this work was to validate their results concerning the MEPs, microbroth dilution was conducted to determine the MICs of the different mutants (see 3.3.1). Of all single deletion mutants, ID40 Δ*mepM1* had the lowest MICs in accordance with the results of the TraDis screening by Sonnabend et al. Deletion of *mepM2* also resulted in higher susceptibility to β-lactam antibiotics,

corresponding to the predictions. A synergistic and striking effect could be observed for the double mutant ID40 Δ*mepM1* Δ*mepM2*, lowering all the MICs under the defined breakpoints with exception of imipenem. Regarding also the growth defect of this mutant, both MepM1 and MepM2 seem to act synergistically rather than redundantly. Deleting the operon *mepH1/2* caused decreased resistance against β-lactams, which is compatible with the lower read counts found in the TraDis for *mepH1* and *mepH2*. Whenever *mepM3* was deleted, the strains were slightly more sensitive than without the deletion. This minor effect could be reproduced in all three mutants carrying a deletion of *mepM3*. In conclusion, deletion of all those MEPs predicted to influence resistance against FEP or MEM, did in fact lower the MICs of β-lactams.

Our findings are in accordance with other results about the influence of PG endopeptidases on resistance determined for other species. To give an example, for *Ec*, it has been shown that overexpression of the MEPs MepS (homologue of *Pa* MepH1 and MepH2), MepM (homologue of *Pa* MepM1) and MepA promotes resistance against mecillinam (Lai et al., 2017). In addition, a *Vibrio cholerae* strain lacking the PG endopeptidase ShyA (homologue of *Ec* MepM) exhibited reduced viability and concomitantly lysed when it was exposed to β-lactams (Dörr et al., 2015). These findings further support our results that suggest MEPs to promote resistance against β-lactam antibiotics.

4.2 Deletion of *mepM1* leads to reduced β-lactamase activity and *ampC* expression

ID40, the MDR *Pa* strain used in this work, carries a point mutation in the *dacB* gene leading to a defective PBP 4, overproduction of AmpC and thereby to high resistance against β-lactam antibiotics (Sonnabend et al., 2019, Moya et al., 2009). Thus, we hypothesized that the decreased resistance after inactivation of certain endopeptidases might be due to a reduction of high AmpC levels. Moreover, previous experiments revealed lower *ampC* expression and β-lactamase activity for ID40 Δ*mepM1* (Sonnabend et al., 2019). For verification of the hypotheses, a qRT-PCR quantifying the expression of the *ampC* gene on

mRNA level and a nitrocefin assay providing information on β-lactamase activity were conducted.

Indeed, our experiments (see 3.3.2) confirmed lower expression levels of *ampC* for ID40 Δ*mepM1*. Additionally, ID40 Δ*mepH1/2* and the double and triple mutants containing a deletion of *mepM1* showed a reduction in *ampC* expression. However, the decrease in the double and triple mutants was not stronger compared to the *mepM1* single deletion mutant. Comparing the results to the determined MICs, it can be assumed that higher susceptibility of ID40 Δ*mepM1* and ID40 Δ*mepH1/2* is at least partly due to reduced *ampC* expression. However, another explanation must be found for the genes *mepM2* and *mepM3*, which do not seem to mediate their effect on resistance via reduced *ampC* expression levels. Furthermore, our expectations that the nitrocefin assay would confirm the results of the qRT-PCR were not quite fulfilled (see 3.3.3). Consistent to the expression levels of *ampC*, the results showed strongly reduced β-lactamase activity for ID40 Δ*mepM1 and* ID40 Δ*mepM1* Δ*mepM2* and no reduction for ID40 Δ*mepM2.* Yet, we see only a slightly reduced β-lactamase activity in ID40 Δ*mepH1/2,* ID40 Δ*mepM1* Δ*mepM3* and the triple mutant, which does not match with the numbers of the *ampC* expression levels. These contradictory results are hard to explain. One possible explanation could be that the performance of the β-lactamase activity assay was problematic. Looking at the results of the different approaches, it can be observed that the absolute amount of nitrocefin turnover varies a lot depending on how the cell lysis was performed. In addition, the result of the third approach is quite different with regard to the ratios of β-lactamase activity of the deletion mutants in comparison with the ID40 WT. Presumably, the first two approaches did not provide sufficient lysis of the bacteria. We suggest that the outcome of the cell lysis varied a lot due to differing cell wall stability among the mutants. Likely, the results of the last experiment can be assessed as being closest to the true numbers, because in this trial cell lysis was performed most thoroughly. Still, for some deletion mutants the results of the β-lactamase activity assay remain inconsistent to the determined MICs, *ampC* expression and our previous expectations. Why does the triple mutant yield higher β-lactamase activity than single deletion of mepM1, even though its MICs are much lower than

the MICs of ID40 Δ*mepM1*? Perhaps certain compensatory mechanisms are initialized by the bacteria, when *mepM3* is deleted. This theory would provide an explanation for the results of the β-lactamase activity assay. Further, it would elucidate why the ID40 Δ*mepM1* Δ*mepM2* has a much stronger growth deficit than the triple mutant (see 3.2). In any case, the β-lactamase activity assay should be repeated with sufficiently lysed bacteria.

Taking the studies of Lai et al. into account, it seems likely that the effect of the MEPs on resistance is not only mediated through *ampC* induction. As described before, overexpression of MEPs in *Ec* could promote resistance against mecillinam (Lai et al., 2017). Since *Ec* does not possess an inducible *ampC* gene (Honoré et al., 1986), another mechanism must lie behind the effects of the MEPs on resistance in *Ec*. Our additional experiments on the expression of the PoxB β-lactamase (3.3.2) or OprD porins (3.3.4) or on the efflux activity (3.3.5) did not provide further decisive explanations. Still, *Pa* employs several other resistance mechanisms (see 1.3) that could be influenced by MEPs. For example, only recently, it was shown that biofilm formation comes along with changes in the PG composition potentially mediated via enzymes degrading PG (Anderson et al., 2020). Hence, experiments on the influence of PG endopeptidases on biofilm formation might reveal new helpful information.

Furthermore, the analysis of knowledge on MEPs in other species might facilitate the development of new theories on how the enzymes influence resistance against β-lactams. Dörr et al. (2015) discovered that the MepM homologue of *Vibrio cholerae* ShyA promotes sphere formation and thereby antibiotic tolerance. They show that *Pa* can also turn into spherical phenotypes in response to meropenem suggesting that the underlying mechanisms might be similar to those in *Vibrio cholerae* (Dörr et al., 2015). Analogous to *Vibrio cholerae*, deletion of MEPs in *Pa* could reduce sphere formation and thereby antibiotic tolerance.

Moreover, knowledge about other enzymes of the PG recycling pathway might provide further ideas on how MEPs affect resistance. For example, the effect of the endopeptidases on the CreBC two-Component system could be investigated. The CreBC two-Component system is a global regulator of cell metabolism found

to play a role in β-lactam resistance. It is activated by *dacB* mutation or inactivation (Moya et al., 2009), so most likely the ID40 strain carries an activated CreBC two-component regulator. Former studies demonstrated that inactivation of other enzymes involved in the PG recycling such as NagZ or AmpG lead to an attenuation of CreBC-regulated gene expression elevated by *dacB* deletion (Zamorano et al., 2014). Maybe, MEPs do also diminish the activation of the CreBC two-component regulator thereby promoting resistance.

Besides, studies about LTs provide interesting theories that might be adaptable for MEPs as both enzymes likely function as PG degradative enzymes in the periplasm: the antisuicide hypothesis by Cavallari et al. (2013) suggests that deletion of LTs has a protective effect on bacteria challenged with β-lactams, because autolysis by these enzymes is inhibited. Accordingly, with exception of the LT Slt, absence of LTs usually results in increased resistance against β-lactams. In *Pa*, Slt deletion mutants show reduced MICs, but interestingly this effect is not due to reduced *ampC* expression (Lamers et al., 2015, Cavallari et al., 2013). It was discovered that deletion of Slt in *Ec* influences the futile cycle upon β-lactam treatment, leading to aberrant crosslinking of PG and thereby to lethal shape changes (Cho et al., 2014). Thus, it might be interesting to investigate whether MEPs influence the downstream processes caused by treatment with β-lactam antibiotics. Additionally, Lamers et al. (2015) performed assays on the permeability of the outer membrane and the integrity of the PG layer. Mutants lacking several membrane-bound LTs exhibited compromised cell envelopes. Whereas single deletion of membrane-bound LTs caused higher resistance against antibiotics, strains lacking several membrane-bound LTs showed increased sensitivity. The authors suggest that the impaired cell envelope effected the reduced resistance. In *Pa*, MepH1, MepH2 and MepM3 are also predicted to be lipoproteins anchored in the outer membrane (Srivastava et al., 2018). To investigate the effect of their deletion on the cell envelope of ID40 might be a good approach. For *Ec* there is some knowledge about how MEPs influence the cell envelope and its processes. As an example, it has been proposed that MEPs such as MepS promote the activity of certain PG synthases (e.g. PBP1b), thereby avoiding the lytic effect of mecillinam (Lai et al., 2017). As

proposed by Banzhaf et al. (see 1.7) the distinct interaction between the degrading hydrolases and the PG synthases might occur through complex formation. According to their results, MepM and MepS, but also PBP4 and PBP7 interact with an outer membrane lipoprotein called NlpI. In addition, an interaction between MepM and MepS is reported. Further, the authors describe the endopeptidases as “space-makers” for incorporation of new PG. Anyways, investigations on how the endopeptidases of *Pa* interact with the cell wall synthases and how their absence influences PG composition appears to be an interesting outlook. Another noteworthy fact is that for *Ec* MepM a subtle role in daughter cell separation was observed. Deletion of *mepM* together with other LytM factors appears to promote lysis upon ampicillin exposition due to a graduate loss of cell shape and integrity (Uehara et al., 2009). Accordingly, *Haemophilus influenzae* strains lacking the MepM homologue YebA exposed aberrant cell morphology but also defects in septum formation and in outer membrane stability. An increased release of outer membrane vesicles was observed (Ercoli et al., 2015). Curiously, *Ec* strains lacking *mepS* were shown to revert a hypervesiculation phenotype caused by deletion of the NlpI (Schwechheimer et al., 2015). Another publication reported that a *Salmonella typhimurium* strain displayed highly increased susceptibility to vancomycin in absence of its *Ec* MepS homologue Spr (Vestö et al., 2018). Usually, Gram-negative bacteria are intrinsically resistant against vancomycin, because it cannot pass their outer membrane. However, the authors suggest that the sensitivity is rather due to distortion of the bacterial cell wall than to higher permeability of the outer membrane. They emphasize the importance of complexes regulating the PG turnover and presume that interference with components of this regulation might lead to altered cell wall composition and thereby to higher sensitivity against antibiotics.

Thus, experiments on daughter cell separation, but also composition and integrity of the cell envelope including the outer membrane could help to understand the mechanisms leading to the susceptibility of our mutants.

To sum up, the increased susceptibility of the ID40 mutants could be explained to some extent by lower *ampC* expression. Furthermore, there are discrepancies between *ampC* expression and β-lactamase activity that remain unclear. It can only be assumed that the deletion of MEPs influences the interplay of other resistance mechanisms, regulatory systems and compensation processes leading to the demonstrated results. In *Pa*, there is still not much knowledge about MEPs and their interactions with each other, but also with other enzymes involved in PG turnover. The findings of Banzhaf et al. (2020) propose a very remarkable and complex interplay of the different enzymes acting in the periplasm. To further understand these interactions should be one focus of future investigation in this field.

4.3 Murein endopeptidases as potential inhibitor targets

The overall goal of this work was the characterization of MEPs and their assessment as targets for adjuvants that re-sensitize MDR *Pa* strains for the treatment with β-lactam antibiotics. The concept of adjuvants implies a potentiation of the activity of the β-lactams through a new compound/inhibitor extending the efficacy spectrum of the antibiotic treatment to MDR strains. Before, other enzymes of the PG recycling pathway have been identified as potential targets for therapeutic adjuvants and for NagZ several inhibitors have been developed (Stubbs et al., 2013). Additionally, LTs and especially Slt are proposed to be suited for targeting (Lamers et al., 2015). Dörr et al. (2015) even suggest the inhibition of ShyA, *Vibrio cholerae's* MepM (*Ec*) homologue, to be a promising approach for the development of new antimicrobial therapies.

In our work, it could indeed be proven that deletion of MepM or MepH proteins causes weakened resistance of *Pa* ID40. The strongest effect of a single deletion mutant on the resistance profile could be observed for deletion mutants lacking *mepM1*. This gene encodes a metallopeptidase of the LytM family, cleaving D-Ala-*m*DAP cross-links (Singh et al., 2012). Consistent with results generated by Sonnabend et al., deletion of *mepM1* resulted in clearly reduced β-lactamase activity and *ampC* expression. Of all examined endopeptidases, deletion of *mepM1* seems to most effectively restore the sensitivity of MDR *Pa* strains.

Targeting more than one of the endopeptidases, however, appears to be a much more potent strategy as proposed by Sonnabend et al. In *Ec*, deletion of the MepM1 homologue MepM together with the endopeptidase MepS was discovered to be lethal (Singh et al., 2012). Besides, for *Vibrio cholerae*, the endopeptidases ShyA and ShyC are essential for growth (Dörr et al., 2013). Even in Gram-positive species (*Bacillus subtilis*) lack of PG endopeptidases causes lethality (Hashimoto et al., 2012). Anyways, these findings enhance the essential role of PG endopeptidases for viability and growth of certain bacteria. Perhaps, absence of the endopeptidases affects the bacterial fitness due to an impaired energy metabolism caused by diminished PG recycling. In accordance with this knowledge, we did not achieve to generate the mutants ID40 Δ*mepM1* Δ*mepH1/2* and ID40 Δ*mepM1* Δ*mepM3* Δ*mepH1/2*. Possibly, the unsuccessful mutagenesis indicates that these endopeptidases are essential for growth and viability of *Pa*. However, to verify this assumption for *Pa*, conditional mutants with inducible genes should be created and their growth should be observed with and without the inducing substance. Combinatory targeting of MepM1, MepH1/2 (and MepM3) seems like a promising approach, which is worth to be verified. What needs to be taken into account, are the regulatory processes of these enzymes: it was shown that MepM1 just as MepH1, MepH2 and MepM3 is inactivated by the carboxy-terminal processing protease CtpA. A *ctpA* deficient mutant of *Pa* exhibited a less virulent phenotype including defective type III secretion system, low salt sensitivity and enhanced surface attachment. An additional deletion of *mepM1* reverted all these phenotypes with exception of the low salt sensitivity (Srivastava et al., 2018). Thus, absence of several substrates of CtpA might lead to enhanced virulence of the *Pa* strains. On the contrary, it has been discovered that in *Yersinia pestis* the MepM homologue YebA is contributing to the virulence of the pathogen. Mice infected with *Yersinia pestis* strains showed strongly reduced mortality when *yebA* was knocked out (Pradel et al., 2014). Hence, to further assess the adequacy of CtpA substrates as targets for antibiotic adjuvants, it should be investigated whether their absence results in changes regarding virulence of *Pa*.

Another combination of MEPs appears worth targeting: double deletion of *mepM1* and *mepM2* had a rather synergistic effect in the microbroth dilution assay, breaking resistance against all tested β-lactam antibiotics except imipenem according to the EUCAST breakpoints. Further deletion of *mepM3* even decreased the MICs slightly more. In addition, ID40 Δ*mepM1* Δ*mepM2* showed a growth deficit in LB medium. Curiously, the mechanisms behind the effects of *mepM2* or *mepM3* deletion remained unclear. Our hypothesis that absence of *mepM2* and *mepM3* would also lead to reduced *ampC* expression was not confirmed. Even though more investigation should be conducted on this behalf, the high susceptibility of the double and triple mutants indicates suitability of combinatory targeting of MepM1, MepM2 and perhaps MepM3. For better estimation on whether it is realistic to develop an inhibitor for several MEPs additional investigation on the exact protein structures should be performed. What we know is that MepM1, MepM2 and MepM3 share the LytM domain defining their active sites (Yakhnina et al., 2015). Structure analyses by Dr. Thales Kronenberger have revealed MepM1 and MepM2 to possess highly similar active catalytic centres forming druggable grooves. Initial in silico analyses, using the available crystal structure of *Pa* MepM2, with docking of the Gly_4Phosphinate (a known inhibitor of *Staphylococcus aureus* LytM, (Grabowska et al., 2015)) followed by molecular dynamics revealed a stable interaction between the phosphinate moiety with the zinc ion located in the active site along the 500 ns of simulation (see 1.8). As a follow-up step virtual screening studies are being conducted to discover potential MEP-inhibitors, using commercially available compound libraries and our in-house computational framework combining docking followed by molecular dynamics simulation of the potential hits. To get further insight about the enzyme's structures, alignments and determination of pairwise identities were performed in our work group. Details about these analyses can be found in the appendix.

The alignment of the endopeptidases belonging to the NlpC/P60 family uncovered MepH1 and MepH2 to be homologues. Both enzymes are predicted to be outer membrane lipoproteins and have also strong similarity with *Ec* MepS (Srivastava et al., 2018). Moreover, there is a homology of the NlpC/P60

endopeptidase domain of MepH1 and MepH2 with *Ec* MepH. Alignments and pairwise identity analysis of the endopeptidases carrying LytM domains yielded high homology between *Ec* MepM and *Pa* MepM1 as described by Srivastava et al. (2018). Both enzymes are predicted to contain a LysM domain, suspected to be responsible for PG binding. All the LytM proteins used in this work were identified to have an actively catalysing LytM domain (Yakhnina et al., 2015). The C-terminal region of the proteins including the active sites with LytM domains was further analysed. The M23 peptidase domain seems to be highly conserved in MepM1, MepM2 and MepM3. Additionally, MepM2 and MepM3 possibly dispose transmembrane helices, so they might be located at the inner membrane of *Pa*. However, the N-terminal regions of the *Pa* MepM proteins show differences and their significance for the protein's functions and potential regulations remain unclear.

Even though combinatory targeting of several MEPs shows great potential, much more knowledge is still required for a convincing assessment. How applicable are our results for other *Pa* strains e.g. strains, which do not overproduce *ampC* like ID40 does? It might be necessary to confirm the results with other *Pa* strains. Besides, the effect of the inhibitor on other species should be estimated. If bacterial species carry homologues of the MEPs, the potential inhibitor more likely might affect them. This is important to forecast the possible application of the inhibitor as treatment of infections with other pathogens, but also to predict side effects of the inhibitor on the physiological flora of patients. An additional inhibitory effect on enteropathogenic *Vibrio cholerae* or *Ec* would be desirable. As mentioned before, both species provide homologues of MEPs. However, many *Ec* strains also form part of the intestinal microbiota, importantly producing vitamin K (Hof and Schlüter, 2019). The physiological microbiota in the gut or in the lung protects the patients against colonization with pathogens and its disturbance upon antibiotic treatment should be minimised (Kamada et al., 2013, Stokell et al., 2015). Especially immunocompromised patients should not be exposed to higher risks of secondary infections during treatment with the potential inhibitor.

As described in 1.6, other players of the PG recycling pathway have been successfully tested as targets for helper drugs. Mutants lacking either NagZ or the permease AmpG reverted β-lactam resistance in vivo (Torrens et al., 2019). For NagZ the first inhibitors have been developed (Stubbs et al., 2013) and for AmpG potential inhibitors have been identified (Collia et al., 2018). However, it has been very challenging to find selective inhibitors, which do not simultaneously provide inhibition of related human enzymes (Stubbs et al., 2013). In addition, the high impermeability of the outer membrane of *Pa* (Bellido et al., 1992) complicates the uptake of adjuvant molecules. A possible solution for the latter problem could be to add subinhibitory concentrations of the permeabilizing agent colistin (Torrens et al., 2017). Other approaches on how to bypass the bacterial cell envelope are being investigated (Zgurskaya et al., 2015). Unlike inhibitors of NagZ, adjuvants targeting MEPs would not have to cross the inner membrane as they are presumably located in the periplasm. Another enzyme of the PG degradative process, which is rated to be a promising target for the development of adjuvants is the LT Slt. Just like our approach of targeting several MEPs simultaneously, one concept developed for the target Slt includes a combinatory inhibition of several enzymes: Bulgecin A is a selective inhibitor of the LTs Slt, MltD, and MltG (Dik et al., 2019). Combinatory treatment of the MDR *Pa* strain PAO1 with β-lactams and Bulgecin A could reduce the MICs 2- to 4-fold (Dik et al., 2019) and suppresses the growth of carbapenem-resistant clinical isolates of *Pa* (Skalweit and Li, 2016). These results confirm the potency of different enzymes of the PG turnover as targets for future antimicrobial therapy.

In summary, the strategy of developing adjuvants that restore the efficiency of antibiotics has been tried and tested with great success. In search of new targets for helper drugs, enzymes of the cell wall metabolism have been identified to be well suited. This work has provided first insights on how MEPs influence resistance of the MDR clinical isolate ID40. Taking all the results into account, we estimate that an inhibitor targeting several MEPs appears to have great potential. The simultaneous knock-out of *mepM1* and *mepM2* could restore sensitivity against many clinically relevant β-lactam antibiotics. Structure analyses suggest both proteins to carry very similar active sites and the development of a

substance that inhibits both enzymes seems a realistic goal. An advantage over inhibitors of NagZ, which acts in the cytosol, is that the MEPs are presumably located in the periplasm. Thus, the inhibitor would only have to pass the outer membrane of the bacterium. However, the development and approval of such an inhibitor still requires much more investigation, for example on selectivity and activity spectrum of the inhibitor or on possible side effects.

The struggle between consistently emerging resistances on the one hand and the development of new antibiotics on the other will continue. Nevertheless, the broad variety of developing antimicrobial therapies including our own approach gives us hope for future combats with MDR pathogens.

5 Summary

Pseudomonas aeruginosa (*Pa*) is a Gram-negative, rod-shaped bacterium, which can infect a broad variety of human tissues. Infections with the opportunistic pathogen mostly occur in nosocomial settings, e.g. during artificial ventilation of patients. Especially for immunocompromised patients, infections with *Pa* can become life-threatening. Just like in other species, the prevalence of MDR *Pa* strains is rising continuously. The bacterium possesses several intrinsic and acquired resistances, which often hamper the treatment with conventional antibiotics. Main resistance mechanisms of *Pa* are the low permeability of its outer membrane as well as the expression of the inducible β-lactamase AmpC. To further guarantee appropriate treatment of infections with *Pa*, investigation on new therapeutic strategies is urgently needed. The concept of using a common antibiotic in combination with an adjuvant that helps to mediate the antibiotic effect even in resistant strains, has been clinically proven over many years. Combining β-lactam antibiotics with β-lactamase inhibitors such as clavulanic acid or tazobactam has been a very successful result of this conception. A new approach includes interference with the induction pathway of the β-lactamase AmpC. The regulation of the *ampC* gene is depending on intermediate products of the cell wall metabolism. Therefore, enzymes such as murein endopeptidases (MEPs), which cleave crosslinks between murein moieties, might be suited as targets for the development of antibiotic adjuvants.

In this work, the influence of MEPs on resistance and growth of MDR clinical isolate ID40 was evaluated. The aim was to submit a first assessment on whether MEPs might serve as potential targets. As a first step deletion mutants of ID40 lacking the different endopeptidases MepM1, MepM2, MepM3, MepH1 and MepH2 were generated. Moreover, the generation of double mutants (ID40 Δ*mepM1* Δ*mepM2*, ID40 Δ*mepM1* Δ*mepM3*) and a triple mutant (ID40 Δ*mepM1* Δ*mepM2* Δ*mepM3*) were implemented. A recently published study by Sonnabend et al. had predicted the MEPs to be involved in resistance of ID40 against cefepime and meropenem. These predictions could be confirmed by tests on

susceptibility of the mutants, which were performed in this work: all deletion mutants showed lower minimal inhibitory concentrations than the ID40 wildtype. The strongest impact could be observed for the deletion of *mepM1*. Strikingly, additional deletion of *mepM2* had a great synergistic effect, breaking resistance against all selected β-lactam antibiotics with exception of imipenem. To find out about the mechanisms behind these effects regarding susceptibility, further experiments were conducted. Expression of *ampC* and β-lactamase activity were clearly reduced in mutants lacking *mepM1*. However, deletion of the other MEPs does not seem to strongly influence the activity of the β-lactamase AmpC. The mechanisms leading to higher susceptibility of the other mutants could not be uncovered. Investigation on the presumably complex interactions of the different enzymes acting in the periplasm of *Pa* might reveal more information as to how MEPs affect resistance against β-lactams. Possibly, deletion of the endopeptidases alters the composition of the bacterial cell envelope, thereby attenuating resistance.

To conclude, the development of an agent that inhibits MepM1 as well as MepM2 seems like a promising approach. Both proteins belong to the same protein family and possess similar active sites. That is why it appears to be a realistic goal to find an inhibitor, which can simultaneously bind to both enzymes. For a final assessment, however, more research regarding protein structures and functionality of MEPs needs to be performed.

6 Deutsche Zusammenfassung

Pseudomonas aeruginosa (*Pa*) ist ein Gram-negatives Stäbchenbakterium, das verschiedenste menschliche Gewebe infizieren kann. Der opportunistische Keim gehört zu den häufigsten nosokomialen Erregern und stellt besonders für immungeschwächte Patient*Innen eine Bedrohung dar. Wie bei vielen anderen Pathogenen ist die Prävalenz von Infektionen mit multiresistenten *Pa* Stämmen steigend. *Pa* besitzt verschiedene intrinsische und erworbene Resistenzen, die die Behandlung mit herkömmlichen Antibiotika erschweren. Dabei spielt vor allem die geringe Permeabilität der äußeren Membran und die induzierbare Expression der β-Laktamase AmpC eine Rolle. Um die Behandlung von Infektionen mit *Pa* weiterhin zu gewährleisten, scheint es dringend notwendig an der Entwicklung neuer antimikrobieller Therapien zu forschen. Ein mittlerweile über viele Jahre erprobtes Konzept ist die Gabe eines bekannten Antibiotikums in Kombination mit einer weiteren Substanz, die die Wirkung des Antibiotikums bei sonst resistenten Bakterien wiederherstellt. Zu dieser Therapiestrategie zählt zum Beispiel die klinisch sehr etablierte Verabreichung eines β-Laktam Antibiotikums in Kombination mit einem β-Laktamase-Inhibitor wie Tazobactam oder Clavulansäure. Ein neuer Ansatz sieht das Eingreifen in den Induktionsweg der β-Laktamase AmpC vor. Da die Regulation des *ampC*-Gens vom Zellwand-Stoffwechsel abhängig ist, könnten Enzyme des Peptidoglykan-Abbaus, wie z.B. Murein-Endopeptidasen (MEPs), mögliche Angriffspunkte sein.

In dieser Arbeit wurde untersucht, inwieweit MEPs Resistenz und Wachstum des klinischen *Pa* Isolats ID40 beeinflussen. Dabei war das übergeordnete Ziel die Beurteilung der MEPs als potenzielle Targets in der Entwicklung neuer Wirkstoffe. Hierzu wurden im ersten Schritt mithilfe eines Allel-Austausches Mutanten des ID40 Stammes generiert, die Deletionen der Endopeptidasen MepM1, MepM2, MepM3, MepH1 und MepH2 aufwiesen. Des Weiteren wurden auch Doppelmutanten (ID40 Δ*mepM1* Δ*mepM2*, ID40 Δ*mepM1* Δ*mepM3*) und eine Tripelmutante (ID40 Δ*mepM1* Δ*mepM2* Δ*mepM3*) hergestellt. Vorangegangene Experimente (Sonnabend et al.) hatten vermuten lassen, dass Murein-Endopeptidasen an der Resistenz von *Pa* gegenüber Cefepim und

Meropenem beteiligt sind. Die Annahme konnte in dieser Arbeit bestätigt werden: Für alle Deletionsmutanten ergaben sich niedrigere minimale Hemmstoffkonzentrationen im Vergleich zum ID40 Wildtyp. Den stärksten Effekt zeigte hierbei die Deletion von *mepM1*. Als besonders vielversprechend erwies sich allerdings die simultane Deletion von *mepM1* und *mepM2*. Die minimalen Hemmstoffkonzentrationen der entsprechende Doppelmutante zeigten mit Ausnahme von Imipenem für alle ausgewählten β-Laktam Antibiotika Werte unterhalb der EUCAST Grenzwerte. Untersuchungen bezüglich der *ampC* Expression und der β-Laktamase-Aktivität der Mutanten resultierten in z.T. widersprüchlichen Ergebnissen. Eindeutig war jedoch festzustellen, dass die Deletion von *mepM1* sowohl die *ampC* Expression als auch die β-Laktamase-Aktivität deutlich senken konnte. Welche Mechanismen sich hinter den Effekten der anderen Deletionsmutanten verbergen, konnte nicht abschließend geklärt werden. Es liegt die Vermutung nahe, dass sich im Periplasma von *Pa* ein komplexes Zusammenspiel von Enzymen des Peptidoglykan-Stoffwechsels ereignet, dessen Prozesse noch weitestgehend im Dunkeln liegen. Außerdem könnte sich eine Deletion von MEPs auch auf die Komposition der bakteriellen Zellhülle auswirken. Diesbezüglich sollte noch weitere Forschung betrieben werden.

Die Entwicklung eines Inhibitors, der sowohl MepM1 als auch MepM2 blockiert, scheint ein vielversprechender Ansatz zu sein. Da beide Proteine zur selben Proteinfamilie gehören und sehr ähnliche aktive Zentren besitzen, ist es durchaus realistisch einen solchen Inhibitor zu finden. Für die abschließende Beurteilung ist es jedoch ratsam noch weitere Untersuchungen hinsichtlich der Proteinstrukturen und der Funktionalität der MEPs durchzuführen.

7 Reference list

ANDERSON, E. M., SYCHANTHA, D., BREWER, D., CLARKE, A. J., GEDDES-MCALISTER, J. & KHURSIGARA, C. M. 2020. Peptidoglycomics reveals compositional changes in peptidoglycan between biofilm- and planktonic-derived Pseudomonas aeruginosa. *J Biol Chem,* 295**,** 504-516.

ARMOUR, A. D., SHANKOWSKY, H. A., SWANSON, T., LEE, J. & TREDGET, E. E. 2007. The impact of nosocomially-acquired resistant Pseudomonas aeruginosa infection in a burn unit. *J Trauma,* 63**,** 164-71.

ASGARALI, A., STUBBS, K. A., OLIVER, A., VOCADLO, D. J. & MARK, B. L. 2009. Inactivation of the glycoside hydrolase NagZ attenuates antipseudomonal beta-lactam resistance in Pseudomonas aeruginosa. *Antimicrob Agents Chemother,* 53**,** 2274-82.

AZGHANI, A. O. 1996. Pseudomonas aeruginosa and epithelial permeability: role of virulence factors elastase and exotoxin A. *Am J Respir Cell Mol Biol,* 15**,** 132-40.

BANZHAF, M., YAU, H. C., VERHEUL, J., LODGE, A., KRITIKOS, G., MATEUS, A., CORDIER, B., HOV, A. K., STEIN, F., WARTEL, M., PAZOS, M., SOLOVYOVA, A. S., BREUKINK, E., VAN TEEFFELEN, S., SAVITSKI, M. M., DEN BLAAUWEN, T., TYPAS, A. & VOLLMER, W. 2020. Outer membrane lipoprotein NlpI scaffolds peptidoglycan hydrolases within multi-enzyme complexes in Escherichia coli. *Embo j,* 39**,** e102246.

BARRETEAU, H., KOVAC, A., BONIFACE, A., SOVA, M., GOBEC, S. & BLANOT, D. 2008. Cytoplasmic steps of peptidoglycan biosynthesis. *FEMS Microbiol Rev,* 32**,** 168-207.

BELLIDO, F., MARTIN, N. L., SIEHNEL, R. J. & HANCOCK, R. E. 1992. Reevaluation, using intact cells, of the exclusion limit and role of porin OprF in Pseudomonas aeruginosa outer membrane permeability. *J Bacteriol,* 174**,** 5196-203.

BERRAZEG, M., JEANNOT, K., NTSOGO ENGUENE, V. Y., BROUTIN, I., LOEFFERT, S., FOURNIER, D. & PLESIAT, P. 2015. Mutations in beta-Lactamase AmpC Increase Resistance of Pseudomonas aeruginosa Isolates to Antipseudomonal Cephalosporins. *Antimicrob Agents Chemother,* 59**,** 6248-55.

BERUBE, B. J., RANGEL, S. M. & HAUSER, A. R. 2016. Pseudomonas aeruginosa: breaking down barriers. *Curr Genet,* 62**,** 109-13.

BIOVISION Beta-Lactamase Activity Colorimetric Assay Kit.

BOTELHO, J., GROSSO, F. & PEIXE, L. 2019. Antibiotic resistance in Pseudomonas aeruginosa - Mechanisms, epidemiology and evolution. *Drug Resist Updat,* 44**,** 100640.

BOUHSS, A., CROUVOISIER, M., BLANOT, D. & MENGIN-LECREULX, D. 2004. Purification and characterization of the bacterial MraY translocase catalyzing the first membrane step of peptidoglycan biosynthesis. *J Biol Chem,* 279**,** 29974-80.

BRAUN, V., GÖTZ, F., SCHULTZ, J. E. & WOHLLEBEN, W. 2015. The bacterial cell envelope: structure, function, and infection interface. *Int J Med Microbiol,* 305**,** 175-7.

BRAZ, V. S., FURLAN, J. P., FERNANDES, A. F. & STEHLING, E. G. 2016. Mutations in NalC induce MexAB-OprM overexpression resulting in high level of aztreonam resistance in environmental isolates of Pseudomonas aeruginosa. *FEMS Microbiol Lett,* 363.

BREIDENSTEIN, E. B., DE LA FUENTE-NUNEZ, C. & HANCOCK, R. E. 2011. Pseudomonas aeruginosa: all roads lead to resistance. *Trends Microbiol,* 19**,** 419-26.

BROWN, K., VIAL, S. C., DEDI, N., WESTCOTT, J., SCALLY, S., BUGG, T. D., CHARLTON, P. A. & CHEETHAM, G. M. 2013. Crystal structure of the Pseudomonas aeruginosa MurG: UDP-GlcNAc substrate complex. *Protein Pept Lett,* 20**,** 1002-8.

BRUCHMANN, S., DOTSCH, A., NOURI, B., CHABERNY, I. F. & HAUSSLER, S. 2013. Quantitative contributions of target alteration and decreased drug accumulation to Pseudomonas aeruginosa fluoroquinolone resistance. *Antimicrob Agents Chemother,* 57**,** 1361-8.

BURNS, J. L., GIBSON, R. L., MCNAMARA, S., YIM, D., EMERSON, J., ROSENFELD, M., HIATT, P., MCCOY, K., CASTILE, R., SMITH, A. L. & RAMSEY, B. W. 2001. Longitudinal assessment of Pseudomonas aeruginosa in young children with cystic fibrosis. *J Infect Dis,* 183**,** 444-52.

BUSH, K. & BRADFORD, P. A. 2016. β-Lactams and β-Lactamase Inhibitors: An Overview. *Cold Spring Harb Perspect Med,* 6.

CABOT, G., OCAMPO-SOSA, A. A., TUBAU, F., MACIA, M. D., RODRIGUEZ, C., MOYA, B., ZAMORANO, L., SUAREZ, C., PENA, C., MARTINEZ-MARTINEZ, L. & OLIVER, A. 2011. Overexpression of AmpC and efflux pumps in Pseudomonas aeruginosa isolates from bloodstream infections: prevalence and impact on resistance in a Spanish multicenter study. *Antimicrob Agents Chemother,* 55**,** 1906-11.

CAVALLARI, J. F., LAMERS, R. P., SCHEURWATER, E. M., MATOS, A. L. & BURROWS, L. L. 2013. Changes to its peptidoglycan-remodeling enzyme repertoire modulate beta-lactam resistance in Pseudomonas aeruginosa. *Antimicrob Agents Chemother,* 57**,** 3078-84.

CENTRES FOR DISEASE CONTROL AND PREVENTION. 2019. ANTIBIOTIC RESISTANCE THREATS IN THE UNITED STATES 2019.

CHATTERJEE, M., ANJU, C. P., BISWAS, L., ANIL KUMAR, V., GOPI MOHAN, C. & BISWAS, R. 2016. Antibiotic resistance in Pseudomonas aeruginosa and alternative therapeutic options. *Int J Med Microbiol,* 306**,** 48-58.

CHO, H., UEHARA, T. & BERNHARDT, T. G. 2014. Beta-lactam antibiotics induce a lethal malfunctioning of the bacterial cell wall synthesis machinery. *Cell,* 159**,** 1300-11.

COLDHAM, N. G., WEBBER, M., WOODWARD, M. J. & PIDDOCK, L. J. V. 2010. A 96-well plate fluorescence assay for assessment of cellular permeability and active efflux in Salmonella enterica serovar Typhimurium and Escherichia coli. *Journal of Antimicrobial Chemotherapy,* 65**,** 1655-1663.

COLLIA, D., BANNISTER, T. D., TAN, H., JIN, S., LANGAEE, T., SHUMATE, J., SCAMPAVIA, L. & SPICER, T. P. 2018. A Rapid Phenotypic Whole-Cell Screening Approach for the Identification of Small-Molecule Inhibitors That Counter β-Lactamase Resistance in Pseudomonas aeruginosa. *SLAS Discov,* 23**,** 55-64.

European Centre of Disease Prevention and Control 2019. Healthcare-associated infections acquired in intensive care units; Annual Epidemiological Report for 2017.

DAURY, L., ORANGE, F., TAVEAU, J. C., VERCHERE, A., MONLEZUN, L., GOUNOU, C., MARREDDY, R. K., PICARD, M., BROUTIN, I., POS, K. M. & LAMBERT, O. 2016. Tripartite assembly of RND multidrug efflux pumps. *Nat Commun,* 7**,** 10731.

DHAR, S., KUMARI, H., BALASUBRAMANIAN, D. & MATHEE, K. 2018. Cell-wall recycling and synthesis in Escherichia coli and Pseudomonas aeruginosa - their role in the development of resistance. *J Med Microbiol,* 67**,** 1-21.

DIK, D. A., MADUKOMA, C. S., TOMOSHIGE, S., KIM, C., LASTOCHKIN, E., BOGGESS, W. C., FISHER, J. F., SHROUT, J. D. & MOBASHERY, S. 2019. Slt, MltD, and MltG of Pseudomonas aeruginosa as Targets of Bulgecin A in Potentiation of β-Lactam Antibiotics. *ACS Chem Biol,* 14**,** 296-303.

DONLAN, R. M. 2002. Biofilms: microbial life on surfaces. *Emerg Infect Dis,* 8**,** 881-90.

DÖRR, T., CAVA, F., LAM, H., DAVIS, B. M. & WALDOR, M. K. 2013. Substrate specificity of an elongation-specific peptidoglycan endopeptidase and its implications for cell wall architecture and growth of Vibrio cholerae. *Mol Microbiol,* 89**,** 949-62.

DÖRR, T., DAVIS, B. M. & WALDOR, M. K. 2015. Endopeptidase-mediated beta lactam tolerance. *PLoS Pathog,* 11**,** e1004850.

DOUAFER, H., ANDRIEU, V., PHANSTIEL, O. T. & BRUNEL, J. M. 2019. Antibiotic Adjuvants: Make Antibiotics Great Again! *J Med Chem,* 62**,** 8665-8681.

DOYLE, R. J., CHALOUPKA, J. & VINTER, V. 1988. Turnover of cell walls in microorganisms. *Microbiol Rev,* 52**,** 554-67.

DRAWZ, S. M. & BONOMO, R. A. 2010. Three decades of beta-lactamase inhibitors. *Clin Microbiol Rev,* 23**,** 160-201.

EICHENBERGER, E. M. & THADEN, J. T. 2019. Epidemiology and Mechanisms of Resistance of Extensively Drug Resistant Gram-Negative Bacteria. *Antibiotics (Basel),* 8.

ERCOLI, G., TANI, C., PEZZICOLI, A., VACCA, I., MARTINELLI, M., PECETTA, S., PETRACCA, R., RAPPUOLI, R., PIZZA, M., NORAIS, N., SORIANI, M. & ARICÒ, B. 2015. LytM proteins play a crucial role in cell separation, outer membrane composition, and pathogenesis in nontypeable Haemophilus influenzae. *mBio,* 6**,** e02575.

FASANI, R. A. & SAVAGEAU, M. A. 2015. Unrelated toxin-antitoxin systems cooperate to induce persistence. *J R Soc Interface,* 12**,** 20150130.

FERNANDEZ, L., BREIDENSTEIN, E. B. & HANCOCK, R. E. 2011. Creeping baselines and adaptive resistance to antibiotics. *Drug Resist Updat,* 14**,** 1-21.

FIRCZUK, M., MUCHA, A. & BOCHTLER, M. 2005. Crystal structures of active LytM. *J Mol Biol,* 354**,** 578-90.

FRITZENWANKER, M., IMIRZALIOGLU, C., HEROLD, S., WAGENLEHNER, F. M., ZIMMER, K. P. & CHAKRABORTY, T. 2018. Treatment Options for

Carbapenem- Resistant Gram-Negative Infections. *Dtsch Arztebl Int,* 115**,** 345-352.

GELLATLY, S. L. & HANCOCK, R. E. 2013. Pseudomonas aeruginosa: new insights into pathogenesis and host defenses. *Pathog Dis,* 67**,** 159-73.

GIBSON, D. G., YOUNG, L., CHUANG, R. Y., VENTER, J. C., HUTCHISON, C. A., 3RD & SMITH, H. O. 2009. Enzymatic assembly of DNA molecules up to several hundred kilobases. *Nat Methods,* 6**,** 343-5.

GIL-PEROTIN, S., RAMIREZ, P., MARTI, V., SAHUQUILLO, J. M., GONZALEZ, E., CALLEJA, I., MENENDEZ, R. & BONASTRE, J. 2012. Implications of endotracheal tube biofilm in ventilator-associated pneumonia response: a state of concept. *Crit Care,* 16**,** R93.

GISIN, J., SCHNEIDER, A., NAGELE, B., BORISOVA, M. & MAYER, C. 2013. A cell wall recycling shortcut that bypasses peptidoglycan de novo biosynthesis. *Nat Chem Biol,* 9**,** 491-3.

GRABOWSKA, M., JAGIELSKA, E., CZAPINSKA, H., BOCHTLER, M. & SABALA, I. 2015. High resolution structure of an M23 peptidase with a substrate analogue. *Sci Rep,* 5**,** 14833.

HANCOCK, R. E. & SPEERT, D. P. 2000. Antibiotic resistance in Pseudomonas aeruginosa: mechanisms and impact on treatment. *Drug Resist Updat,* 3**,** 247-255.

HANDFIELD, J., GAGNON, L., DARGIS, M. & HULETSKY, A. 1997. Sequence of the ponA gene and characterization of the penicillin-binding protein 1A of Pseudomonas aeruginosa PAO1. *Gene,* 199**,** 49-56.

HASHIMOTO, M., OOIWA, S. & SEKIGUCHI, J. 2012. Synthetic lethality of the lytE cwlO genotype in Bacillus subtilis is caused by lack of D,L-endopeptidase activity at the lateral cell wall. *J Bacteriol,* 194**,** 796-803.

HAUSER, A. R. 2009. The type III secretion system of Pseudomonas aeruginosa: infection by injection. *Nat Rev Microbiol,* 7**,** 654-65.

HMELO, L. R., BORLEE, B. R., ALMBLAD, H., LOVE, M. E., RANDALL, T. E., TSENG, B. S., LIN, C., IRIE, Y., STOREK, K. M., YANG, J. J., SIEHNEL, R. J., HOWELL, P. L., SINGH, P. K., TOLKER-NIELSEN, T., PARSEK, M. R., SCHWEIZER, H. P. & HARRISON, J. J. 2015. Precision-engineering the Pseudomonas aeruginosa genome with two-step allelic exchange. *Nat Protoc,* 10**,** 1820-41.

HOF, H. & SCHLÜTER, D. 2019. *Medizinische Mikrobiologie, 7th edition*, Thieme.

HONG, D. J., BAE, I. K., JANG, I. H., JEONG, S. H., KANG, H. K. & LEE, K. 2015. Epidemiology and Characteristics of Metallo-beta-Lactamase-Producing Pseudomonas aeruginosa. *Infect Chemother,* 47**,** 81-97.

HONORÉ, N., NICOLAS, M. H. & COLE, S. T. 1986. Inducible cephalosporinase production in clinical isolates of Enterobacter cloacae is controlled by a regulatory gene that has been deleted from Escherichia coli. *Embo j,* 5**,** 3709-14.

IKEDA, M., WACHI, M., JUNG, H. K., ISHINO, F. & MATSUHASHI, M. 1991. The Escherichia coli mraY gene encoding UDP-N-acetylmuramoyl-pentapeptide: undecaprenyl-phosphate phospho-N-acetylmuramoyl-pentapeptide transferase. *J Bacteriol,* 173**,** 1021-6.

IRAZOKI, O., HERNANDEZ, S. B. & CAVA, F. 2019. Peptidoglycan Muropeptides: Release, Perception, and Functions as Signaling Molecules. *Front Microbiol,* 10**,** 500.

JACOBS, C., FRERE, J. M. & NORMARK, S. 1997. Cytosolic intermediates for cell wall biosynthesis and degradation control inducible beta-lactam resistance in gram-negative bacteria. *Cell,* 88**,** 823-32.

JACOBS, C., HUANG, L. J., BARTOWSKY, E., NORMARK, S. & PARK, J. T. 1994. Bacterial cell wall recycling provides cytosolic muropeptides as effectors for beta-lactamase induction. *Embo j,* 13**,** 4684-94.

JACOBS, C., JORIS, B., JAMIN, M., KLARSOV, K., VAN BEEUMEN, J., MENGIN-LECREULX, D., VAN HEIJENOORT, J., PARK, J. T., NORMARK, S. & FRÈRE, J. M. 1995. AmpD, essential for both beta-lactamase regulation and cell wall recycling, is a novel cytosolic N-acetylmuramyl-L-alanine amidase. *Mol Microbiol,* 15**,** 553-9.

JACQUES, I., DERELLE, J., WEBER, M. & VIDAILHET, M. 1998. Pulmonary evolution of cystic fibrosis patients colonized by Pseudomonas aeruginosa and/or Burkholderia cepacia. *Eur J Pediatr,* 157**,** 427-31.

JONES, P., BINNS, D., CHANG, H. Y., FRASER, M., LI, W., MCANULLA, C., MCWILLIAM, H., MASLEN, J., MITCHELL, A., NUKA, G., PESSEAT, S., QUINN, A. F., SANGRADOR-VEGAS, A., SCHEREMETJEW, M., YONG, S. Y., LOPEZ, R. & HUNTER, S. 2014. InterProScan 5: genome-scale protein function classification. *Bioinformatics,* 30**,** 1236-40.

JUAN, C., MACIA, M. D., GUTIERREZ, O., VIDAL, C., PEREZ, J. L. & OLIVER, A. 2005. Molecular mechanisms of beta-lactam resistance mediated by AmpC hyperproduction in Pseudomonas aeruginosa clinical strains. *Antimicrob Agents Chemother,* 49**,** 4733-8.

KAMADA, N., CHEN, G. Y., INOHARA, N. & NÚÑEZ, G. 2013. Control of pathogens and pathobionts by the gut microbiota. *Nat Immunol,* 14**,** 685-90.

KING, J. D., KOCÍNCOVÁ, D., WESTMAN, E. L. & LAM, J. S. 2009. Review: Lipopolysaccharide biosynthesis in Pseudomonas aeruginosa. *Innate Immun,* 15**,** 261-312.

KLEIN, K., SONNABEND, M. S., FRANK, L., LEIBIGER, K., FRANZ-WACHTEL, M., MACEK, B., TRUNK, T., LEO, J. C., AUTENRIETH, I. B., SCHUTZ, M. & BOHN, E. 2019. Deprivation of the Periplasmic Chaperone SurA Reduces Virulence and Restores Antibiotic Susceptibility of Multidrug-Resistant Pseudomonas aeruginosa. *Front Microbiol,* 10**,** 100.

KLOCKGETHER, J., CRAMER, N., WIEHLMANN, L., DAVENPORT, C. F. & TUMMLER, B. 2011. Pseudomonas aeruginosa Genomic Structure and Diversity. *Front Microbiol,* 2**,** 150.

KONG, K. F., AGUILA, A., SCHNEPER, L. & MATHEE, K. 2010. Pseudomonas aeruginosa β-lactamase induction requires two permeases, AmpG and AmpP. *BMC Microbiol,* 10**,** 328.

KONG, K. F., JAYAWARDENA, S. R., INDULKAR, S. D., DEL PUERTO, A., KOH, C. L., HØIBY, N. & MATHEE, K. 2005. Pseudomonas aeruginosa AmpR is a global transcriptional factor that regulates expression of AmpC and PoxB beta-lactamases, proteases, quorum sensing, and other virulence factors. *Antimicrob Agents Chemother,* 49**,** 4567-75.

KORZA, H. J. & BOCHTLER, M. 2005. Pseudomonas aeruginosa LD-carboxypeptidase, a serine peptidase with a Ser-His-Glu triad and a nucleophilic elbow. *J Biol Chem,* 280**,** 40802-12.

KRACHLER, A. M. & ORTH, K. 2013. Targeting the bacteria-host interface: strategies in anti-adhesion therapy. *Virulence,* 4**,** 284-94.

LAI, G. C., CHO, H. & BERNHARDT, T. G. 2017. The mecillinam resistome reveals a role for peptidoglycan endopeptidases in stimulating cell wall synthesis in Escherichia coli. *PLoS Genet,* 13**,** e1006934.

LAM, J. S., TAYLOR, V. L., ISLAM, S. T., HAO, Y. & KOCÍNCOVÁ, D. 2011. Genetic and Functional Diversity of Pseudomonas aeruginosa Lipopolysaccharide. *Front Microbiol,* 2**,** 118.

LAMBERT, P. A. 2002. Mechanisms of antibiotic resistance in Pseudomonas aeruginosa. *J R Soc Med,* 95 Suppl 41**,** 22-6.

LAMERS, R. P., NGUYEN, U. T., NGUYEN, Y., BUENSUCESO, R. N. & BURROWS, L. L. 2015. Loss of membrane-bound lytic transglycosylases increases outer membrane permeability and beta-lactam sensitivity in Pseudomonas aeruginosa. *Microbiologyopen,* 4**,** 879-95.

LANGAEE, T. Y., GAGNON, L. & HULETSKY, A. 2000. Inactivation of the ampD gene in Pseudomonas aeruginosa leads to moderate-basal-level and hyperinducible AmpC beta-lactamase expression. *Antimicrob Agents Chemother,* 44**,** 583-9.

LARKIN, M. A., BLACKSHIELDS, G., BROWN, N. P., CHENNA, R., MCGETTIGAN, P. A., MCWILLIAM, H., VALENTIN, F., WALLACE, I. M., WILM, A., LOPEZ, R., THOMPSON, J. D., GIBSON, T. J. & HIGGINS, D. G. 2007. Clustal W and Clustal X version 2.0. *Bioinformatics,* 23**,** 2947-8.

LEE, M., HESEK, D., BLAZQUEZ, B., LASTOCHKIN, E., BOGGESS, B., FISHER, J. F. & MOBASHERY, S. 2015. Catalytic spectrum of the penicillin-binding protein 4 of Pseudomonas aeruginosa, a nexus for the induction of beta-lactam antibiotic resistance. *J Am Chem Soc,* 137**,** 190-200.

LEE, M., HESEK, D., DIK, D. A., FISHOVITZ, J., LASTOCHKIN, E., BOGGESS, B., FISHER, J. F. & MOBASHERY, S. 2017. From Genome to Proteome to Elucidation of Reactions for All Eleven Known Lytic Transglycosylases from Pseudomonas aeruginosa. *Angew Chem Int Ed Engl,* 56**,** 2735-2739.

LEGAREE, B. A., DANIELS, K., WEADGE, J. T., COCKBURN, D. & CLARKE, A. J. 2007. Function of penicillin-binding protein 2 in viability and morphology of Pseudomonas aeruginosa. *J Antimicrob Chemother,* 59**,** 411-24.

LI, H., LUO, Y. F., WILLIAMS, B. J., BLACKWELL, T. S. & XIE, C. M. 2012. Structure and function of OprD protein in Pseudomonas aeruginosa: from antibiotic resistance to novel therapies. *Int J Med Microbiol,* 302**,** 63-8.

LI, X. Z. & NIKAIDO, H. 2009. Efflux-mediated drug resistance in bacteria: an update. *Drugs,* 69**,** 1555-623.

LISTER, P. D., GARDNER, V. M. & SANDERS, C. C. 1999. Clavulanate induces expression of the Pseudomonas aeruginosa AmpC cephalosporinase at physiologically relevant concentrations and antagonizes the antibacterial activity of ticarcillin. *Antimicrob Agents Chemother,* 43**,** 882-9.

LISTER, P. D., WOLTER, D. J. & HANSON, N. D. 2009. Antibacterial-resistant Pseudomonas aeruginosa: clinical impact and complex regulation of

chromosomally encoded resistance mechanisms. *Clin Microbiol Rev,* 22**,** 582-610.

LYCZAK, J. B., CANNON, C. L. & PIER, G. B. 2000. Establishment of Pseudomonas aeruginosa infection: lessons from a versatile opportunist. *Microbes Infect,* 2**,** 1051-60.

MAISONNEUVE, E. & GERDES, K. 2014. Molecular mechanisms underlying bacterial persisters. *Cell,* 157**,** 539-48.

MASUDA, N., SAKAGAWA, E., OHYA, S., GOTOH, N., TSUJIMOTO, H. & NISHINO, T. 2000. Substrate specificities of MexAB-OprM, MexCD-OprJ, and MexXY-oprM efflux pumps in Pseudomonas aeruginosa. *Antimicrob Agents Chemother,* 44**,** 3322-7.

MAYER, C. 2019. Peptidoglycan Recycling, a Promising Target for Antibiotic Adjuvants in Antipseudomonal Therapy. *J Infect Dis,* 220**,** 1713-1715.

MITCHELL, A. L., ATTWOOD, T. K., BABBITT, P. C., BLUM, M., BORK, P., BRIDGE, A., BROWN, S. D., CHANG, H. Y., EL-GEBALI, S., FRASER, M. I., GOUGH, J., HAFT, D. R., HUANG, H., LETUNIC, I., LOPEZ, R., LUCIANI, A., MADEIRA, F., MARCHLER-BAUER, A., MI, H., NATALE, D. A., NECCI, M., NUKA, G., ORENGO, C., PANDURANGAN, A. P., PAYSAN-LAFOSSE, T., PESSEAT, S., POTTER, S. C., QURESHI, M. A., RAWLINGS, N. D., REDASCHI, N., RICHARDSON, L. J., RIVOIRE, C., SALAZAR, G. A., SANGRADOR-VEGAS, A., SIGRIST, C. J. A., SILLITOE, I., SUTTON, G. G., THANKI, N., THOMAS, P. D., TOSATTO, S. C. E., YONG, S. Y. & FINN, R. D. 2019. InterPro in 2019: improving coverage, classification and access to protein sequence annotations. *Nucleic Acids Res,* 47**,** D351-d360.

MOHAMMADI, T., VAN DAM, V., SIJBRANDI, R., VERNET, T., ZAPUN, A., BOUHSS, A., DIEPEVEEN-DE BRUIN, M., NGUYEN-DISTÈCHE, M., DE KRUIJFF, B. & BREUKINK, E. 2011. Identification of FtsW as a transporter of lipid-linked cell wall precursors across the membrane. *Embo j,* 30**,** 1425-32.

MONDON, M., HUR, S., VADLAMANI, G., RODRIGUES, P., TSYBINA, P., OLIVER, A., MARK, B. L., VOCADLO, D. J. & BLÉRIOT, Y. 2013. Selective trihydroxyazepane NagZ inhibitors increase sensitivity of Pseudomonas aeruginosa to β-lactams. *Chem Commun (Camb),* 49**,** 10983-5.

MORADALI, M. F., GHODS, S. & REHM, B. H. 2017. Pseudomonas aeruginosa Lifestyle: A Paradigm for Adaptation, Survival, and Persistence. *Front Cell Infect Microbiol,* 7**,** 39.

MOYA, B., DOTSCH, A., JUAN, C., BLAZQUEZ, J., ZAMORANO, L., HAUSSLER, S. & OLIVER, A. 2009. Beta-lactam resistance response triggered by inactivation of a nonessential penicillin-binding protein. *PLoS Pathog,* 5**,** e1000353.

MULCAHY, L. R., BURNS, J. L., LORY, S. & LEWIS, K. 2010. Emergence of Pseudomonas aeruginosa strains producing high levels of persister cells in patients with cystic fibrosis. *J Bacteriol,* 192**,** 6191-9.

NIKAIDO, H. 2003. Molecular basis of bacterial outer membrane permeability revisited. *Microbiol Mol Biol Rev,* 67**,** 593-656.

PAGE, M. G. & HEIM, J. 2009. Prospects for the next anti-Pseudomonas drug. *Curr Opin Pharmacol,* 9**,** 558-65.

PANG, Z., RAUDONIS, R., GLICK, B. R., LIN, T. J. & CHENG, Z. 2019. Antibiotic resistance in Pseudomonas aeruginosa: mechanisms and alternative therapeutic strategies. *Biotechnol Adv,* 37**,** 177-192.

PATERSON, D. L. & BONOMO, R. A. 2005. Extended-spectrum beta-lactamases: a clinical update. *Clin Microbiol Rev,* 18**,** 657-86.

PERCIVAL, S. L., SULEMAN, L., VUOTTO, C. & DONELLI, G. 2015. Healthcare-associated infections, medical devices and biofilms: risk, tolerance and control. *J Med Microbiol,* 64**,** 323-334.

PFAFFL, M. W. 2001. A new mathematical model for relative quantification in real-time RT-PCR. *Nucleic Acids Res,* 29**,** e45.

POOLE, K. 2001. Multidrug efflux pumps and antimicrobial resistance in Pseudomonas aeruginosa and related organisms. *J Mol Microbiol Biotechnol,* 3**,** 255-64.

POOLE, K. 2007. Efflux pumps as antimicrobial resistance mechanisms. *Ann Med,* 39**,** 162-76.

PRADEL, E., LEMAÎTRE, N., MERCHEZ, M., RICARD, I., REBOUL, A., DEWITTE, A. & SEBBANE, F. 2014. New insights into how Yersinia pestis adapts to its mammalian host during bubonic plague. *PLoS Pathog,* 10**,** e1004029.

PUTMAN, M., VAN VEEN, H. W. & KONINGS, W. N. 2000. Molecular properties of bacterial multidrug transporters. *Microbiol Mol Biol Rev,* 64**,** 672-93.

PUZARI, M. & CHETIA, P. 2017. RND efflux pump mediated antibiotic resistance in Gram-negative bacteria Escherichia coli and Pseudomonas aeruginosa: a major issue worldwide. *World J Microbiol Biotechnol,* 33**,** 24.

RAWAT, D. & NAIR, D. 2010. Extended-spectrum beta-lactamases in Gram Negative Bacteria. *J Glob Infect Dis,* 2**,** 263-74.

RESTREPO, M. I., BABU, B. L., REYES, L. F., CHALMERS, J. D., SONI, N. J., SIBILA, O., FAVERIO, P., CILLONIZ, C., RODRIGUEZ-CINTRON, W. & ALIBERTI, S. 2018. Burden and risk factors for Pseudomonas aeruginosa community-acquired pneumonia: a multinational point prevalence study of hospitalised patients. *Eur Respir J,* 52.

RICE, L. B. 2008. Federal funding for the study of antimicrobial resistance in nosocomial pathogens: no ESKAPE. *J Infect Dis,* 197**,** 1079-81.

ROUJEINIKOVA, A. 2008. Crystal structure of the cell wall anchor domain of MotB, a stator component of the bacterial flagellar motor: implications for peptidoglycan recognition. *Proc Natl Acad Sci U S A,* 105**,** 10348-53.

RUEDEN, C. T., SCHINDELIN, J., HINER, M. C., DEZONIA, B. E., WALTER, A. E., ARENA, E. T. & ELICEIRI, K. W. 2017. ImageJ2: ImageJ for the next generation of scientific image data. *BMC Bioinformatics,* 18**,** 529.

SABUDA, D. M., LAUPLAND, K., PITOUT, J., DALTON, B., RABIN, H., LOUIE, T. & CONLY, J. 2008. Utilization of colistin for treatment of multidrug-resistant Pseudomonas aeruginosa. *Can J Infect Dis Med Microbiol,* 19**,** 413-8.

SADIKOT, R. T., BLACKWELL, T. S., CHRISTMAN, J. W. & PRINCE, A. S. 2005. Pathogen-host interactions in Pseudomonas aeruginosa pneumonia. *Am J Respir Crit Care Med,* 171**,** 1209-23.

SCHAEFER, P. & BAUGH, R. F. 2012. Acute otitis externa: an update. *Am Fam Physician,* 86**,** 1055-61.

SCHLEIFER, K. H. & KANDLER, O. 1972. Peptidoglycan types of bacterial cell walls and their taxonomic implications. *Bacteriol Rev,* 36**,** 407-77.

SCHMIDTKE, A. J. & HANSON, N. D. 2008. Role of ampD homologs in overproduction of AmpC in clinical isolates of Pseudomonas aeruginosa. *Antimicrob Agents Chemother,* 52**,** 3922-7.

SCHWECHHEIMER, C., RODRIGUEZ, D. L. & KUEHN, M. J. 2015. NlpI-mediated modulation of outer membrane vesicle production through peptidoglycan dynamics in Escherichia coli. *Microbiologyopen,* 4**,** 375-89.

SEO, J. & DARWIN, A. J. 2013. The Pseudomonas aeruginosa periplasmic protease CtpA can affect systems that impact its ability to mount both acute and chronic infections. *Infect Immun,* 81**,** 4561-70.

SHAM, L. T., BUTLER, E. K., LEBAR, M. D., KAHNE, D., BERNHARDT, T. G. & RUIZ, N. 2014. Bacterial cell wall. MurJ is the flippase of lipid-linked precursors for peptidoglycan biogenesis. *Science,* 345**,** 220-2.

SHEPP, D. H., TANG, I. T., RAMUNDO, M. B. & KAPLAN, M. K. 1994. Serious Pseudomonas aeruginosa infection in AIDS. *J Acquir Immune Defic Syndr (1988),* 7**,** 823-31.

SHIGEMURA, K., OSAWA, K., KATO, A., TOKIMATSU, I., ARAKAWA, S., SHIRAKAWA, T. & FUJISAWA, M. 2015. Association of overexpression of efflux pump genes with antibiotic resistance in Pseudomonas aeruginosa strains clinically isolated from urinary tract infection patients. *J Antibiot (Tokyo),* 68**,** 568-72.

SHU, J. C., KUO, A. J., SU, L. H., LIU, T. P., LEE, M. H., SU, I. N. & WU, T. L. 2017. Development of carbapenem resistance in Pseudomonas aeruginosa is associated with OprD polymorphisms, particularly the amino acid substitution at codon 170. *J Antimicrob Chemother,* 72**,** 2489-2495.

SIEVERS, F., WILM, A., DINEEN, D., GIBSON, T. J., KARPLUS, K., LI, W., LOPEZ, R., MCWILLIAM, H., REMMERT, M., SÖDING, J., THOMPSON, J. D. & HIGGINS, D. G. 2011. Fast, scalable generation of high-quality protein multiple sequence alignments using Clustal Omega. *Mol Syst Biol,* 7**,** 539.

SILBY, M. W., WINSTANLEY, C., GODFREY, S. A., LEVY, S. B. & JACKSON, R. W. 2011. Pseudomonas genomes: diverse and adaptable. *FEMS Microbiol Rev,* 35**,** 652-80.

SINGH, S. K., SAISREE, L., AMRUTHA, R. N. & REDDY, M. 2012. Three redundant murein endopeptidases catalyse an essential cleavage step in peptidoglycan synthesis of Escherichia coli K12. *Mol Microbiol,* 86**,** 1036-51.

SIRIYONG, T., SRIMANOTE, P., CHUSRI, S., YINGYONGNARONGKUL, B. E., SUAISOM, C., TIPMANEE, V. & VORAVUTHIKUNCHAI, S. P. 2017. Conessine as a novel inhibitor of multidrug efflux pump systems in Pseudomonas aeruginosa. *BMC Complement Altern Med,* 17**,** 405.

SKALWEIT, M. J. & LI, M. 2016. Bulgecin A as a β-lactam enhancer for carbapenem-resistant Pseudomonas aeruginosa and carbapenem-resistant Acinetobacter baumannii clinical isolates containing various resistance mechanisms. *Drug Des Devel Ther,* 10**,** 3013-3020.

SONNABEND, M. S., KLEIN, K., BEIER, S., ANGELOV, A., KLUJ, R., MAYER, C., GROSS, C., HOFMEISTER, K., BEUTTNER, A., WILLMANN, M., PETER, S., OBERHETTINGER, P., SCHMIDT, A., AUTENRIETH, I. B., SCHUTZ, M. & BOHN, E. 2019. Identification of drug-resistance determinants in a clinical isolate of Pseudomonas aeruginosa by high-density transposon mutagenesis. *Antimicrob Agents Chemother*.

SPENCER, R. C. 1996. Predominant pathogens found in the European Prevalence of Infection in Intensive Care Study. *Eur J Clin Microbiol Infect Dis,* 15**,** 281-5.

SRIVASTAVA, D., SEO, J., RIMAL, B., KIM, S. J., ZHEN, S. & DARWIN, A. J. 2018. A Proteolytic Complex Targets Multiple Cell Wall Hydrolases in Pseudomonas aeruginosa. *MBio,* 9.

STEWART, P. S. 2002. Mechanisms of antibiotic resistance in bacterial biofilms. *Int J Med Microbiol,* 292**,** 107-13.

STEWART, P. S. & COSTERTON, J. W. 2001. Antibiotic resistance of bacteria in biofilms. *Lancet,* 358**,** 135-8.

STOKELL, J. R., GHARAIBEH, R. Z., HAMP, T. J., ZAPATA, M. J., FODOR, A. A. & STECK, T. R. 2015. Analysis of changes in diversity and abundance of the microbial community in a cystic fibrosis patient over a multiyear period. *J Clin Microbiol,* 53**,** 237-47.

STOVER, C. K., PHAM, X. Q., ERWIN, A. L., MIZOGUCHI, S. D., WARRENER, P., HICKEY, M. J., BRINKMAN, F. S., HUFNAGLE, W. O., KOWALIK, D. J., LAGROU, M., GARBER, R. L., GOLTRY, L., TOLENTINO, E., WESTBROCK-WADMAN, S., YUAN, Y., BRODY, L. L., COULTER, S. N., FOLGER, K. R., KAS, A., LARBIG, K., LIM, R., SMITH, K., SPENCER, D., WONG, G. K., WU, Z., PAULSEN, I. T., REIZER, J., SAIER, M. H., HANCOCK, R. E., LORY, S. & OLSON, M. V. 2000. Complete genome sequence of Pseudomonas aeruginosa PAO1, an opportunistic pathogen. *Nature,* 406**,** 959-64.

STROMINGER, J. L. & TIPPER, D. J. 1965. Bacterial cell wall synthesis and structure in relation to the mechanism of action of penicillins and other antibacterial agents. *Am J Med,* 39**,** 708-21.

STUBBS, K. A., BACIK, J. P., PERLEY-ROBERTSON, G. E., WHITWORTH, G. E., GLOSTER, T. M., VOCADLO, D. J. & MARK, B. L. 2013. The development of selective inhibitors of NagZ: increased susceptibility of Gram-negative bacteria to β-lactams. *Chembiochem,* 14**,** 1973-81.

STUBBS, K. A., BALCEWICH, M., MARK, B. L. & VOCADLO, D. J. 2007. Small molecule inhibitors of a glycoside hydrolase attenuate inducible AmpC-mediated beta-lactam resistance. *J Biol Chem,* 282**,** 21382-91.

STUBBS, K. A., SCAFFIDI, A., DEBOWSKI, A. W., MARK, B. L., STICK, R. V. & VOCADLO, D. J. 2008. Synthesis and use of mechanism-based protein-profiling probes for retaining beta-D-glucosaminidases facilitate identification of Pseudomonas aeruginosa NagZ. *J Am Chem Soc,* 130**,** 327-35.

SU, M. Y., SOM, N., WU, C. Y., SU, S. C., KUO, Y. T., KE, L. C., HO, M. R., TZENG, S. R., TENG, C. H., MENGIN-LECREULX, D., REDDY, M. & CHANG, C. I. 2017. Structural basis of adaptor-mediated protein degradation by the tail-specific PDZ-protease Prc. *Nat Commun,* 8**,** 1516.

SUGAWARA, E., NESTOROVICH, E. M., BEZRUKOV, S. M. & NIKAIDO, H. 2006. Pseudomonas aeruginosa porin OprF exists in two different conformations. *J Biol Chem,* 281**,** 16220-9.

TACCONELLI, E., CARRARA, E., SAVOLDI, A., HARBARTH, S., MENDELSON, M., MONNET, D. L., PULCINI, C., KAHLMETER, G., KLUYTMANS, J., CARMELI, Y., OUELLETTE, M., OUTTERSON, K., PATEL, J., CAVALERI, M., COX, E. M., HOUCHENS, C. R., GRAYSON, M. L., HANSEN, P., SINGH, N., THEURETZBACHER, U. & MAGRINI, N. 2018. Discovery, research, and development of new antibiotics: the WHO priority list of antibiotic-resistant bacteria and tuberculosis. *Lancet Infect Dis,* 18**,** 318-327.

TEMPLIN, M. F., URSINUS, A. & HOLTJE, J. V. 1999. A defect in cell wall recycling triggers autolysis during the stationary growth phase of Escherichia coli. *Embo j,* 18**,** 4108-17.

TORRENS, G., PEREZ-GALLEGO, M., MOYA, B., MUNAR-BESTARD, M., ZAMORANO, L., CABOT, G., BLAZQUEZ, J., AYALA, J. A., OLIVER, A. & JUAN, C. 2017. Targeting the permeability barrier and peptidoglycan recycling pathways to disarm Pseudomonas aeruginosa against the innate immune system. *PLoS One,* 12**,** e0181932.

TORRENS, G., SANCHEZ-DIENER, I., JORDANA-LLUCH, E., BARCELO, I. M., ZAMORANO, L., JUAN, C. & OLIVER, A. 2019. In Vivo Validation of Peptidoglycan Recycling as a Target to Disable AmpC-Mediated Resistance and Reduce Virulence Enhancing the Cell-Wall-Targeting Immunity. *J Infect Dis,* 220**,** 1729-1737.

UEHARA, T., DINH, T. & BERNHARDT, T. G. 2009. LytM-domain factors are required for daughter cell separation and rapid ampicillin-induced lysis in Escherichia coli. *J Bacteriol,* 191**,** 5094-107.

VAN DEN BERG VAN SAPAROEA, H. B., LUBELSKI, J., VAN MERKERK, R., MAZURKIEWICZ, P. S. & DRIESSEN, A. J. 2005. Proton motive force-dependent Hoechst 33342 transport by the ABC transporter LmrA of Lactococcus lactis. *Biochemistry,* 44**,** 16931-8.

VANDENHEUVEL, D., LAVIGNE, R. & BRÜSSOW, H. 2015. Bacteriophage Therapy: Advances in Formulation Strategies and Human Clinical Trials. *Annu Rev Virol,* 2**,** 599-618.

VAZIRANI, J., WURITY, S. & ALI, M. H. 2015. Multidrug-Resistant Pseudomonas aeruginosa Keratitis: Risk Factors, Clinical Characteristics, and Outcomes. *Ophthalmology,* 122**,** 2110-4.

VESTÖ, K., HUSEBY, D. L., SNYGG, I., WANG, H., HUGHES, D. & RHEN, M. 2018. Muramyl Endopeptidase Spr Contributes to Intrinsic Vancomycin Resistance in Salmonella enterica Serovar Typhimurium. *Front Microbiol,* 9**,** 2941.

VOLLMER, W. & BERTSCHE, U. 2008. Murein (peptidoglycan) structure, architecture and biosynthesis in Escherichia coli. *Biochim Biophys Acta,* 1778**,** 1714-34.

VOLLMER, W., JORIS, B., CHARLIER, P. & FOSTER, S. 2008. Bacterial peptidoglycan (murein) hydrolases. *FEMS Microbiol Rev,* 32**,** 259-86.

WATERHOUSE, A. M., PROCTER, J. B., MARTIN, D. M., CLAMP, M. & BARTON, G. J. 2009. Jalview Version 2--a multiple sequence alignment editor and analysis workbench. *Bioinformatics,* 25**,** 1189-91.

WEAVER, A. I., MURPHY, S. G., UMANS, B. D., TALLAVAJHALA, S., ONYEKWERE, I., WITTELS, S., SHIN, J. H., VANNIEUWENHZE, M., WALDOR, M. K. & DÖRR, T. 2018. Genetic Determinants of Penicillin Tolerance in Vibrio cholerae. *Antimicrob Agents Chemother,* 62.

WEINER-LASTINGER, L. M., ABNER, S., EDWARDS, J. R., KALLEN, A. J., KARLSSON, M., MAGILL, S. S., POLLOCK, D., SEE, I., SOE, M. M., WALTERS, M. S. & DUDECK, M. A. 2019. Antimicrobial-resistant pathogens associated with adult healthcare-associated infections: Summary of data reported to the National Healthcare Safety Network, 2015-2017. *Infect Control Hosp Epidemiol***,** 1-18.

WEISSMAN, B. A., MONDINO, B. J., PETTIT, T. H. & HOFBAUER, J. D. 1984. Corneal ulcers associated with extended-wear soft contact lenses. *Am J Ophthalmol,* 97**,** 476-81.

WILLIAMS, B. J., DEHNBOSTEL, J. & BLACKWELL, T. S. 2010. Pseudomonas aeruginosa: host defence in lung diseases. *Respirology,* 15**,** 1037-56.

WILLMANN, M., KLIMEK, A. M., VOGEL, W., LIESE, J., MARSCHAL, M., AUTENRIETH, I. B., PETER, S. & BUHL, M. 2014. Clinical and treatment-related risk factors for nosocomial colonisation with extensively drug-resistant Pseudomonas aeruginosa in a haematological patient population: a matched case control study. *BMC Infect Dis,* 14**,** 650.

WU, Y. T., WILLCOX, M., ZHU, H. & STAPLETON, F. 2015. Contact lens hygiene compliance and lens case contamination: A review. *Cont Lens Anterior Eye,* 38**,** 307-16.

YAKHNINA, A. A., MCMANUS, H. R. & BERNHARDT, T. G. 2015. The cell wall amidase AmiB is essential for Pseudomonas aeruginosa cell division, drug resistance and viability. *Mol Microbiol,* 97**,** 957-73.

ZAMORANO, L., MOYÀ, B., JUAN, C., MULET, X., BLÁZQUEZ, J. & OLIVER, A. 2014. The Pseudomonas aeruginosa CreBC two-component system plays a major role in the response to β-lactams, fitness, biofilm growth, and global regulation. *Antimicrob Agents Chemother,* 58**,** 5084-95.

ZAMORANO, L., REEVE, T. M., DENG, L., JUAN, C., MOYA, B., CABOT, G., VOCADLO, D. J., MARK, B. L. & OLIVER, A. 2010. NagZ inactivation prevents and reverts beta-lactam resistance, driven by AmpD and PBP 4 mutations, in Pseudomonas aeruginosa. *Antimicrob Agents Chemother,* 54**,** 3557-63.

ZAMORANO, L., REEVE, T. M., JUAN, C., MOYA, B., CABOT, G., VOCADLO, D. J., MARK, B. L. & OLIVER, A. 2011. AmpG inactivation restores susceptibility of pan-beta-lactam-resistant Pseudomonas aeruginosa clinical strains. *Antimicrob Agents Chemother,* 55**,** 1990-6.

ZGURSKAYA, H. I., LÖPEZ, C. A. & GNANAKARAN, S. 2015. Permeability Barrier of Gram-Negative Cell Envelopes and Approaches To Bypass It. *ACS Infect Dis,* 1**,** 512-522.

ZHANG, W., LEE, M., HESEK, D., LASTOCHKIN, E., BOGGESS, B. & MOBASHERY, S. 2013. Reactions of the three AmpD enzymes of Pseudomonas aeruginosa. *J Am Chem Soc,* 135**,** 4950-3.

ZIMMERMANN, L., STEPHENS, A., NAM, S. Z., RAU, D., KÜBLER, J., LOZAJIC, M., GABLER, F., SÖDING, J., LUPAS, A. N. & ALVA, V. 2018. A Completely Reimplemented MPI Bioinformatics Toolkit with a New HHpred Server at its Core. *J Mol Biol,* 430**,** 2237-2243.

ZINCKE, D., BALASUBRAMANIAN, D., SILVER, L. L. & MATHEE, K. 2016. Characterization of a Carbapenem-Hydrolyzing Enzyme, PoxB, in Pseudomonas aeruginosa PAO1. *Antimicrob Agents Chemother,* 60**,** 936-45.

8 Appendix

8.1 Protein analysis

8.1.1 Alignments

8.1.1.1 NlpC/P60 peptidase family

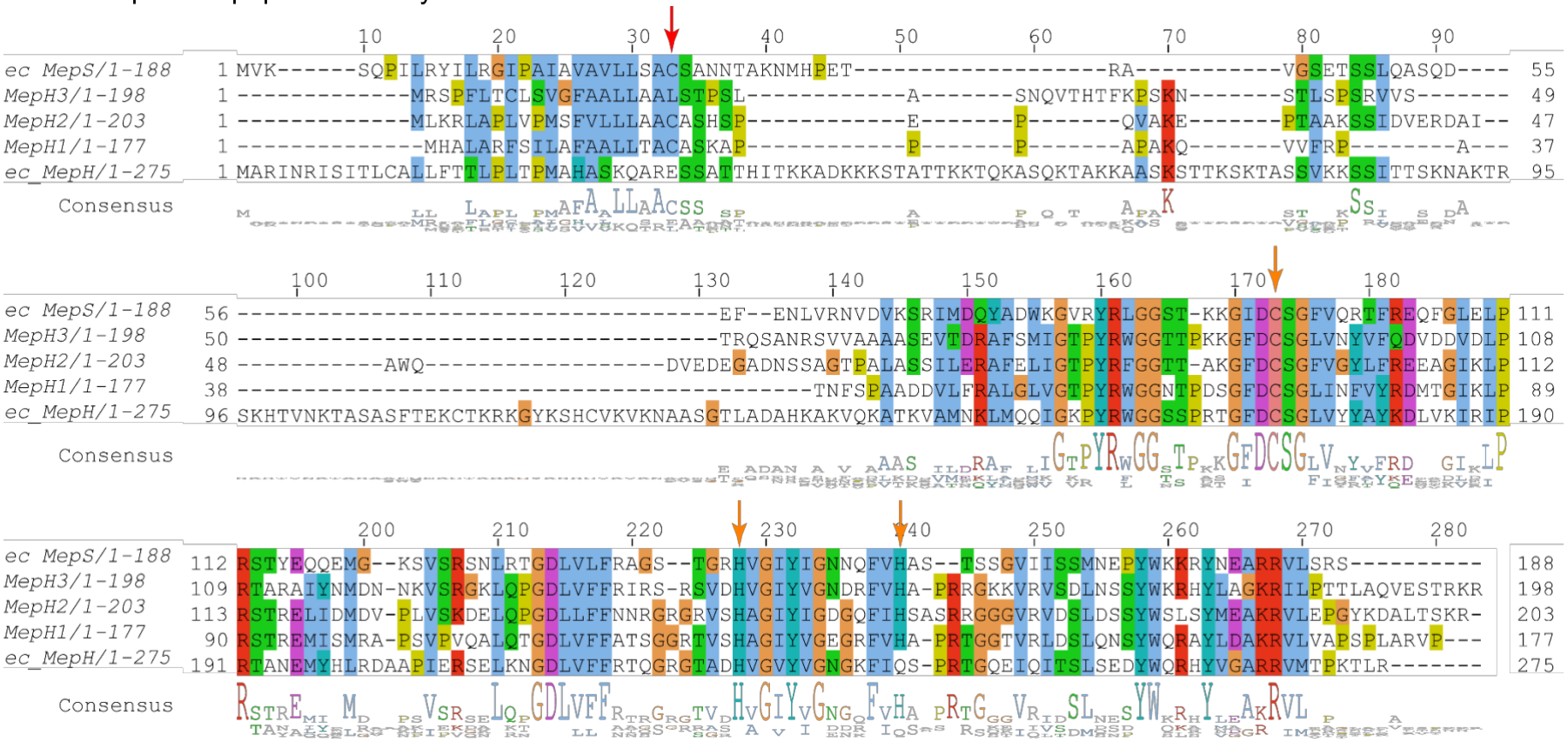

Figure 27: ***Alignments of Ec MepS, Ec MepH, Pa MepH1, Pa MepH2 and Pa MepH3***

The sequences of Pa MepH1, MepH2 and MepH3 and Ec MepH and MepS proteins were aligned using clustalΩ (Sievers et al., 2011, Zimmermann et al., 2018) and colour-coded according to conservation with clustalX (Larkin et al., 2007). A consensus sequence logo was generated and is depicted below the sequence alignment to highlight conserved residues. The sequence alignment view was prepared with Jalview (Waterhouse et al., 2009). Marked with a red arrow the palmytoylation/ diacylglycerolylation site of Ec MepS (https://www.uniprot.org/uniprot/P0AFV4) is displayed. The membrane-anchoring lipid is attached at this site. Orange arrows indicate the catalytic "H-H-C" triade of NlpC/P60 domains based on NMR structure (2k1g) of Ec MepS. The alignment was kindly provided by Dr. Fabian Renschler.

8.1.1.2 M23 peptidase domains of LytM proteins

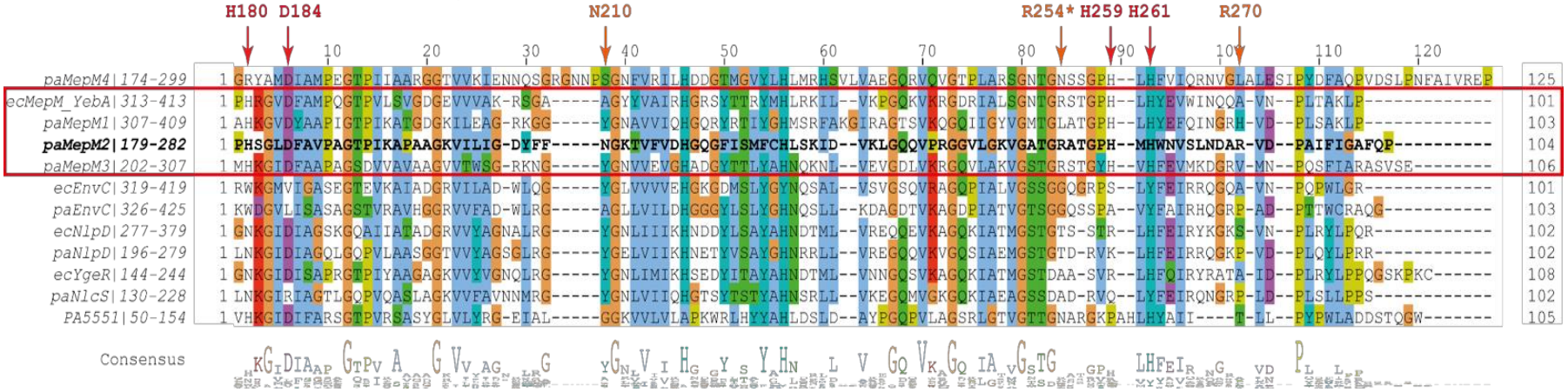

Figure 28: ***Alignment of the M23 peptidase domains of Ec and Pa LytM proteins***

To visualize their conservation, the sequences of M23 peptidase domains of the different members of the LytM protein family were aligned using clustalΩ (Sievers et al., 2011, Zimmermann et al., 2018) and colour-coded according to conservation with clustalX (Larkin et al., 2007). A consensus sequence logo was generated and is depicted below the sequence alignment to highlight conserved residues. The sequence alignment view was prepared with Jalview (Waterhouse et al., 2009). Because the N-termini of the LytM proteins vary greatly, the alignment is restricted to the M23 peptidase domains. The red box shows the catalytical component of the MepM proteins indicated by the presence of Zn^{2+}-coordinating residues which are highlighted by the red arrows (H180, D184, H259, H261). The Zn^{2+}-coordinating residues are based on a crystal structure of Pa MepM2 (PDB-ID: 2hsi). Orange arrows (N210, R254, R270) mark the catalytic centre/substrate interactions based on docking of $(Gly)_4$Phospinate into the crystal structure of Pa MepM2 (2hsi) performed by Dr. Thales Kronenberger. * indicates the interactions mediated by backbone atoms. The sequence of Pa MepM2 is highlighted in bold. The alignment was kindly provided by Dr. Fabian Renschler.*

8.1.2 Phylogenetic trees and pairwise identities

8.1.2.1 NlpC/P60 peptidase family

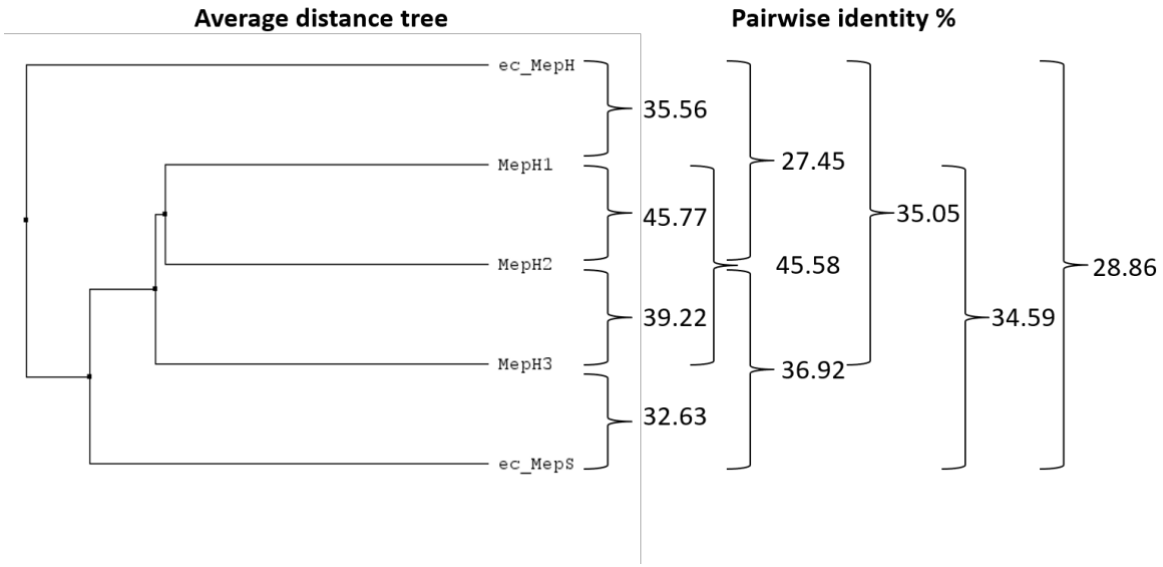

Figure 29: ***Average distance tree and pairwise identities in % of Ec MepS, Ec MepH, Pa MepH1, Pa MepH2 and Pa MepH3***

An average distance tree shows how the different proteins of the NlpC/P60 family are phylogenetically related. The tree was calculated from the clustalΩ alignment in Jalview using the BLOSUM62 matrix (Waterhouse et al., 2009). Pairwise identities were calculated using Jalview (Waterhouse et al., 2009), representing the extent (%) to which the amino acid sequences are invariant. The calculation of pairwise identities also depended on the alignment displayed in 8.1.1.1. The figure was kindly provided by Dr. Fabian Renschler.

8.1.2.2 Average distance tree of the M23 domains of *Ec* and *Pa* LytM proteins

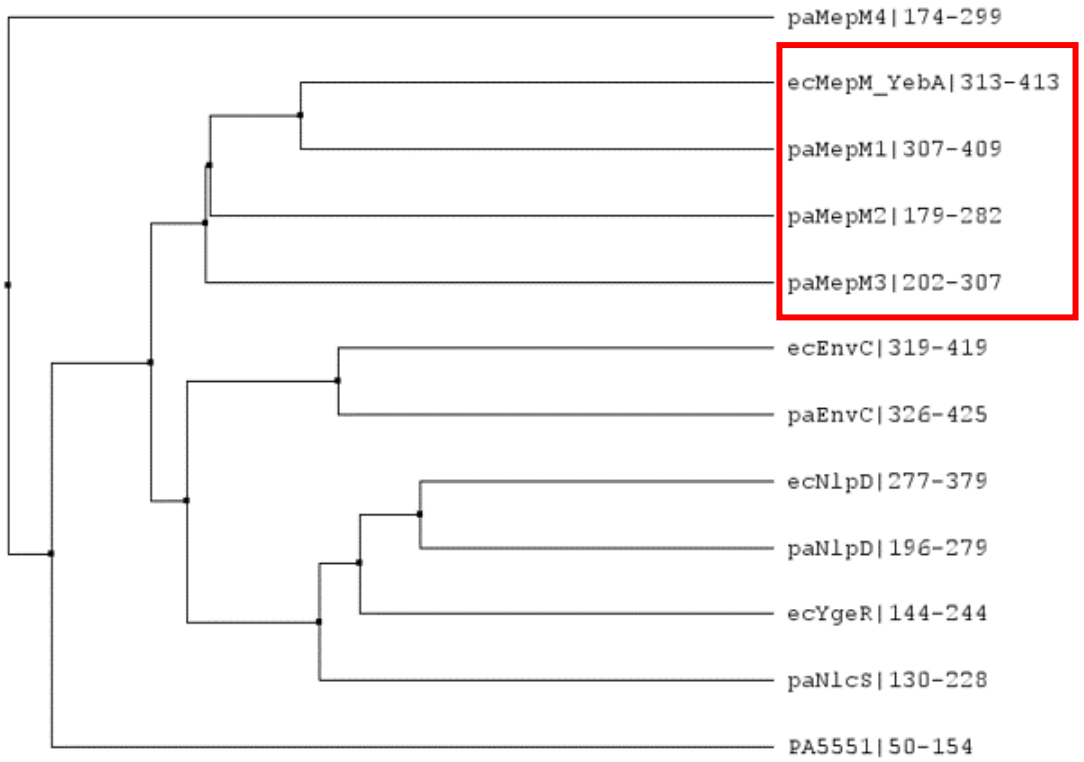

Figure 30: ***Average distance tree of the M23 domains of Ec and Pa LytM proteins***

The average distance tree shows how the different M23 domains of Ec and Pa LytM proteins are phylogenetically related. Highlighted with the red box, it includes the M23 domains of the LytM proteins used in this work (Pa MepM1, Pa MepM2 and Pa MepM3) as well as Ec MepM. The tree was calculated from the clustalΩ alignment in Jalview using the BLOSUM62 matrix (Waterhouse et al., 2009). The numbers displayed behind the protein's names indicate the position within the protein's amino acid sequence used for the alignment. The figure was kindly provided by Dr. Fabian Renschler.

8.1.2.3 Pairwise identities of M23 domains of LytM proteins

Table 31: ***Pairwise identities of M23 domains of Ec MepM, Pa MepM1, Pa MepM2 and Pa MepM3***

Pairwise identities were calculated using Jalview (Waterhouse et al., 2009), representing the extent (%) to which the amino acid sequences of the M23 domains are invariant. The calculation of pairwise identities also depended on the alignment displayed in 9.1.1.2. The figure was kindly provided by Dr. Fabian Renschler.

	Ec MepM	*Pa* MepM1	*Pa* MepM2	*Pa* MepM3
Ec MepM		47.57	40.38	41.58
Pa MepM1	47.57		38.68	39.81
Pa MepM2	40.38	38.68		40.38
Pa MepM3	41.58	39.81	40.38	

8.1.3 Domain organisation of the MepM proteins

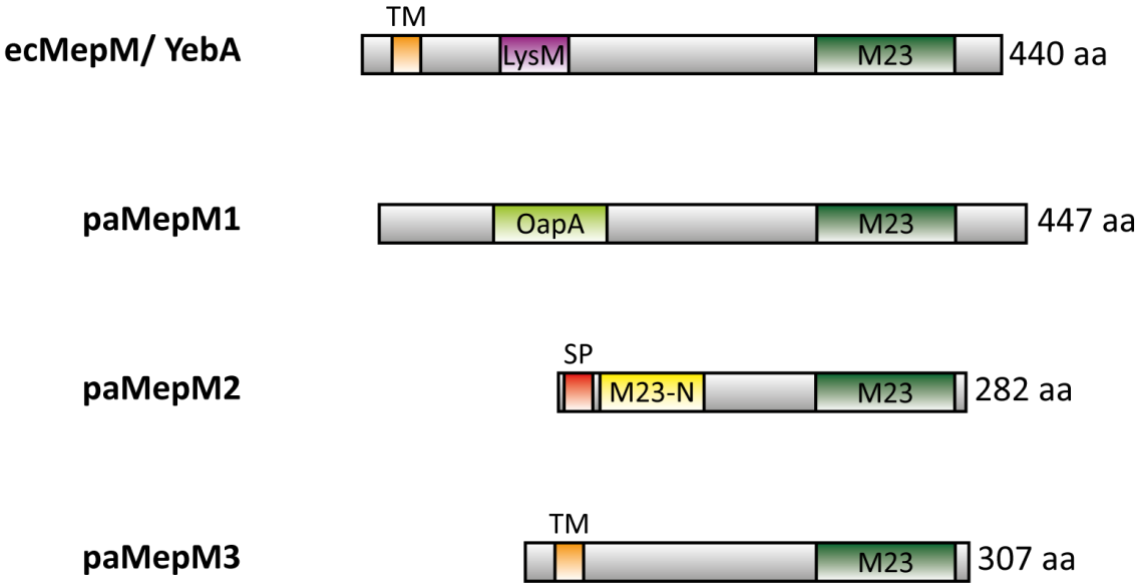

Figure 31: ***Simplified scheme of MepM domain organisation***

The sequences of all four proteins were scanned for their domain organization using InterProScan (Jones et al., 2014) from InterPro (Mitchell et al., 2019). The ecMepM/ YebA protein contains an N-terminal transmembrane helix (TM, orange) followed by a Lysine motif (LysM, purple) domain and a peptidase M23 (M23, dark green) domain at the C-terminus. The C-terminal part after the TM helix is periplasmic. The paMepM1 protein comprises an Opacity-associated protein A (OapA, green) domain at the N-terminus and a C-terminal M23 domain. Of note, OapA domains are distantly related with LysM domains. PaMepM2 contains a signal peptide (SP, red) for the Sec translocon at its N-terminus followed by a Peptidase family M23 N-terminal domain (M23-N, yellow) as well as a M23 domain. In paMepM3, a N-terminal TM helix and a C-terminal M23 domain were identified. Figure and description were kindly provided by Dr. Fabian Renschler.

9 Erklärung zum Eigenanteil

Die Arbeit wurde am Interfakultären Institut für Mikrobiologie und Infektionsmedizin (Tübingen) unter Betreuung von PD Dr. Erwin Bohn durchgeführt.

Die Konzeption des Projekts erfolgte durch PD Dr. Erwin Bohn und PD Dr. Monika Schütz.

Sämtliche Versuche wurden nach Einarbeitung durch die Labormitglieder PD Dr. Erwin Bohn, PD Dr. Monika Schütz, Dr. Fabian Renschler, Dr. Michael Sonnabend und Elias Walter von mir eigenständig durchgeführt. Um die Mutagenese zu beschleunigen übernahm PD Dr. Erwin Bohn einzelne Schritte an Wochenenden. Dr. Fabian Renschler führte die Alignments und Berechnung der pairwise identities der Proteine durch und erstellte die phylogenetischen Bäume, die im Appendix zu finden sind.

Die statistische Auswertung erfolgte nach Anleitung durch PD Dr. Erwin Bohn durch mich.

Ich versichere, das Manuskript selbständig verfasst zu haben und keine weiteren als die von mir angegebenen Quellen verwendet zu haben.

Tübingen, den 28.09.2020

Johanna Kemper

10 Danksagung

An dieser Stelle möchte ich mich ganz herzlich bei allen bedanken, die mich während der Anfertigung meiner Promotion unterstützt haben. Mein besonderer Dank gilt hierbei PD Dr. Erwin Bohn, der mein Projekt ermöglicht und mich über die ganze Zeit sehr verlässlich und kompetent betreut hat. Ganz herzlich möchte ich mich bei der gesamten AG Schütz/Bohn bedanken, namentlich bei PD Dr. Monika Schütz, Elias Walter, Dr. Michael Sonnabend, Dr. Fabian Renschler, Dr. Kristina Klein, Karolin Leibiger, Tanja Späth, Sara Pereira und Noelle Wackler. Während meiner gesamten Zeit im Labor, während zahlreicher Labmeetings, aber auch in meiner Schreibphase während der Corona-Pandemie, konnte ich immer auf Eure fachkundige Unterstützung zählen. Ich habe mich durch das wirklich nette Arbeitsklima immer wohl gefühlt, was mir die Arbeit sicher sehr erleichtert hat.

Des Weiteren möchte ich dem DZIF für die großzügige Förderung meiner Promotion danken. Zusätzlich danke ich auch den Verantwortlichen des IZKF Promotionskolleg der medizinischen Fakultät in Tübingen, durch die ich viele weitere Einblicke in das wissenschaftliche Arbeiten erlangt habe.

Auch meiner Familie gilt besonderer Dank, weil sie mich immer unterstützt hat.